PROBING THE STRUCTURES OF PROTONATED AND METALATED GLYCINE COMPLEXES USING INFRARED MULTIPLE PHOTON DISSOCIATION SPECTROSCOPY

CHAD GARRY ATKINS

Probing the Structures of Protonated and Metalated Glycine Complexes using Infrared Multiple Photon Dissociation Spectroscopy

by

Chad Garry Atkins

A thesis

presented to Memorial University

in fulfillment of the thesis requirement

for the degree of Master of Science

in Chemistry

St. John's, Newfoundland & Labrador, Canada, 2009

Abstract

The determination of gas-phase ion structures has been a prominent goal for many researchers within the field of mass spectrometry. The techniques to achieve this goal have evolved tremendously and absolute characterization is becoming an exciting reality. In the studies to be discussed, experimental results led to the conclusive assignment of a particular structure being the largest contributor of all ions present in the gas phase.

The proton- and the sodium ion-bound glycine homodimers were studied by a combination of infrared multiple photon dissociation (IRMPD) spectroscopy in the N-H and O-H stretching region and electronic structure calculations. The IRMPD spectrum for the proton-bound dimer confirmed that the lowest-energy structure was an ion-dipole complex between N-protonated glycine and the carboxyl group of the other glycine. The IRMPD spectrum for the sodium ion-bound dimer confirmed that the lowest energy structure was two bidentate glycine molecules bound to Na^+. In both cases, higher-energy structures could be ruled out using spectroscopic and/or thermodynamic arguments.

In the second study to be discussed, IRMPD spectroscopy, collision-induced dissociation (CID) spectrometry and theoretical calculations were combined to provide new insights into the structure and dissociation of lead(II) complexed with the amino acid glycine in the presence and absence of solvent. Unexpectedly, these experiments revealed the main lead(II) coordination sites to glycine were the deprotonated amino group and the carbonyl group. Such information is useful because of the biological implications which lead(II) has towards physiological systems. Structural knowledge of this system can be extended to include other amino acids and provide insight into the coordination of lead(II) with peptides responsible for detoxification.

Acknowledgements

As I recall the sequence of events which led me to where I am today, the individuals along the way who provided invaluable advice and assistance are countless. While I can't say it was my childhood dream to obtain a graduate degree in chemistry (space is overrated anyhow), the entire experience has been a meaningful one. My first thanks are therefore extended to the people who instinctively knew which direction to push me in. Harvey & Debbie MacEachern, thanks!

Once the papers were signed to attend the University of Waterloo for my chemistry undergrad, life changed drastically. Many thanks to **Andrew**, **Travis**, and **Vince** who provided numerous outlets as I coped with my late night study-habits. As the early undergrad years progressed, my curiosity towards the physical nature of chemistry was only just being stimulated. It wasn't until taking a class on mass spectrometry that my path to satiating this curiosity became clearer. The culmination of my quest was finally resolved with my fourth year honours work done in the McMahon laboratory at Waterloo. The McMahon group was influential in creating not only a strong passion for research, but also a meaningful comradery. For these reasons combined, I extend my thanks to **Terry, Rob, Rick, Matt, Jon**, and **Kris**.

Looking to build upon the foundation of the Waterloo experience, my next choice fell into my lap. Having been born in St. John's and raised nearby, the decision to return was strengthened two-fold; 1) the prospect of re-uniting with old friends, and 2) the chance to work with Dr. Travis Fridgen , former post-doc of Terry McMahon and a prior professor of mine for an aforementioned mass spectrometry class. It's difficult for me to properly convey my gratitude for Travis. Not only was he inspiring as a professor, but his easy-going, friendly, and exuberant

nature as a supervisor have made the last two years a scintillating adventure. At the conclusion of my degree, Travis will have taken me to three conferences and have mentored in the publication of two papers. The appreciation I have for Travis goes well beyond the scope of such tangible results. His ability to manage his research group while being a model husband to Lisa and loving father to four children is something to really be admired. Travis, **Thanks** for your support, your trust, and your belief that I would somehow come through in the clutch! I need to also extend thanks to Travis' research group; **Negar, Elizabeth, Osama, Julie**, and others, thanks! Extended thanks go out to **Mark**, who sat in the trenches with me and engaged in battle with the Pb^{2+} ion, and also to **Mike**; if it wasn't for our daily conversations on topics regarding (but not exclusive to) each other's sanity, international news, and *sometimes* chemistry, I wouldn't have been able to pull this all together. Mike, you're an archetypal friend and our esoteric discussions will be missed!

Finally, the only force in my life that has been constant over the course of this story has been my family. **Garry, Audrey**, and **Krista**, your never-ending love and support are truly appreciated. To my parents : the check-up phone calls, the e-mails, the snail-mail cards - while I may have been busy or preoccupied with other things, having your support in my corner is an unfathomable asset that I am only starting to appreciate now. Thank you! Garry, I think I finally get it! After all these years, you *may* indeed know a thing or two! I guess I have years of advice to catch up on, huh? Audrey, "I'll love you forever I'll like you for always as long as I'm living my Mommy you'll be."

†† For My Family ††

Table of Contents

List of Figures

List of Tables

List of Abbreviations

ω	angular frequency
Δ	change in
ΔG^o_{calc}	calculated standard Gibbs free energy charge
ΔG^o_{exp}	measured standard Gibbs free energy change
ΔG_{rel}	standard Gibbs free energy change relative to lowest-energy isomer
ΔG^o_{rxn}	standard Gibbs free energy change for a reaction
ΔH^o_{calc}	calculated standard enthalpy change
ΔH^o_{exp}	measured standard enthalpy change
ΔH_{rel}	standard enthalpy change relative to lowest-energy isomer
ΔH^o_{rxn}	standard enthalpy change for a reaction
ΔS^o_{calc}	calculated entropy change
ΔS^o_{exp}	measured entropy change
ΔS_{rel}	standard entropy change relative to lowest-energy isomer
ΔS^o_{rxn}	standard enttropy change for a reaction
BIRD	blackbody infrared radiative dissociation
B3LYP	Becke's adaptation of density functional theory using the correlation of Lee, Yang, and Parr
CID	collision-induced dissociation
DFT	density functional theory
DNA	deoxyribonucleic acid
ECD	electron capture dissociation
EI	electron impact
ESI	electrospray ionization
FAB	fast-atom bombardment

FEL	free-electron laser
FID	free induction decay
FT-ICR	Fourier transform ion cyclotron resonance
FTMS	Fourier transform mass spectrometer
H-bond	hydrogen bond
HPMS	high-pressure mass spectrometry
ICR	ion cyclotron resonance
IR	infrared
IRMPD	infrared multiple photon dissociation
IVR	intramolecular vibrational-energy redistribution
K_{eq}	equilibrium constant
MALDI	matrix-assisted laser desorption ionization
MIKES	mass-analyzed ion kinetic energy spectrometry
MP2	second order Møller-Plesset perturbation theory
MS	mass spectrometry
MS^n	tandem mass spectrometry with n levels of separation
OPG	optical parametric generation
OPO	optical parametric oscillation
OPA	optical parametric amplification
QqTOF	hybrid quadrupole time-of-flight mass spectrometer
T_{eff}	empirical effective temperature parameter
ZPE	zero-point energy

Chapter 1

Introduction

1.1 General Introduction

It is impossible to overlook the importance of mass spectrometry (MS) as a tool for understanding the world around us. Since its earliest inception by J. J. Thompson, who devised a means for separating isotopes of neon based on their mass-to-charge ratios,[1] the tool has evolved tremendously. Commercial applications of the technique are now widespread and its usage is no longer limited to the physical chemist studying the most fundamental of processes; it is instead commonplace to see mass spectrometry assisting chemists with diverse backgrounds. Throughout this evolution, new theories and revised ideas have repeatedly been adapted and implemented to the mass spectrometer, solidifying its ability to study almost any available problem. As scientific research continues to delve from the macroscopic world into the realm of the microscopic, mass spectroscopists have courageously been able to stay on track and remain on the cutting edge.

Of the major scientific discoveries in the last century, Watson and Crick`s elucidation of the double helix structure for deoxyribonucleic acid (DNA) is inarguably one of the most important.[2] While the connection may not seem direct, their breakthrough significantly influenced the field of biochemistry and created great interest towards understanding the interactions of nucleotides. This then led to an explosion of research in genomics and the more recent field of proteomics, where investigations have been centered on evaluating protein function, describing protein folding, interpreting post-translational modifications, and identifying

structural features. It is this latter goal which has captivated the focus of many mass spectrometry research groups.

The basic operating components for any mass spectrometer (ion source, mass analyzer, detector) have been well-defined and will not be reiterated here.[3-5] It is worth noting, however, that the key requirement for any analyte in a MS analysis is that it must be in the form of a gaseous ion. This may seem like a debilitating feature for proteomics work considering that biological samples are non-volatile and difficult to introduce into the gas-phase without disrupting native structure. With the advent of 'soft' ionization methods such as matrix-assisted laser desorption ionization (MALDI)[6] and electrospray ionization (ESI),[7] this significant problem has been eliminated. These techniques allow the introduction and ionization of non-volatile biological molecules into the gas phase without undesirable fragmentation. In reality, the key requirement becomes a subtle benefit as biological research is inherently intertwined with ionic systems. Accurately modeling systems of interest in the gas phase is *not* the real challenge of mass spectrometry. The real challenge arises when trying to relate gas phase systems (typically measured in the absence of water and counter ions) with the same systems *in vivo*. This concept of `bridging-the-gap` between the gas phase and the condensed phase has therefore been studied rigorously and remains the objective of many studies today.

One of the most prevalent goals of any research in chemistry is to understand what is occurring on a fundamental level. To develop a better picture of protein chemistry and how proteins interact in real biological systems, they must first be understood from the simplest foundation. Proteins are composed of building blocks known as amino acids, of which there are twenty variations recognized as being the "standard amino acids".[8-10] By definition, an amino

acid contains an amino and carboxyl functional group and they adhere to the general formula $H_2NCHRCOOH$, where R represents an organic side chain native to each acid. Amino acids have historically been studied by mass spectrometry for decades. However, the collection and interpretation of data has been very progressive and reliant on previous studies, corresponding to what type of information can be obtained with the available procedure at the time. For example, proton affinities,[11] binding energies,[12] and other thermodynamic values have been established for certain amino acid systems for quite some time. While such data can provide insight towards the strength of bonds and fundamental interactions, it is impossible to fully characterize a complete picture of structural features for the given ion of interest. Without this information, it becomes difficult to extrapolate the information obtained from an amino acid system towards a more complicated protein. One of the goals for these introductory chapters is to describe a scintillating procedure known as infrared multiple photon dissociation (IRMPD) by which structural characterization can be achieved, and to bring forward exciting examples which have been thoroughly examined. Determining structures of gas-phase amino acids when complexed with metal ions, protic solvents, etc., is the first step towards `bridging-the-gap` and ultimately emulating what one may find in solution. The proceeding section will examine some techniques used in mass spectrometry to characterize structural features of ions, followed by a more in-depth examination of work done presently by the Fridgen group at Memorial University.

1.2 Determining Structures of Gas-Phase Ions

Mass spectrometry is a tool for detecting and analyzing a wide variety of substances. It was and still is heralded for its high selectivity and sensitivity. While determining reliable ion mass is useful for some studies, the early mass spectrometer could offer very little information

on the structure of a mass-selected ion. To compensate for this inadequacy, the following approaches have been adapted to *infer* structural features: 1) low- and high-energy collision-induced dissociation (CID),[13-15] 2) electron capture dissociation (ECD),[16-19] and 3) thermochemistry arguments,[20-22] to name a few. For the most part, these techniques are based on increasing the internal energy of a molecular ion and then analyzing its fragmentation pattern. They are indeed capable of elucidating structural features yet they can provide only limited information on *actual* three-dimensional ion structure; a more exhaustive means of structural analysis is desired. To meet the demand for such functionality, a technique that could perform infrared (IR) spectroscopy on an isolated ion and generate a representative gas-phase IR spectrum has been developed. This spectrum, much like an IR spectrum obtained in solution, depicts characteristic absorption bands as a direct indicator for the presence of certain structural features. Combined with theoretical calculations (see section 2.3), the interpreter would be able to produce a valid three-dimensional structure of the ion studied. Before discussing how this IR technique works, the reader must be aware of a certain functionality known as tandem mass spectrometry. This functionality is commonly seen in some of the approaches listed above, and discussing its basic definition will provide some insight into how the mass spectrometer can be utilized in its various ways to infer structural information.

1.2.1 Tandem Mass Spectrometry

Tandem mass spectrometry is conceptually similar to the combination of chromatography devices with mass spectrometers (i.e., GC/MS, LC/MS).[23] It involves multiple steps of mass selection (MS^n, where n = number of separation events) with some form of fragmentation occurring between each step. The separation stages can occur in space (multiple

mass analyzers) or in time (one mass analyzer, multiple stages), depending on the instrumentation available. Double focusing mass spectrometers based on magnetic and electrostatic sectors were the first instruments used for CID studies.[24] Pioneering work done by McLafferty in 1968 demonstrated the application of CID towards distinguishing between isomeric structures.[25] However, a setup which is based solely on sectors suffered from poor precursor and product ion resolution. Recent advances in combining mass analyzers have led to experiment-specific instrumental arrangements. For 'high-energy' (keV collision energy) CID, the older sector approach is sufficient. For the more-common 'low-energy' (eV collision energy) CID, tandem quadrupoles and quadrupole hybrids are preferred. It is these low-energy experiments which are favored when analyzing biological samples, as unnecessary side-chain cleavage causes interference with expected fragmentation patterns. Not only has combining mass analyzers shown promise for tandem MS, but newer analyzers such as the Fourier transform ion cyclotron resonance cell (FT-ICR, described in section 2.2.1) have been adapted to permit both ECD and IR spectroscopy. On the whole, using tandem mass spectrometry for the investigation of peptides and proteins has started to supplant the traditional method of *N*-terminal Edman sequencing. An entire MS^n analysis can be done in minutes and very cost-effectively, while the traditional sequencing approach is timely and can accrue a hefty price.[26]

The next sections describe the capabilities of CID and two pertinent thermochemical approaches, namely ion-molecule reactions and Cooks' kinetic method. The following discussion shows how these methods are used for inferring structural information of a gaseous ion.

1.2.2 Collision-Induced Dissociation (CID)

J. J. Thomson is credited with being the first to perform a CID experiment, even though it may not have explicitly been his intention.[1] CID is a simple procedure by which precursor ions of interest are fragmented in a mass spectrometer. It occurs when ions produced from the ion source are imparted with large amounts of kinetic energy through acceleration and are directed into a collision cell with neutral gas molecules (most commonly helium or argon).[27] This step is known as "ion activation" and its purpose is to insert sufficient energy into an ion so that fragmentation can eventually occur. The CID mechanism is thought to occur in two steps;

$$M_p^+ + N \xrightarrow{KE} M_p^{+*} + N' \quad (1.1)$$

$$M_p^{+*} \rightarrow dissociation\ ions + neutrals \quad (1.2)$$

When the precursor ion (M_p^+) impacts the neutral molecule (N), the kinetic energy contained in these species is converted into internal energy and the energized precursor ion is promoted to an excited state, as seen in Eq. 1.1. The second step is dependent on the competitive unimolecular dissociation pathways for the precursor ion, which influence the identities of the product ions and neutrals formed in Eq. 1.2. These fragments are detected and information pertaining to the parent ion's structure can be deduced.[28] This process reveals the importance of tandem mass spectrometry as an innovative approach for obtaining structural information. As shown below, the evolution of tandem mass spectrometry has also played a role in the historical capability of CID.

With approaches for ionizing, transmitting, and detecting protein complexes in the mass spectrometer being well-established, structure elucidation of such species has become a challenge. The objective is centered on inducing the disassembly of a given protein to obtain information about its composition and organization. While an absolute three-dimensional structure cannot be obtained directly due to the complexity of proteins and protein folding, the field of proteomics has shown heavy reliance on CID.[29,30] This is because the experimental procedure for CID is relatively easy and provides the ability to create fingerprints for various proteins. As such, *identification* and **not** structural characterization becomes simplified.

A recent example from the scientific literature[31] demonstrates the use of CID to study cobalt-cysteine ions. Examination of fragmentation pathway mechanisms reveals that the cobalt ion is strongly bound to the sulphur atom of the cysteine. The experiments were carried out on a Q-star Pulsar tandem quadrupole time-of-flight (QqTOF) mass spectrometer, which was equipped with an electrospray source. Solutions are typically dilute when using an electrospray source, and here cobalt-cysteine mixtures (0.5 mM and 0.1 mM, respectively) were made in 50/50 methanol/water. Three main ion species were observed experimentally: 1) ions with cobalt and cysteine, such as $[Co(Cys)_n\text{-}H]^+$ with n = 1-3, 2) ions with cobalt and methanol, such as $[Co(CH_3OH)_n\text{-}H]^+$ with n = 1-3, and 3) complexes with two ligands such as $[Co(Cys)(CH_3OH)\text{-}H]^+$. The most abundant ion species was from the first category and is $[Co(Cys)\text{-}H]^+$, or m/z = 179.

To gain insight into the formation mechanism and structure of the most abundant $[Co(Cys)\text{-}H]^+$ ion, Buchmann et al. isolated the ion and performed CID experiments. The resulting data was displayed in a mass spectrum depicting the detected product ions (Figure 1.1), as well as via a breakdown graph highlighting the abundance of fragment ions as a function of collision energy (Figure 1.2).

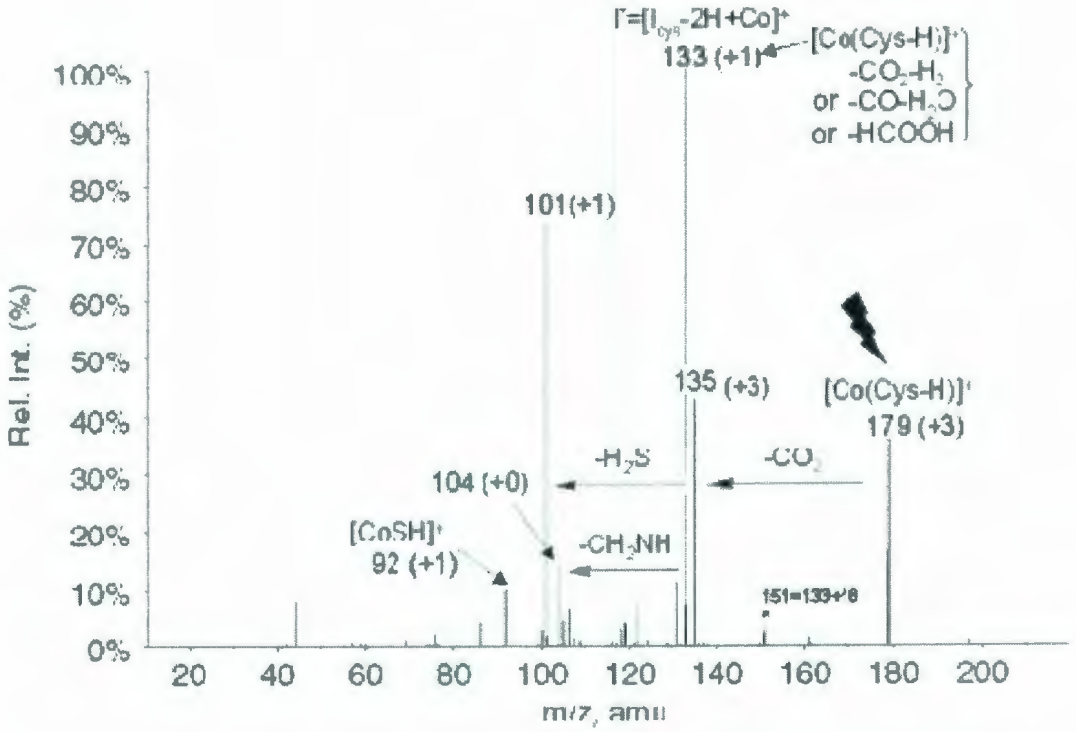

Figure 1.1 – MS/MS CID spectrum of m/z = 179 $[Co(Cys)-H]^+$ ion with CE = 20 eV. Deuterium labeling experiments are in parentheses.[31] Figure reprinted with permission fron. *Journal of Mass Spectrometry,* 2007, *42*, 517. Copyright 2007 Wiley.

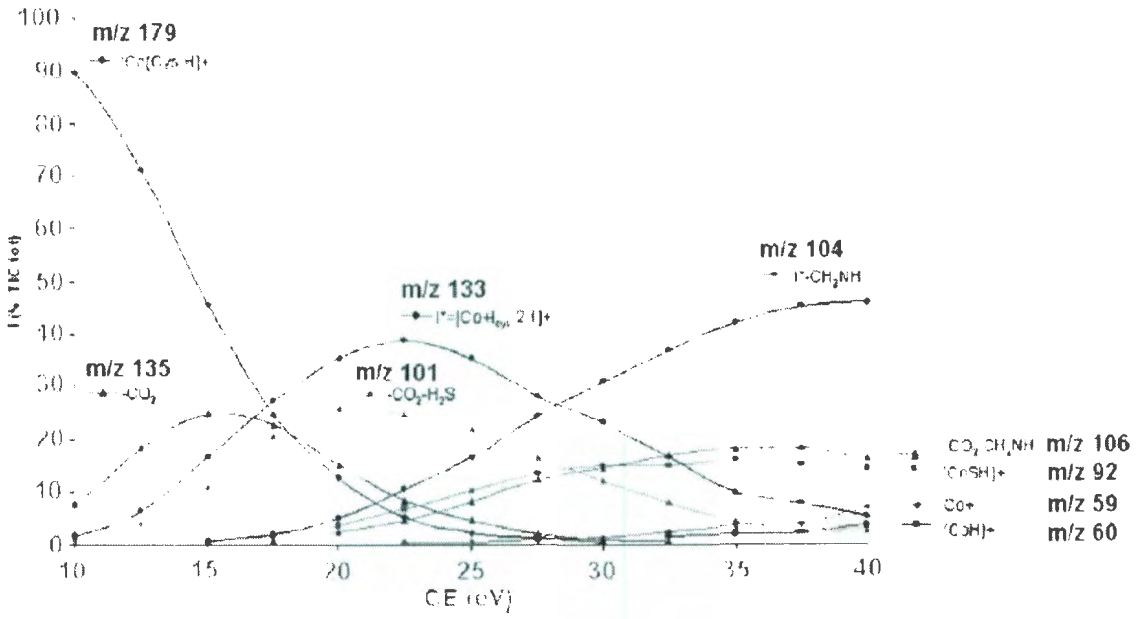

Figure 1.2 – Evolution of ion intensity from $[Co(Cys)-H]^+$ as a function of CE.[31] Figure reprinted with permission from *Journal of Mass Spectrometry* 2007, *42*, 517. Copyright 2007 Wiley.

Figure 1.1 reveals product ion identities using mass differences from the parent ion *m/z* = 179. Common neutral molecules which are lost during fragmentation are well known for such amino acid systems. At lower collision energies *m/z* = 135 is the main fragment peak due to the loss of a fragment with 44 mass units, likely CO_2. Figure 1.2 demonstrates that as the collision energies get higher (>20 eV), the most abundant product ion becomes *m/z* = 133. This *m/z* = 133 fragment is due to a loss of 46 mass units which has previously been attributed to losses of HCOOH, $CO_2 + H_2$, or $CO + H_2O$. The identity of the *m/z* = 133 ion is assigned as being the immonium fragment of cysteine minus two hydrogens but with a cobalt ion. At the highest attainable collision energies, this ion loses 29 mass units, $[M-(CH_2=NH)]^+$, resulting in the most abundant product ion at *m/z* = 104. Other peaks present at collision energies >30 eV are *m/z* = 106 and *m/z* = 92. The former corresponds to successive losses of CO_2 and CH_2=NH from *m/z* = 179, while the latter results from a loss of CH_2=CH-NH_2 and is identified as $[CoSH]^+$. As argued by the authors through evidence presented in their proposed pathways, the presence of ions at *m/z* = 135, 133, 104, 106, and 92 confirms the strong affinity of the cobalt metal ion for the sulfur atom of cysteine. This is evident by the fact that among these product ions there is no indication of sulfur fragmentation. Their conclusion represents an important structural *inference* towards cobalt-cysteine complexes, which is representative of the technique, on the whole.

CID relies on complementary approaches and experiments to help validate conclusions. A common tool for a majority of gas-phase experiments is the use of theoretical electronic structure calculations. The energetic arguments presented by such calculations enable a researcher to propose a plausible mechanistic scheme for a given fragmentation pathway, and eliminate contributions from disfavored routes. This functions to narrow possible reaction schemes and allow for more reliable interpretations.

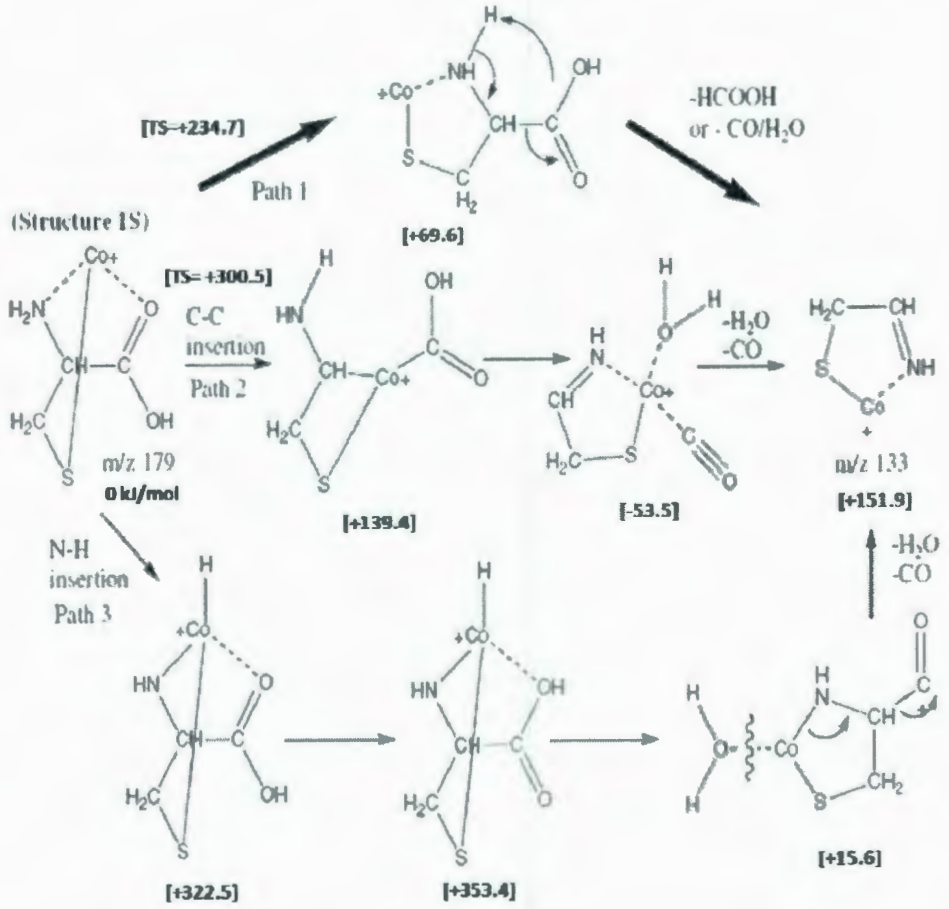

Figure 1.3 – Possible pathways of m/z = 179 $[Co(Cys)-H]^+$ fragmenting into m/z = 133. Relative energies are indicated in brackets.[31] Figure is modified from reference 31 to depict energies in kJ mol^{-1}, and is reprinted with permission from *Journal of Mass Spectrometry,* 2007, *42*, 517. Copyright 2007 Wiley.

As shown in Figure 1.3, the simplest pathway would be the two-step path 1. Energy arguments (in brackets) made available by B3LYP/6-31++G(d,p) theoretical calculations show that this would be the most likely route. While path 2 contains a stable intermediate (ΔG° = -53.5 kJ mol^{-1}), it is disfavoured by its very high first barrier (TS = +300.5 kJ mol^{-1}). Path 3 is similarly disfavoured on energetic grounds as the first two intermediates are higher in energy than the first transition state of path 2. Arguments such as these are extremely useful to CID experiments and data interpretation. Meanwhile, to assist in classifying fragment products simple deuterium labeling experiments can be implemented to observe the patterns created when all exchangeable hydrogens undergo H/D exchange. Such techniques were used above by Buchmann et al. to assist in their investigation.

1.2.3 Thermochemistry : Ion-Molecule Reactions and the Kinetic Method

Gas-phase ion thermochemistry is an area that has garnered immense interest within the mass spectrometry community. Research in this area revolves around the prediction and/or experimental determination of basic thermodynamic quantities, including Gibbs free energy (G), enthalpy (H), and entropy (S). This type of knowledge can provide tremendous insight for a wide range of properties, including; binding enthalpies,[32] solvation energies,[33] ion affinities,[34,35] and experimental reaction mechanisms.[36] When used in conjunction with theoretical calculations, it becomes possible to make structural assignments for gaseous complexes. Two approaches for evaluating the thermodynamic quantities mentioned above using mass spectrometry will now be discussed; the study of ion-molecule reactions and Cooks' kinetic method.

1.2.3.1 Ion-Molecule Reactions

When dealing with ion-molecule clustering reactions, thermodynamic quantities can be established using the principle of chemical equilibrium. The equilibrium shown in Eq. 1.3 is the simplest type of reaction, where a produced ion (A^+) interacts with a neutral molecule (B) to yield the complex of interest (AB^+). The coefficients α, β, and σ indicate stoichiometric contribution from each species. While other reaction types are common, they follow the same experimental approach to be described.

$$\alpha A^+ + \beta B \rightleftharpoons \sigma AB^+ \tag{1.3}$$

Chemical equilibrium designates an experimental condition whereby the concentrations of reactants and products are unchanged over time. The standard equation for determining the equilibrium constant of a system such as Eq. 1.3 is shown below in Eq. 1.4.

$$K_{eq} = \frac{[AB^+]^\sigma}{[A^+]^\alpha [B]^\beta} \tag{1.4}$$

The instrumentation most often used for thermochemical determinations is high-pressure mass spectrometry (HPMS). Such an apparatus would deal with gas-phase systems only, so that the equation for chemical equilibrium above would be in terms of pressures and not concentrations, as shown in Eq. 1.5, where P_{AB}^+, P_A^+, and P_B represent partial pressures and P_o is the standard pressure of 1 bar.

1.2.3.1 Ion-Molecule Reactions

When dealing with ion-molecule clustering reactions, thermodynamic quantities can be established using the principle of chemical equilibrium. The equilibrium shown in Eq. 1.3 is the simplest type of reaction, where a produced ion (A^+) interacts with a neutral molecule (B) to yield the complex of interest (AB^+). The coefficients α, β, and σ indicate stoichiometric contribution from each species. While other reaction types are common, they follow the same experimental approach to be described.

$$\alpha A^+ + \beta B \rightleftharpoons \sigma AB^+ \tag{1.3}$$

Chemical equilibrium designates an experimental condition whereby the concentrations of reactants and products are unchanged over time. The standard equation for determining the equilibrium constant of a system such as Eq. 1.3 is shown below in Eq. 1.4.

$$K_{eq} = \frac{[AB^+]^\sigma}{[A^+]^\alpha [B]^\beta} \tag{1.4}$$

The instrumentation most often used for thermochemical determinations is high-pressure mass spectrometry (HPMS). Such an apparatus would deal with gas-phase systems only, so that the equation for chemical equilibrium above would be in terms of pressures and not concentrations, as shown in Eq. 1.5, where P_{AB}^+, P_A^+, and P_B represent partial pressures and P_o is the standard pressure of 1 bar.

$$K_{eq} = \frac{P_{AB^+}}{P_{A^+} \times P_B} P_o \tag{1.5}$$

In HPMS experiments, ions are usually generated by electron impact (EI) ionization. A short electron pulse created via an electron gun interacts with a bath gas mixture containing an analyte of interest. Collisions between the high-energy electrons and the bath gas molecules results in positive ionization accompanied by the production of secondary electrons which further enhances ionization. Due to the high pressure environment of the source, there are approximately 10^8 collisions per second which thermalize the A^+ ions. These produced ions are then able to participate in chemical reactions with neutral B molecules added to the mixture to yield AB^+ complexes of interest.

Determining the partial pressures of each species is not practical. Ion populations of A^+ and the complex AB^+ are instead measured individually. If these species attain a state of equilibrium, then it is believed that their decays will occur at the same rate. Inspecting the time evolution of the detected populations reveals that the establishment of chemical equilibrium between the two ions can be observed. The first step is to normalize the time-resolved ion intensity profiles of each species with one another, shown in Eq. 1.6 and 1.7, to remove the common effect of diffusion-controlled discharging of the ions to the wall.

$$I_{A^+} = \frac{I_{A^+}}{I_{A^+} + I_{AB^+}} \tag{1.6}$$

$$I_{AB^+} = \frac{I_{AB^+}}{I_{AB^+} + I_{A^+}} \tag{1.7}$$

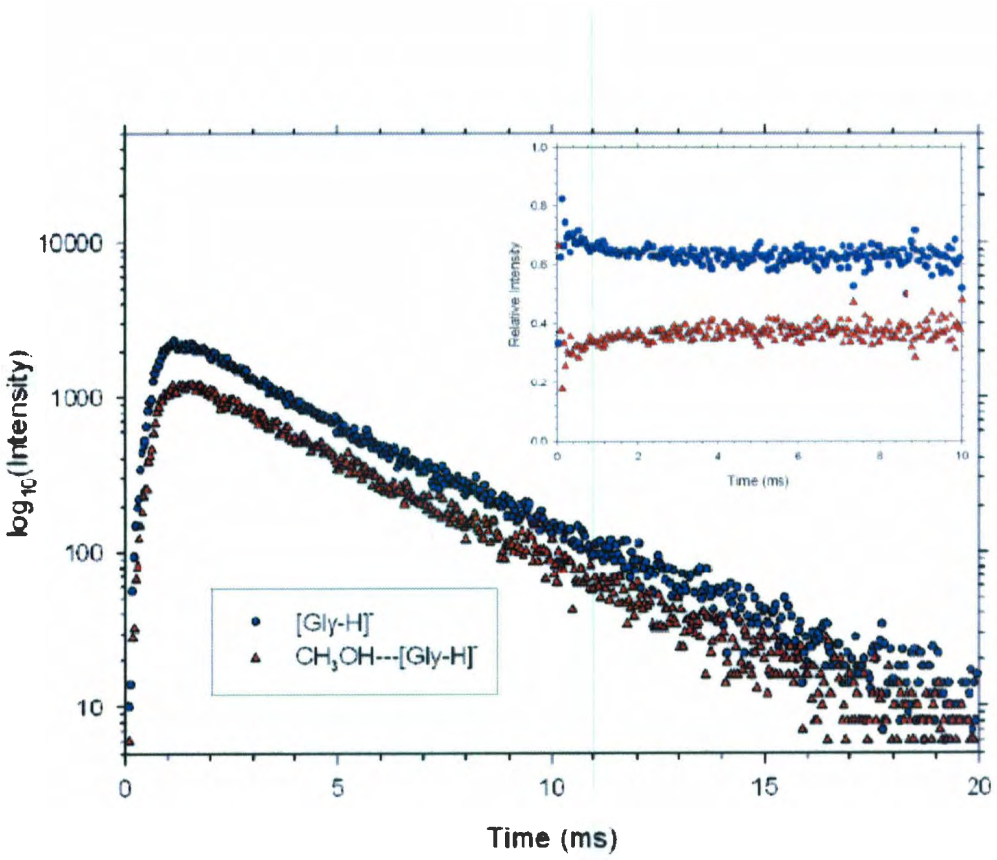

Figure 1.4 – Typical log_{10}(intensity) - time profile. Inset: normalized conditions showing equilibrium.[38] Figure reproduced from Nieckarz et al., *ChemPhysChem*, 2008, *9*, 2816 with permission from the author.

$$\Delta G^{o}_{rxn} = -RT \ln(K_{eq}(T)) \quad (1.10)$$

$$\Delta G^{o}_{rxn}(T) = \Delta H^{o}_{rxn} - T\Delta S^{o}_{rxn} \quad (1.11)$$

$$\ln(K_{eq}(T)) = -\frac{\Delta H^{o}_{rxn}}{RT} + \frac{\Delta S^{o}_{rxn}}{R} \quad (1.12)$$

Plotting $\ln(K_{eq})$ vs T^{-1} yields a linear plot with enthalpy and entropy obtainable via the slope and intercept, respectively. This is where the ability to infer structural information becomes possible. Evaluating thermochemical values obtained for theoretical structures and comparing them with experimental results allows researchers to make reasonable conclusions regarding the structure of observed gas-phase ions. However, as convincing as such an approach may be, absolute characterization is not possible. There are inherent limitations which could contribute to inadequate structural conclusions, such as in a situation where low-barrier isomerization channels exist or when a mixture of isomeric structures is present. In the case where there is a low-barrier, lower temperatures would favor the isomer having a significant enthalpic advantage while higher temperatures would favor another isomer having a significant entropic advantage. Experimentally this would appear as a 'bent' van't Hoff plot composed of two linear portions displaying thermochemical data representative for each isomer.[39] Without recognizing the presence of such a low-barrier, it would be possible to interpret the van't Hoff plot incorrectly and make an erroneous structural conclusion. In the case where mixtures of isomers having similar free energies are experimentally accessible, a linear van't Hoff plot would be observed

producing agreeable enthalpy values but very misleading entropy results. This is due to the entropy of mixing which finds its origin grounded in statistical mechanics. Such circumstances could contribute to incorrect structural conclusions.

In past applications, the study of gas-phase amino acids using HPMS was extremely difficult due to their non-volatile nature. However, this limitation was resolved when the McMahon group at the University of Waterloo started to directly introduce a solid sample of the amino acid into their heated ion source, resulting in sublimation of the amino acid.[40] A recent HPMS study was published by Nieckarz, Atkins and McMahon.[38] These researchers intended to investigate the interactions of polar protic solvents, such as water, methanol, and ethanol, with glycine in its deprotonated form. All measurements were performed using a VG 8-80 HPMS, containing a single magnetic-sector mass analyzer and a home-built pulsed-ionization high-pressure ion source. A solid sample of glycine was placed in the ion source at above 120°C which produced a sufficient density of sublimed glycine to provide a usable ion signal. The deprotonated glycine ion was obtained by introducing N_2O which has been shown to produce a gaseous OH^- ion upon electron bombardment. Clustering of the deprotonated glycine with each of the protic solvents was then investigated. K_{eq} values were determined from knowing the ratio of product to reactant ion intensities during the period of time when the two ions were in equilibrium. The van't Hoff plots depicted by Nieckarz, Atkins & McMahon for each equilibrium reaction of deprotonated glycine + solvent were linear and ranged from approximately 120°C - 180°C (Figure 1.5). $\Delta H°_{exp}$ and $\Delta S°_{exp}$ were then obtained from the slope and intercept, respectively (Table 1.1).

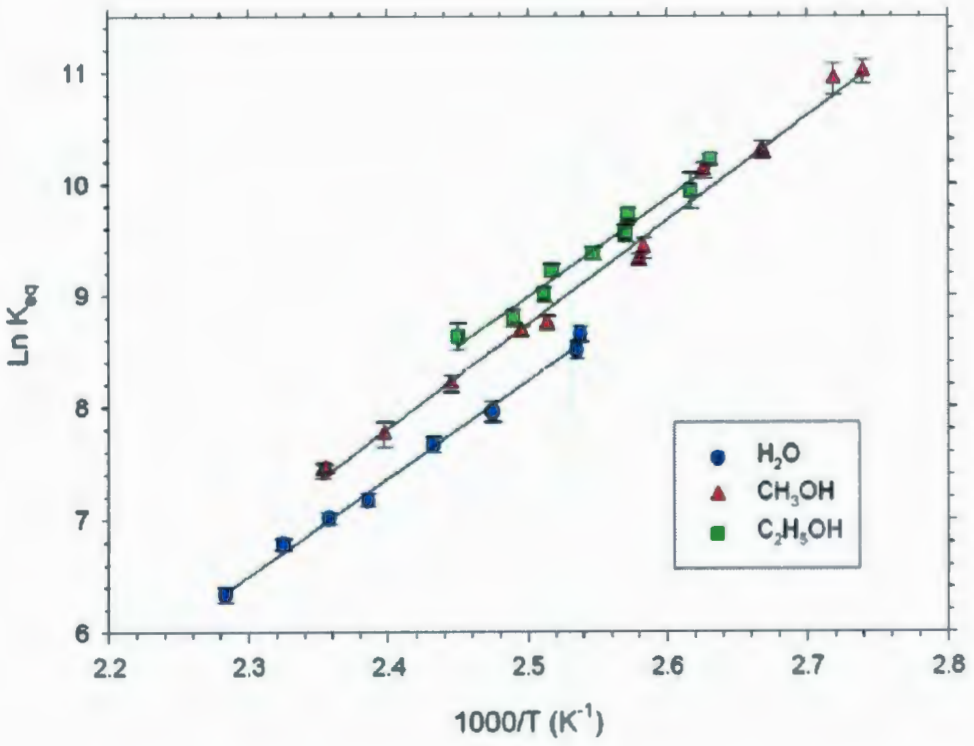

Figure 1.5 – van't Hoff plot for the clustering of $[Gly\text{-}H]^-$ with H_2O, CH_3OH, C_2H_5OH.[38] Figure reproduced from Nieckarz et al., *ChemPhysChem*, 2008, *9*, 2816 with permission from the author.

Table 1.1 – Experimental thermochemical properties.[38] Table contains data from Nieckarz et al., *ChemPhysChem* 2008, *9*, 2816.

Cluster		ΔH^o_{obs}	ΔS^o_{obs}	$\Delta G^o_{298,obs}$
$[\boldsymbol{M-H}]^-$	ROH	$(\pm 2.0\ kJ\ mol^{-1})$	$(\pm 10.0\ J\ K^{-1}\ mol^{-1})$	$(\pm 4.1\ kJ\ mol^{-1})$
$[\boldsymbol{Gly-H}]^-$	H_2O	-72.5	-112.7	-38.9
	CH_3OH	-71.1	-105.5	-39.6
	C_2H_5OH	-73.5	-109.0	-41.0

The supporting B3LYP/6-311++G(d,p) calculations performed in this study demonstrated that the gaseous OH^- ion favoured the removal of a proton from glycine's carboxyl functional group. As such, the calculations also demonstrated that two basic types of clusters were present for all systems. The first class was attachment of the ROH solvent to the carboxylate moiety, and the second class was the attachment of the solvent to the amine moiety. Through investigation of the thermochemical properties for each in comparison to the experimentally obtained values, it was deemed that the former class was considerably more favourable. It is through such comparisons that structural information is gained with this HPMS approach. For this literature example, the lowest-energy structures for the three systems (Figure 1.6) agreed favourably with experimental results (Table 1.2).

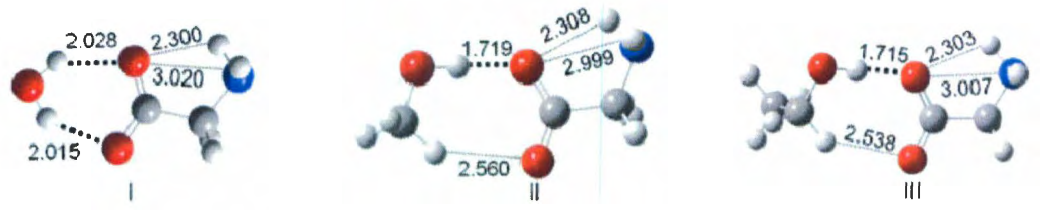

Figure 1.6 – Lowest energy theoretical structures for each $[Gly\text{-}H]^-\cdots ROH$ system.[38] All were optimized using B3LYP/6-311++G(d,p). Figure reproduced from Nieckarz et al., *ChemPhysChem*, 2008, *9*, 2816 with permission from the author.

Table 1.2 – Comparison of experimental data with theoretically-obtained Data.[38] Table contains data from Nieckarz et al., *ChemPhysChem* 2008, *9*, 2816.

Cluster	ΔH^o $(kJ\ mol^{-1})$	ΔS^o $(kJ\ mol^{-1})$	ΔG^o_{298} $(\pm 2.0\ kJ\ mol^{-1})$	Method
$H_2O \cdots [Gly-H]^-$	-72.5±2.0	-112.7±10.0	-38.9±4.1	a
	-70.3	-113.6	-36.5	b
	-73.1	-122.7	-36.6	c
	-53.7	-110.6	-20.7	d
$CH_3OH \cdots [Gly-H]^-$	-71.1±2.0	-105.5±10.0	-39.6±4.1	a
	-68.9	-105.3	-37.6	b
	-71.4	-120.9	-35.4	c
	-57.2	-116.4	-22.5	d
$C_2H_5OH \cdots [Gly-H]^-$	-73.5±2.0	-109.0±10.0	-41.0±4.1	a
	-73.9	-110.1	-41.1	b
	-74.5	-121.0	-38.4	c
	-58.3	-120.5	-22.3	d

[a] HPMS. [b] Calculated for distribution of all isomers. [c] Calculated for lowest-energy isomer. [d] Calculated for solvent attachment to the amine group of the deprotonated glycine.

The best agreement occurred for the water system, as the isomeric distribution was shown to consist of one major isomer and a small number of less significant ones. In both the methanol and ethanol systems, large discrepancies were present between the entropy values determined experimentally and the entropy values from the lowest-energy calculated structures. Closer inspection revealed that an isomeric distribution was expected to occur for methanol over the given temperature range, so by taking into account all isomers the entropy difference between experiment and theory was reduced from 15.4 J K^{-1} mol^{-1} to 0.5 J K^{-1} mol^{-1}. Similarly for ethanol, taking into account the presence of all significant isomers reduced the entropy difference from 11.0 J K^{-1} mol^{-1} to 1.0 J K^{-1} mol^{-1}.

For the deprotonated glycine··ROH solvent complex, it is demonstrated that a distribution of isomers within an HPMS ion source will affect the measured thermochemical properties. Correlating this conclusion with the theme of this thesis, it becomes clear that a more conclusive means of isolating and identifying individual structural features is required.

1.2.3.2 Kinetic Method

The kinetic method is considered to be highly successful because of its simplicity and convenience of use.[41] It was first introduced in 1977 by Cooks and Kruger using mass-analyzed ion kinetic energy spectroscopy (MIKES).[42] The method is said to be of the 'thermokinetic' type, whereby the thermodynamic data to be obtained relies on the evaluation of *reaction rates*.[43] The initial intent of the method was to provide the relative affinities of two competitive fragmentation channels by means of comparing their rate constants. As time progressed, the experimental approach became more refined and was capable of evaluating a wider variety of

systems and contributing to structural inquiries. While the overall method has improved since its initial introduction, the standard approach remains the foundation for all enhanced versions.

The kinetic method involves formation and dissociation of heterodimeric cluster ions, in which two molecules are connected via a central ion.[44] The typical situation involves molecule A (with unknown thermochemistry) binding to a central ion along with molecule B (one of a homologous set of reference compounds, all with known affinity and having 'similar' structure to A). The first step in this process is to mass-select the cluster ion within a tandem mass spectrometer. The loosely bound complex A···X^+···B (bound by either a proton, cation, electron, etc.) can dissociate through two major pathways as in Figure 1.7;

$$AX^+ + B \overset{k_1}{\leftarrow} A \cdots X^+ \cdots B \overset{k_2}{\rightarrow} A + BX^+ \tag{1.13}$$

The rate constants for the unimolecular dissociation reactions are given above as k_1 and k_2. The ratio of these rate constants are directly proportional to product concentrations, or ion abundances.[45]

$$\frac{k_1}{k_2} = \frac{[\mathrm{BX}^+]}{[\mathrm{AX}^+]} \tag{1.14}$$

The simplest approach to obtain thermochemical information from experimental kinetics is through the Arrhenius equation as shown in Eq. 1.15;

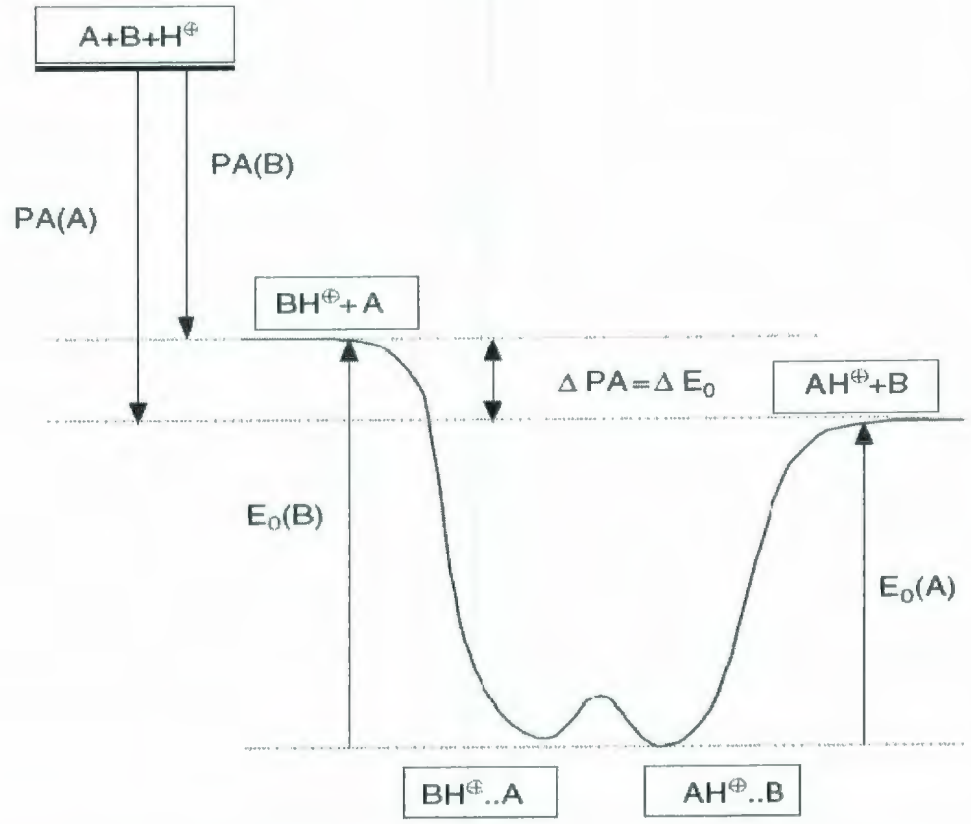

Figure 1.7 – Schematic of kinetic method.[45] PA is proton affinity, E_o is the activation energy. Figure reprinted with permission from *Journal of Mass Spectrometry*, 2003, *38*, 1025. Copyright 2007 Wiley.

$$k_i(T_{eff}) = A_i e^{(\frac{Ea_i}{RT_{eff}})} \quad (1.15)$$

where T_{eff} is the effective temperature (empirical term accounting for the lack of thermal equilibrium),[46] A_i is the pre-exponential factor, and Ea_i is the activation energy, both for the *i*th dissociation channel. The term T_{eff} was introduced to evaluate a temperature determined from a smoothly varying, but non-Boltzmann, distribution of internal energies. The term does not provide a quantitative estimate of the dimer ion internal energy, but will provide a qualitative estimate.[47] The exponential function in Eq. 1.15 is undesirable and can be removed by taking a natural logarithm of both sides to obtain;

$$\ln\left(\frac{k_1}{k_2}\right) = \ln A_1 - \ln A_2 + (\frac{E_{a2}-E_{a1}}{RT_{eff}}) \quad (1.16)$$

The pre-exponential terms, which account for the entropy of activation, are assumed to be similar for each of these competing channels and cancel.[48] This happens for complexes where A and B are of similar chemical structure and therefore their transition states are also similar. Due to these similarities, the energy and entropy difference between the two ompetitive products will be almost the same as the differences between their transition states. Eq. 1.16 can be represented by a familiar version from transition state theory (involving partition functions),[35] but is not required because the fragmentation of the dimers is assumed to proceed without a reverse reaction barrier.[44] This means that the reaction does not have an ordinary transition

state, but rather a very loose one. Under these conditions, the difference in activation energies of the branching processes, $Ea_1 - Ea_2$, becomes numerically equivalent to the difference in the proton affinities of A and B, $\Delta H_1 - \Delta H_2$. The final representation of the standard method is shown below in Eq. 1.17;

$$\ln\left(\frac{AX^+}{BX^+}\right) = \ln\left(\frac{k_1}{k_2}\right) = \left(\frac{\Delta H_2 - \Delta H_1}{RT_{eff}}\right) = \frac{\Delta(\Delta H)}{RT_{eff}} \qquad (1.17)$$

The idea behind the method is that a linear trend results from plotting $\ln(k_1/k_2)$ versus the known ΔH_2, with a slope of $1/RT_{eff}$. From this slope, T_{eff} can be evaluated, and the unknown ΔH_1 can be determined through direct input (of the known ΔH_2 and the obtained T_{eff}) into Eq. 1.17. The method is attractive because it is conceptually simple, yields reproducible results, does not require special instrumentation, and can be used to determine various thermochemical properties such as proton affinities or gas-phase basicities.[48] The criticisms include the fact that the method is only approximate; there is no consistency to the assumption that the entropy of the two competitive pathways is similar and the differences negligible.

A recent example from the scientific literature highlights how approximate structural information was obtained for an amino acid system using aspects of the kinetic method. Cerda and Wesdemiotis in 2000[49] investigated the affinities of alkali metal ions between an amino acid and its corresponding methyl ester by monitoring the dissociation of a heterodimer. Experiments were performed using a modified Micromass AutoSpec tandem mass spectrometer of E_1BE_2 geometry. Alkali metal ion-bound heterodimers of amino acids and their derivatives,

designated as A_1–M^+–A_2 or $[A_1 + A_2]M^+$, were produced by fast-atom bombardment (FAB) with Cs^+ ions accelerated to 12 keV. These precursor ions were mass selected by the first electrostatic sector (E_1) and allowed to dissociate spontaneously in the field-free region between the magnetic sector (B) and the second electrostatic sector (E_2). The fragment ions formed there were mass-analyzed by E_2 and detected.

The kinetic method procedure allows for the evaluation of relative heterodimer dissociation rates as they dissociate into their individually metallated monomers. As mentioned, assuming A_1 and A_2 have closely related structures their entropies of M^+ attachment would be similar ($\Delta(\Delta S°_M) = 0$). The experimentally measured k_1/k_2 ratios would provide a direct measure of the difference of bond enthalpies ($\Delta(\Delta H°_M)$)between the A_1-M^+ and A_2-M^+ bonds. However, the goal here is not to simply determine bond enthalpies but to use such information to infer some degree of structural information.

The authors demonstrated that the M^+ affinity order should adhere to the order of free acid (canonical) < alkyl ester < carboxylate (zwitterion). Their argument is that the alkyl ester of an amino acid is expected to display a higher M^+ affinity than the corresponding free acid due to its better ability for inductive stabilization of the metallated complex. In a similar logic, they argue that an amino acid carrying a negatively charged carboxylate group, as in an amino acid zwitterion, should have a higher M^+ affinity than the ester because of its larger dipole moment. Thus, comparison of the alkali M^+ affinities of an amino acid and its alkyl ester should provide insight into the structure of the corresponding [amino acid + M]$^+$ complex and whether or not the structure is comprised of its zwitterionic or canonical form.

An obvious starting place for such a study was with the arginine amino acid. Previous publications had demonstrated that, while not a zwitterion in the gas phase, the energy levels of its zwitterionic and canonical forms differed by very little. This is in contrast to the simplest amino acid gylcine where the difference between its zwitterion and canonical form is greater than 70 kJ mol^{-1}. Using the kinetic method, the competing dissociations of [Arg + ArgOMe]M^+ indicate that the relative affinities of Arg and ArgOMe depend on the identity of the metal ion. Heterodimers with Li^+ and Na^+ were shown to produce more [ArgOMe]M^+ than [Arg]M^+, while those with K^+ and Cs^+ lead to more abundant [Arg]M^+ than [ArgOMe]M^+.[49] These results directly imply that ArgOMe has a higher Li^+ and Na^+ affinity but a lower K^+ and Cs^+ affinity than Arg. While this may not seem directly useful, given the expected M^+ affinity order outlined above (free acid < methyl ester < zwitterion), the observed trends correlate well to the idea that canonical arginine is favoured in the Li^+ and Na^+ complexes but zwitterionic arginine becomes stabilized for the K^+ and Cs^+ complexes. Such a simple study relays very little absolute structural information, but the inferred implication of arginine's structural preference is very valuable. The main conclusion is that large alkali metal ions can interact simultaneously with both oxygen atoms of a carboxylate, thereby stabilizing the zwitterionic structure. Small alkali metal ions having a high charge density tend to maximize the electron density around them which is best achieved through the electrostatic interactions present with a canonical structure. [49]

Further analysis of amino acid zwitterionic structures and their stabilization is discussed in section 2.4. To conclude this section, results from this study can only be treated qualitatively as it would be impossible to determine whether the structure of arginine in a cationic heterodimer (cationic arginine bound to the methyl ester of arginine) would be the same as that of the ***isolated***, cationic amino acid.[49] This indirect information therefore needs to be expanded

upon and further characterization must be obtained. At the conclusion of this chapter, a variety of approaches used in mass spectrometry for inferring structural information have been discussed. The following chapter will focus solely on the method of IR spectroscopy and its value for absolute characterization of ions in the gas-phase.

1.3 References

(1) Thomson, J. J. *Rays of Positive Electricity and Their Application to Chemical Analysis*; Longmans, Green, & co: London, 1913; Vol. 40.

(2) Watson, J. D.; Crick, F. H. *Nature* **1953**, *171*, 737.

(3) Craig, R. D.; Bateman, R. H.; Green, B. N.; Millington, D. S. *Phil. Trans. R. Soc. A.* **1979**, *293*, 135.

(4) Cooks, R. G.; Hoke, S. H., II; Morand, K. L.; Lammert, S. A. *Int. J. Mass Spectrom. Ion Processes* **1992**, *118-119*, 1.

(5) Domon, B.; Aebersold, R. *Science* **2006**, *312*, 212.

(6) Strupat, K.; Karas, M.; Hillenkamp, F. *Int. J. Mass Spectrom. Ion Processes* **1991**, *72*, 89.

(7) Fenn, J. B.; Mann, M.; Meng, C. K.; Wong, S. F.; Whitehouse, C. M. *Science* **1989**, *246*, 64.

(8) Uy, R.; Wold, F. *Science* **1977**, *198*, 890.

(9) Weber, A. L.; Miller, S. L. *J. Mol. Evol.* **1981**, *17*, 273.

(10) Lu, Y.; Freeland, S. *Genome Biol.* **2006**, *7*, 102.

(11) Gorman, G. S.; Speir, J. P.; Turner, C. A.; Amster, I. J. *J. Am. Chem. Soc.* **1992**, *114*, 3986.

(12) Price, W. D.; Schnier, P. D.; Williams, E. R. *J. Phys. Chem. B* **1997**, *101*, 664.

(13) Rogalewicz, F.; Hoppilliard, Y.; Ohanessian, G. *Int. J. Mass Spectrom.* **2001**, *206*, 45.

(14) Rogalewicz, F.; Louazel, G.; Hoppilliard, Y.; Ohanessian, G. *Int. J. Mass Spectrom.* **2003**, *228*, 779.

(15) Liu, J.; Huang, T.-Y.; McLuckey, S. A. *Anal. Chem.* **2009**, *81*, 1433.

(16) Adams, C. M.; Kjeldsen, F.; Zubarev, R. A.; Budnik, B. A.; Haselmann, K. F. *J. Am. Soc. Mass Spectrom.* **2004**, *15*, 1087.

(17) Breuker, K.; Oh, H.; Lin, C.; Carpenter, B. K.; McLafferty, F. W. *PNAS* **2004**, *101*, 14011.

(18) Zubarev, R. A.; Horn, D. M.; Fridriksson, E. K.; Kelleher, N. L.; Kruger, N. A.; Lewis, M. A.; Carpenter, B. K.; McLafferty, F. W. *Anal. Chem.* **2000**, *72*, 563.

(19) Cooper, H. J.; Hakansson, K.; Marshall, A. G. *Mass Spectrom. Rev.* **2005**, *24*, 201.

(20) Wu, R.; McMahon, T. B. *J. Am. Chem. Soc.* **2008**, *130*, 3065.

(21) Bouchoux, G.; Desaphy, S.; Bourcier, S.; Malosse, C.; Bimbong, R. N. B. *J. Phys. Chem. B* **2008**, *112*, 3410.

(22) Mayer, P. M.; Keister, J. W.; Baer, T.; Evans, M.; Ng, C. Y.; Hsu, C.-W. *J. Phys. Chem. A* **1997**, *101*, 1270.

(23) McLafferty, F. W. *Acc. Chem. Res.* **1980**, *13*, 33.

(24) McLafferty, F. W.; Bente, P. F., III; Kornfeld, R.; Tsai, S.-C.; Howe, I. *J. Am. Chem. Soc.* **1973**, *95*, 2120.

(25) Haddon, W. F.; McLafferty, F. W. *J. Am. Chem. Soc.* **1968**, *90*, 4745.

(26) Dufresne, C. P.; Wood, T. D.; Hendrickson, C. L. *J. Am. Soc. Mass Spectrom.* **1998**, *9*, 1222.

(27) Sleno, L.; Volmer, D. A. *J. Mass Spectrom.* **2004**, *39*, 1091.

(28) Mayer, P. M.; Poon, C. *Mass Spectrom. Rev.* **2009**, *28*, 608.

(29) Aebersold, R.; Goodlet, D. R. *Chem. Rev.* **2001**, *101*, 269.

(30) Biemann, K.; Scoble, H. A. *Science* **1987**, *237*, 992.

(31) Buchmann, W.; Spezia, R.; Tournois, G.; Cartailler, T.; Tortajada, J. *J. Mass Spectrom.* **2007**, *42*, 517.

(32) Brown, P. H.; Beckett, D. *Biochem.* **2005**, *44*, 3112.

(33) Jockusch, R. A.; Lemoff, A. S.; Williams, E. R. *J. Phys. Chem. A* **2001**, *105*, 10929.

(34) Gapeev, A.; Dunbar, R. C. *Int. J. Mass Spectrom.* **2003**, *228*, 825.

(35) McLuckey, S. A.; Cameron, D.; Cooks, R. G. *J. Am. Chem. Soc.* **1981**, *103*, 1313.

(36) Marta, R. A.; McMahon, T. B.; Fridgen, T. D. *J. Phys. Chem. A* **2007**, *111*, 8792.

(37) McMahon, T. B. *NATO ASI Ser., Ser. C* **1999**, *535*, 259.

(38) Nieckarz, R. J.; Atkins, C. G.; McMahon, T. B. *ChemPhysChem* **2008**, *9*, 2816.

(39) Norrman, K.; McMahon, T. B. *J. Am. Chem. Soc.* **1996**, *118*, 2449.

(40) Raspopov, S. A.; McMahon, T. B. *J. Mass Spectrom.* **2005**, *40*, 1536.

(41) Armentrout, P. B. *J. Mass Spectrom.* **1999**, *34*, 74.

(42) Cooks, R. G.; Kruger, T. L. *J. Am. Chem. Soc.* **1977**, *99*, 1279.

(43) Cooks, R. G.; Koskinen, J. T.; Thomas, P. D. *J. Mass Spectrom.* **1999**, *34*, 85.

(44) Wesdemiotis, C. *J. Mass Spectrom.* **2004**, *39*, 998.

(45) Drahos, L.; Vekey, K. *J. Mass Spectrom.* **2003**, *38*, 1025.

(46) Drahos, L.; Vekey, K. *J. Mass Spectrom.* **1999**, *34*, 79.

(47) Cooks, R. G.; Patrick, J. S.; Kotiaho, T.; McLuckey, S. A. *Mass Spectrom. Rev.* **1994**, *13*, 287.

(48) Ervin, K. M. *Chem. Rev.* **2001**, *101*, 391.

(49) Cerda, B. A.; Wesdemiotis, C. *Analyst* **2000**, *125*, 657.

Chapter 2

Experimental and Theory

2.1 Introduction

The purpose of this section is centered on describing a procedure known as infrared multiple photon dissociation (IRMPD), by which direct structural characterization can be achieved. The discussion thus far has been focused on gathering the reader`s attention and directing it to the various techniques using mass spectrometry which enables one to elucidate structural information for gaseous ions. With the field of proteomics growing exponentially, it has been demonstrated in the scientific literature how CID can assist in the identification of protein composition using tandem mass spectrometry.[1,2] Similarly, it has been established in Chapter 1 that techniques relying on obtaining thermochemical data, such as the study of ion-molecule reactions or analysis using Cooks` kinetic method, can infer structural information within a certain degree of reliability. This leaves one remaining structural technique to be investigated; IRMPD spectroscopy. The recently-constructed Fridgen laboratory at Memorial University has the capability of performing this technique, through the coupling of a tunable IR bench-top laser system with a Fourier Transform Mass Spectrometer (FTMS). These instruments are introduced in this chapter, along with other experimental and theoretical aspects.

It may not seem immediately obvious why obtaining a complete three-dimensional structure of a gas-phase ion is necessary. To relieve the reader of this doubt, examples can be cited which highlight the importance of absolute characterization. The first example comes from biochemistry, where the nucleobase uracil, which binds to adenine in the Watson-Crick base pairing,[3] is found in its neutral form as a dioxo tautomer.[4] This is true for both the condensed and gas phases. There is an alternative tautomeric form of uracil, however, which can be formed

upon a proton transfer reaction (Figure 2.1). The foundation for many protein studies is deciphering the formation of point mutations developed during nucleic acid replication.[5] Through understanding the possible tautomers of uracil, it becomes possible to determine whether a different structure is the cause of such a mutation. A second example involves the impact that metal ions have on chemical behaviour inside cells. It is known that heavy metal ions are toxic as they are able to coordinate strongly and compete effectively for binding sites of essential metal ions.[6] Knowing how these metal ions interact with certain amino acids and to what functionalities they bind is integral to comprehending their toxic effects. These two examples merely scratch the surface of the potential knowledge that can be gained from structurally investigating these biological systems.

2.2 Experimental

Any study of gas-phase systems whereby dissociation is initiated from the absorption of radiation can be categorized broadly as photodissociation. Such studies tend to be straight-forward in terms of experimental requirements. Gas-phase ions are prepared by some form of ionization, isolated and stored in an ion trapping device, and dissociated after interacting with the supplied radiation. The dissociated fragments then provide chemical information inherent to the system. The only difference between typical photodissociation experiments and IRMPD spectroscopy is that the radiation source must be tunable. This feature will be highlighted in section 2.2.2.2.

As interest in the Fridgen group often has a connection to biologically-relevant systems, the preparation of ions is achieved using electrospray ionization. Solution flow rates range

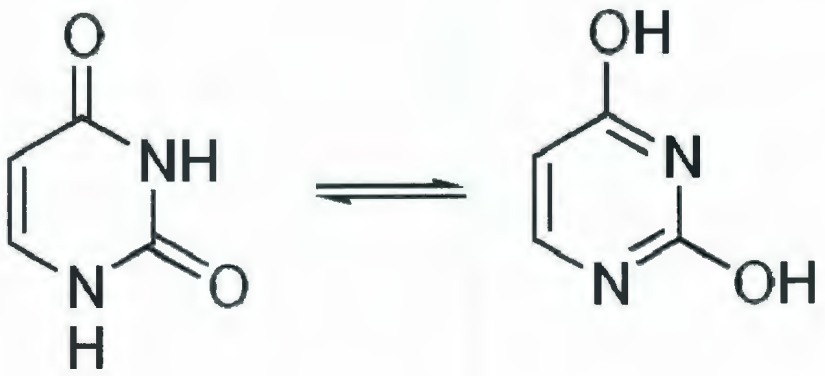

Figure 2.1 – Tautomerization of uracil

from 50 to 150 μl hr^{-1}. Once the ions have been created, they are focused and guided through the instrument using a series of ion optics into the ICR cell. In this transfer region there is an option of mass-selection via a quadrupole trap. The main region of mass-selection occurs within the ICR cell which also functions as its own detector and is discussed further in section 2.2.1. The cell sits inside a 7 Tesla superconducting-magnet and is famous for its ability to store trapped ions for long periods of time. This described instrumentation was commercially obtained and is known as a Bruker Apex® Qe 70 FTMS. See Figure 2.2 for a picture of the instrument and Figure 2.3 for a more in-depth schematic.

2.2.1 Fourier Transform Ion Cyclotron Resonance Mass Spectrometry (FTMS)

The theory of ion cyclotron resonance is based on the well-known motion of an ion when subjected to a magnetic field. If the magnetic field is static and uniform, an ion will perpetuate in a circular motion due to the Lorentz force, as shown in Figure 2.4.[7] This is known as cyclotron motion. It can be shown that the physics of this motion can be used for measuring the mass of the ion upon introduction into a mass spectrometer. This is because the angular frequency (ω) of cyclotron motion is a function of magnetic field strength, elementary charge, the number of charges on the ion, and the mass of the ion as shown in Eq. 2.1.

$$\omega = \frac{zeB}{m} \tag{2.1}$$

Figure 2.2 – Bruker Apex® Qe 70 FTMS as located at Memorial University.

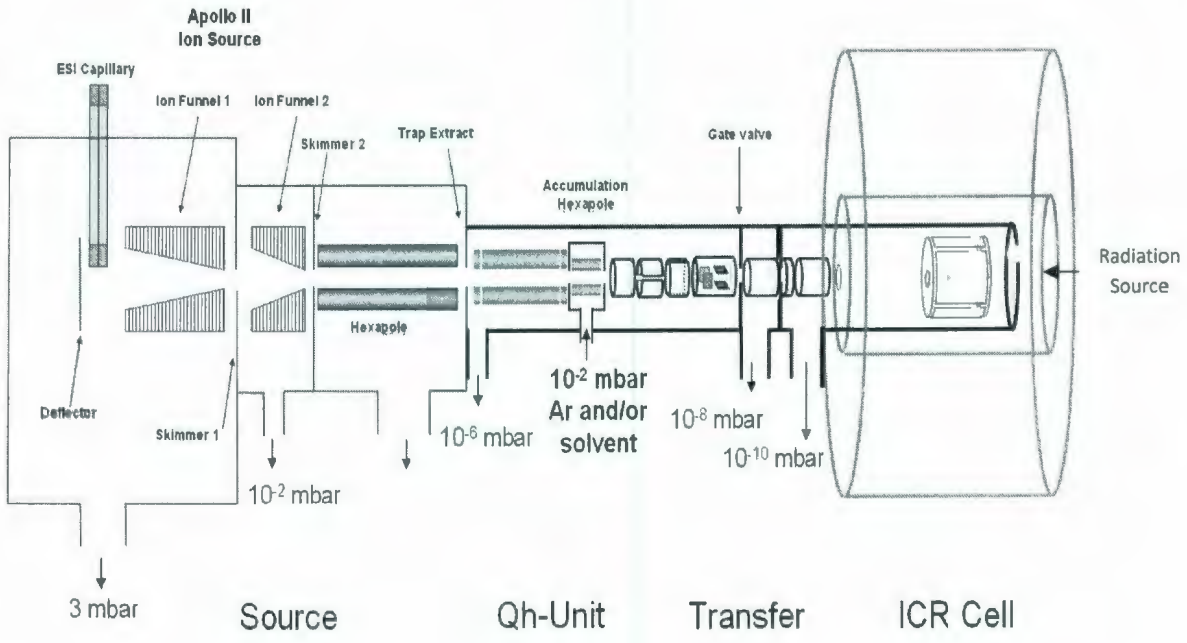

Figure 2.3 - Schematic showing the source, Q_h region, ion transfer optics, ICR cell and radiation entrance.

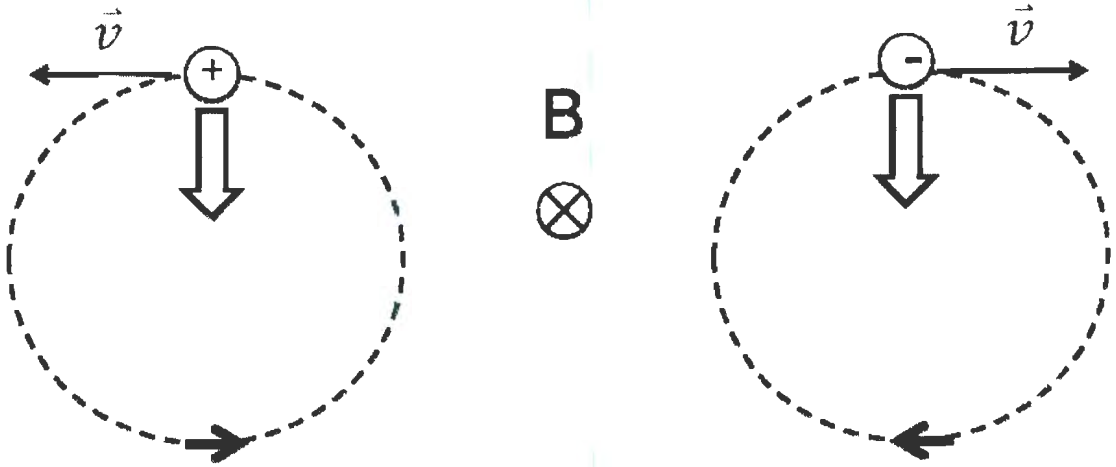

Figure 2.4 – Motion of ions when subjected to a magnetic field (directed into the plane of the page).

The significant conclusion obtained from this equation is that any ion of a given mass-to-charge ratio will have the same cyclotron frequency (which is independent of their velocity). This highlights the benefit which separates ICR mass-selection from other mass-analyzing theories in mass spectrometry; no additional translational energy focusing is required.[7]

Figure 2.5 is a picture of the ICR cell, also known as a "Penning trap". The Penning trap at Memorial University has a six centimetre diameter and is composed of trapping plates, excitation plates, and detecting plates. A static magnetic field applied in the z-direction confines ions only in the x- and y-directions. To prevent ions from escaping in the z-direction, a small potential (approximately 1 volt) is applied to each of the trapping plate electrodes. The ICR cell is able to store charged particles in three-dimensions for prolonged periods using a strong axial magnetic field and a direct current potential, respectively.

The major difference of FTMS from other mass spectrometry techniques is that the ions are not detected through secondary means such as measuring an electron cascade produced from an electron multiplier when an ion strikes it. Instead, the motion of the ions is detected directly. A detection event occurs after a packet of trapped ions traveling in its intrinsic cyclotron pathway becomes accelerated to a larger radius through an excitation waveform. Given that the dimensions of the cell are fixed, this radius can only be increased by a finite amount. The approach of the ion packet towards the detection plates creates an oscillating image charge which is actually detected as an image current. The resulting time-domain signal is called a free induction decay (FID) or a transient, and consists of superimposed sine waves. Each individual sine wave is representative of a particular ion packet, or more specifically, an exact *m/z*. The frequency-domain spectrum is converted to a mass domain spectrum and is extracted

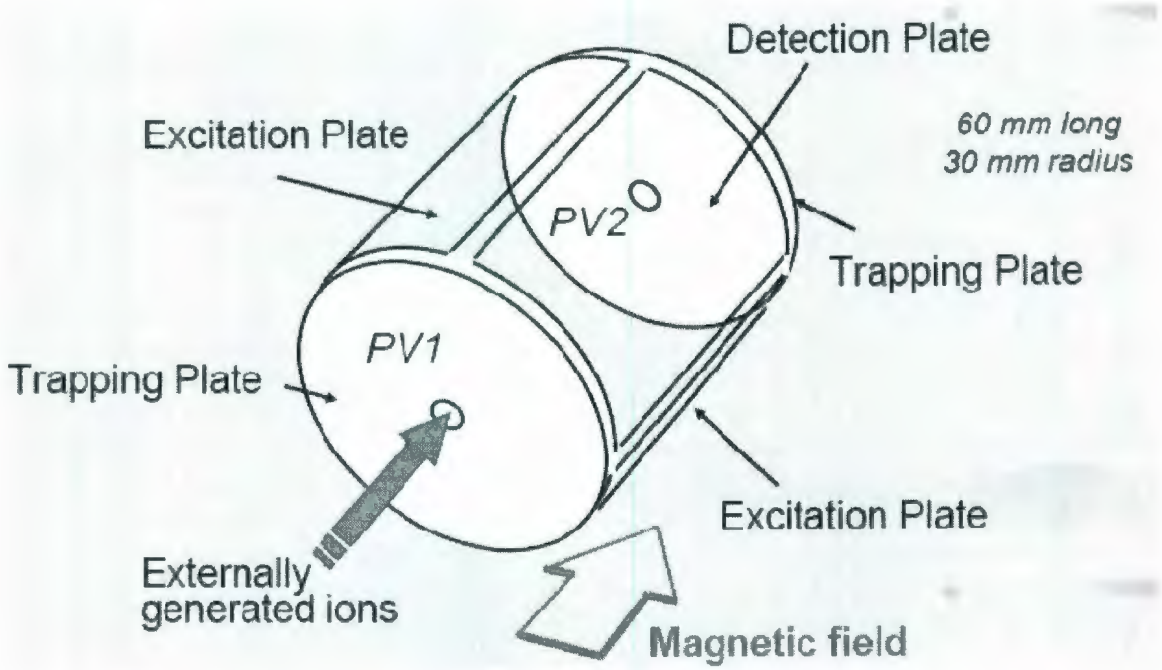

Figure 2.5 – Cylindrical ICR cell composed of trapping, excitation & detection plates.

from this raw data by performing a Fourier transform (Figure 2.6). Additionally, the masses are not resolved in space or time as with other tandem techniques but only in frequency. The different ion packets are therefore not detected in different places or at different times but all ions are detected simultaneously over a defined period of time.[8]

The preceding paragraph explains the procedure of ion detection using an ICR cell. The route through which all ion packets are detected simultaneously through mass-selection may not be clear. For the ICR cell to function as a tandem mass spectrometer, the elimination of unwanted ions must be accomplished. By irradiating the ions with a specific radio frequency (rf) across the excitation plates, it is possible to excite a certain packet of ions having a defined *m/z*, without affecting the other ions. One can, then, eject a particular *m/z* from the ICR cell.[7] On the other hand, one could irradiate the ICR cell with a sweep of all radio frequency values across the excitation plates excluding one which would correspond to a single *m/z*. By irradiating all ions except one, it is possible to isolate a specific *m/z*. Re-arranging Eq. 2.1 above, we see that the frequency of the applied potential excitation waveform (f) will dictate which specific *m/z* ion packet will be in resonance at a given time, as demonstrated by Eq. 2.2. Selectivity of ion removal is therefore attainable.

$$\frac{m}{z} = \frac{eB}{2\pi f} \tag{2.2}$$

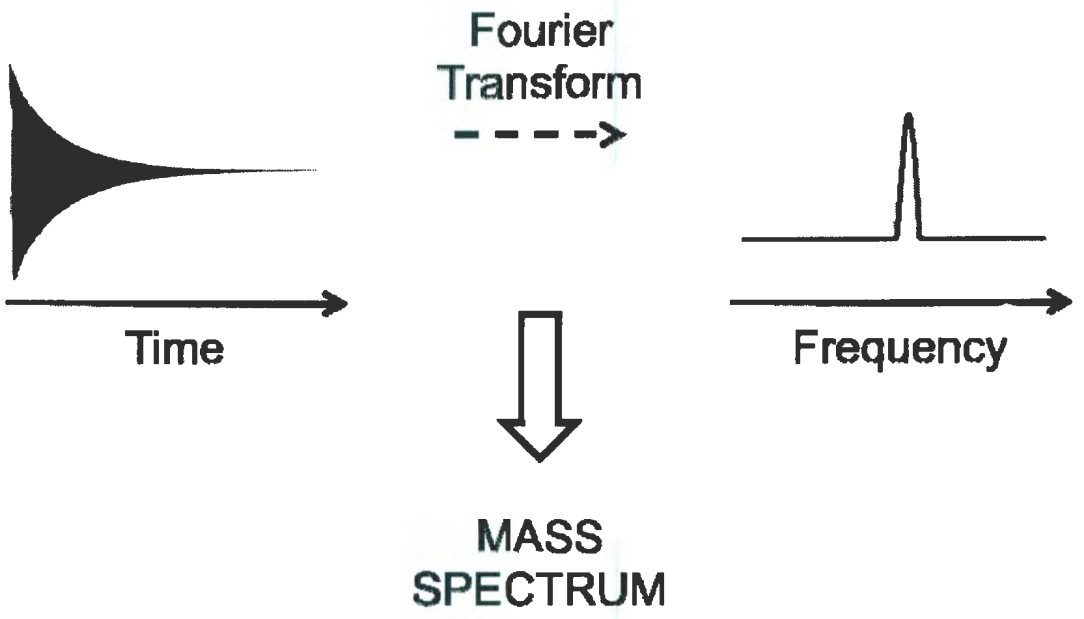

Figure 2.6 – Initial time-domain spectrum becomes Fourier transformed into the more useful frequency-domain. This can then be depicted as a m/z mass spectrum.

Fourier transform ion cyclotron resonance mass spectrometry provides very high resolution (in excess of 10^6) enabling masses of ions to be resolved with great accuracy.[9] Its uses are widespread, from evaluating compositions of large proteins to examining isotopic distributions to assist in complex mixture analysis. An FT-ICR permits the storage of mass-selected ions in a collision-free environment for up to several minutes, hours, or days and is sufficiently adaptable to allow the introduction of a radiation source to induce dissociation (via collision gas, electron capture, laser beam, etc.).[10]

2.2.2 Infrared Multiple Photon Dissociation (IRMPD)

Chapter 1 demonstrated key techniques that have been utilized by mass spectrometrists to deduce structural information of gaseous ions. The information obtained from such studies is extremely influential in our understanding of ion structure and the techniques will likely remain to have a role in future determinations. However, as suggested previously, the implementation of IR spectroscopy as an approach to investigate gas phase ion structures has become the preferred means of such studies. The Fridgen laboratory at Memorial University has the capability of performing this technique using an FTMS, and now that ion isolation with an ICR cell has been discussed, IRMPD can be thoroughly investigated. The following will be an in-depth analysis of this approach, covering its history, mechanism, and improvements over the past few decades.

2.2.2.1 Historical Development of IRMPD

Traditional (or 'normal') infrared spectroscopy is an efficient probe of molecular species. As suggested by the name, the procedure is dependent on the interaction of a molecule with an impinging form of infrared radiation. By measuring the attenuation of the radiation as it is absorbed by the sample, direct information is relayed on the vibrational modes present within the molecule, which can include CO, NH, and OH oscillators. However, can this traditional infrared spectroscopy be directly applied to ionic systems in the gas-phase? The shc ·t answer is no, not very effectively. The main limitation for using traditional IR spectroscopy on gaseous ions is the necessity to trap and store the molecular ions of interest. The mass-analyzers capable of this requirement, Paul and Penning traps (quadrupole ion trap and ICR cell, respectively), can sufficiently isolate ions so that they can interact with a radiation source for extended lapses. The deficiency arises from knowing the fact that there is an extremely low ion density since the normal IR attenuation approach is very insensitive.[11] A different approach to performing IR spectroscopy on trapped ions was introduced and is labeled "consequence spectroscopy". This name comes from the notion that it is not the attenuation of radiation that is bein~ measured but the consequence of photon absorption on the mass spectrum. The absorption of IR photons that are resonant with a vibrational mode will cause an increase in the internal energy for the ions of interest and, depending on the energy of the impinging radiation, dissociation may occur. Given the high sensitivity of mass spectrometry, the dissociation products and the depletion of the parent ion can be accurately detected. It has been shown that in the gas-phase, such a multiple photon absorption approach can be applied and yield structural information in a comparable way to the more traditional one-photon IR absorption. This technique has been therefore been called infrared multiple-photon dissociation, or IRMPD spectroscopy. Historically,

the 'consequence' modification to the field of IR spectroscopy has been credited to being instituted by Y.T. Lee and co-workers.[12]

Another difference which separates traditional IR spectroscopy from the gas-phase IRMPD approach is the source of radiation. Given that IRMPD is a multiple photon process, a more intense source is required. In its earliest of implementations, instrumentation performing IRMPD were fitted with continuous-wave carbon dioxide (CO_2) lasers exclusively, as they were the only available IR-option with sufficient intensity to dissociate an observable number of ions.[13] Unfortunately, these lasers have a limited and discontinuous tuning range. As we will see in section 2.2.2.2, newly developed radiation technologies have vastly improved the range and the quality of IRMPD spectra.

2.2.2.2 Radiation Sources and Spectral Analysis in IRMPD

Interest in having the capability to perform IRMPD in a research environment has grown tremendously over the past few decades. Given that CO_2 lasers were inadequate due to their limited tuning range,[14] an advanced alternative was heavily desired. The experimental revolution which followed coincided with the advent of free-electron lasers (FELs). FELs are based on the radiation generated by accelerated relativistic electrons.[15] Relativistic electron bunches of many MeV are created, commonly using linear accelerators. These bunches are attenuated and injected into a periodic magnetic field device, called an undulator, which induces a "wiggling" (or, angular acceleration) motion as a result of the Lorentz force.[15] This wiggling generates the radiation upon which the laser is based. As IRMPD requires radiation tunability, a means of

determining and ultimately controlling the wavelength is required. This is done by resolving the energy of the electons and varying the magnetic field strength of the undulator.[16]

There are two major facilities which house the instrumentation to perform IRMPD with an FEL. These facilities are referred to as FELIX, located at the FOM-Institute for Plasma Physics Rijnhuizen in Nieuwegein, Netherlands[17] and the "Centre Laser Infrarouge Orsay" (CLIO) facility in Orsay, France.[18] The CLIO FEL delivers electron kinetic energies in the 10–50 MeV range. The accessible wavelength range goes from 3 to 120 μm and has a high peak power well suited for IRMPD studies.[19] The "actual" usable wavelength range for IRMPD is limited to the fingerprint region, which is defined as mid-IR and ~500-2000 cm^{-1}.

Some of the first IRMPD experiments employing a FEL were performed on polyaromatic hydrocarbon cations of astrophysical interest that were stored in a Paul trap.[20] Although it is possible to couple a FEL to either a Paul or Penning trap, the most common arrangement at the CLIO facility is to couple it with the Penning. In this arrangement which has been described previously,[21] the IR laser beam is focused in the middle of the ICR cell. Although the beam's dimension in the middle of the cell is smaller than the ion cloud, when irradiating ions for more than one second photofragmentation ratios as high as 80% can be observed which safely indicates that most ions eventually interact with laser. The irradiation time is controlled by a fast electromechanical shutter synchronized with the FEL.[19]

The Instrumentation required for operation of such a laser is large enough to occupy a building. Although the mating of the FEL with ion trapping devices has created the ability to perform IRMPD effectively, cost and space issues arise for an individual researcher attempting to set-up in their own lab. The previously mentioned FEL centers very graciously allow for booking

of their laser time, but more-feasible alternatives were actively sought by the research community. With the demand came yet another revolution in the field of laser application, this time coinciding with the performance of tunable IR bench-top laser systems. The bench-top arrangements that have been recently utilized as cost-effective FEL alternatives are based on the theories of optical parametric oscillation and amplification (OPO/OPA).[11,14,22] Such bench-top systems are capable of producing radiation in the mid -IR (2500–4000 cm^{-1}) and newer modifications are enabling such systems to extend into the fingerprint region. However, while it may appear that a bench-top apparatus is capable of scanning the same IR regions as an FEL, it cannot replicate its functionality. Bench-top systems are far less intense and therefore unable to induce dissociation in stronger systems. It is not a matter of replacing the costly FEL with these bench-top alternatives, but more so a case of effectively obtaining conclusive structural information that may or may not be enhanced by complementary data that could be obtained with an FEL. As will be demonstrated in Chapter 4, it is possible to make structural conclusions based solely on IRMPD using a bench-top laser in the mid-IR range.

The actual operation of the bench-top laser system, as installed at Memorial University, will now be briefly discussed. All bench-top laser methods are based on some form of optical parametric generation (OPG). The fundamentals of OPGs were initially laid out in 1962[23], with the first operational OPO demonstration dating back to 1965.[24] Although it appears as if the technology has existed for a while, early usage of these methods was not satisfactory due to the unavailability of suitable nonlinear optical materials and poor beam characteristics. The alternative approach of using dye lasers soon became the commercial standard. It is only recently that OPOs have become prevalent again, as solid-state materials (acting as nonlinear crystals) having good optical properties and high damage threshold have become more

accessible.[25]

OPG methods are founded on a nonlinear optical procedure that involves the energy conversion of a fixed frequency initial laser wave ω_p (called the pump beam) into two lower energy beams, the signal beam at ω_s and the idler beam at ω_i.[26] These two new photons are formed concurrently via the process of stimulated emission.[25] In practice, an OPO is composed of a nonlinear solid-state crystal that is placed within an optical resonator which serves to resonate with at least one of the signal or idler waves. There is much more optic theory behind the operation of the OPO,[25] but it is unnecessary for the purpose of this thesis. Continuing the discussion with real experimental parameters, to produce tunable IR radiation in the 1.5 to 3.2 μm range, the fundamental 1064 nm line from a Q-switched Nd:YAG pumps a $KTiOPO_4$ (KTP) crystal. The pump radiation can also be directed to a $LiNbO_3$ crystal which is tunable from 2.5 to 4.3 μm.[11] The radiation is directed through a BaF_2 window to the center of the ICR cell where it interacts with the ionic species of interest. The optics table containing the laser, as well as the entire path of IR radiation to the ICR cell, is purged with dry air and N_2 to eliminate the absorption of the laser by water vapor.[11]

Dissociation products are monitored as a function of the incoming radiation wavelength.[14] The IRMPD efficiency is defined in Eq. 2.3. Plotting the IRMPD efficiency as a function of wavelength produces an IRMPD "consequence" spectrum.

$$IRMPD\ efficiency = -\log\left(\frac{I_{parent}}{I_{parent} + \sum i\ I_{fragment(i)}}\right) \qquad (2.3)$$

Any invested internal energy will be entirely utilized for the dissociation of products, so this equation requires that all accessible dissociation pathways during the IRMPD process be accounted for. The given system and the input energy make it possible to observe competition for accessing a particular dissociation pathway. Fridgen et al. in their 2006 study on alcohol proton-bound dimers[27] observed two dissociation routes for all systems; formation of an S_N2 intermediate leading to elimination of water, and a simple loss of the neutral alcohol. It was shown that the branching ratio of these routes was dependent upon the wavelength of the initial radiation. Furthermore, Fridgen demonstrated that a strong IR absorption favoured the simple loss of a neutral alcohol from the dimer, while a weaker IR absorption favoured the opposite channel. The barrier for the S_N2 water loss is lower than that of the simple alcohol route loss. However, when the vibrational mode activation is strong, extra photons are quickly absorbed which accounts for the kinetic difference.[11]

Another interesting point to mention about IRMPD spectra, which is also observed in traditional IR spectroscopy, is the effect noncovalent interactions have on the expected band positions for certain absorptions. It is well-known that for biological systems involving hydrogen bonds (H-bond), the stretching vibrations of N-H or O-H groups that are the H-bonding donor exhibit a strong red-shift (shift to lower energy) accompanied by a broadening of the band.[28] Placing significant meaning on the absolute intensity of the band is much more difficult to do, as a variety of factors influence the contribution. Bush et al. list some of these parameters, including the absorption cross section at a given wavelength, the energy distribution across internal modes of the precursor ion, and the magnitude of the lowest dissociation channel. [29] If the magnitude of this latter parameter is large, a kinetic effect in the IRMPD process can be

induced whereby the spectrum is diminished if the time scale of the experiment is not long enough to access the channel.

2.2.2.3 IRMPD Mechanism

The mechanism of IRMPD has been well described in the scientific literature[30] and, due to its relevance to the subject of this thesis, features will be reiterated here. The physical nature involves the sequential absorption of photons by trapped ions, which causes an increase in the internal energy of the ions until they dissociate through the lowest energy channel.

This absorption of a photon occurs when it is in resonance with a vibrational transition from the v=0 to the v=1 state. As mentioned, IRMPD is not a single-photon process so how and why do multiple photons become necessary? Due to anharmonicity, the v=0 to the v=1 transition is no longer resonant with the incoming radiation after the first absorption. However, if there is sufficient anharmonic coupling between the mode that is absorbing and other modes in the ion, a rapid process (10^{-12} s) known as intramolecular vibrational energy redistribution (IVR) occurs. This process acts to statistically remove the energy present in the v=1 populated states to all other vibrational degrees of freedom, such that resonance between the radiation source and the v=0 to the v=1 transition is restored.[11,22] This allows the absorption of the second photon, and the IVR cycle repeats itself until the population of high energy states is so high that ion dissociation results when sufficient energy is put into this bath of vibrational levels ('quasi-continuum' regime). The number of photons this requires could be anywhere from one to a hundred[31], depending on the energy of the irradiating photons and the dissociation energy of the ion. Experimentally speaking, the dissociation can then be monitored as the population of

the dissociation channel fragment increases while that of the precursor decreases. Figure 2.7 presents a generic representation of the IRMPD mechanism.

2.2.2.4 Advantages/Disadvantages of IRMPD Spectroscopy

It is important to recap the advantages and disadvantages of the IRMPD technique to fully appreciate its value. It is also important to note a subtle discrepancy that may exist in practice with applications of IRMPD. In the Fridgen group, IRMPD is used as a spectr scopic tool to produce IR-like spectra with the purpose of elucidating structural information. The most obvious advantage of IRMPD as a spectroscopic tool is the unparalleled structural characterization which it provides when coupled with theoretical calculations. Chapters 3 and 4 serve to provide more evidence for this claim. A less obvious advantage involves the fundamental insight gained after a structural characterization is complete. For example, with any given system it is possible to examine and separate the effects of individual interactions that are caused through the addition of a water molecule, a metal cation, or another solvent.[32] Separating such effects allows for the deduction of the relative contribution of each.

The IRMPD disadvantages arise from the intrinsic effects that are difficult to avoid, and attempts can only be made to account for these complications. The first expected disadvantage is the difficulty in correcting for anharmonicity. The presence of anharmonicity causes peaks to be shifted and broadened in an undesirable fashion, making peak assignment difficult.[33,34] Other disadvantages are specific to the system being studied. A strongly-bound ion-complex will not efficiently undergo the IRMPD process, while a system lacking anharmonic mode coupling may

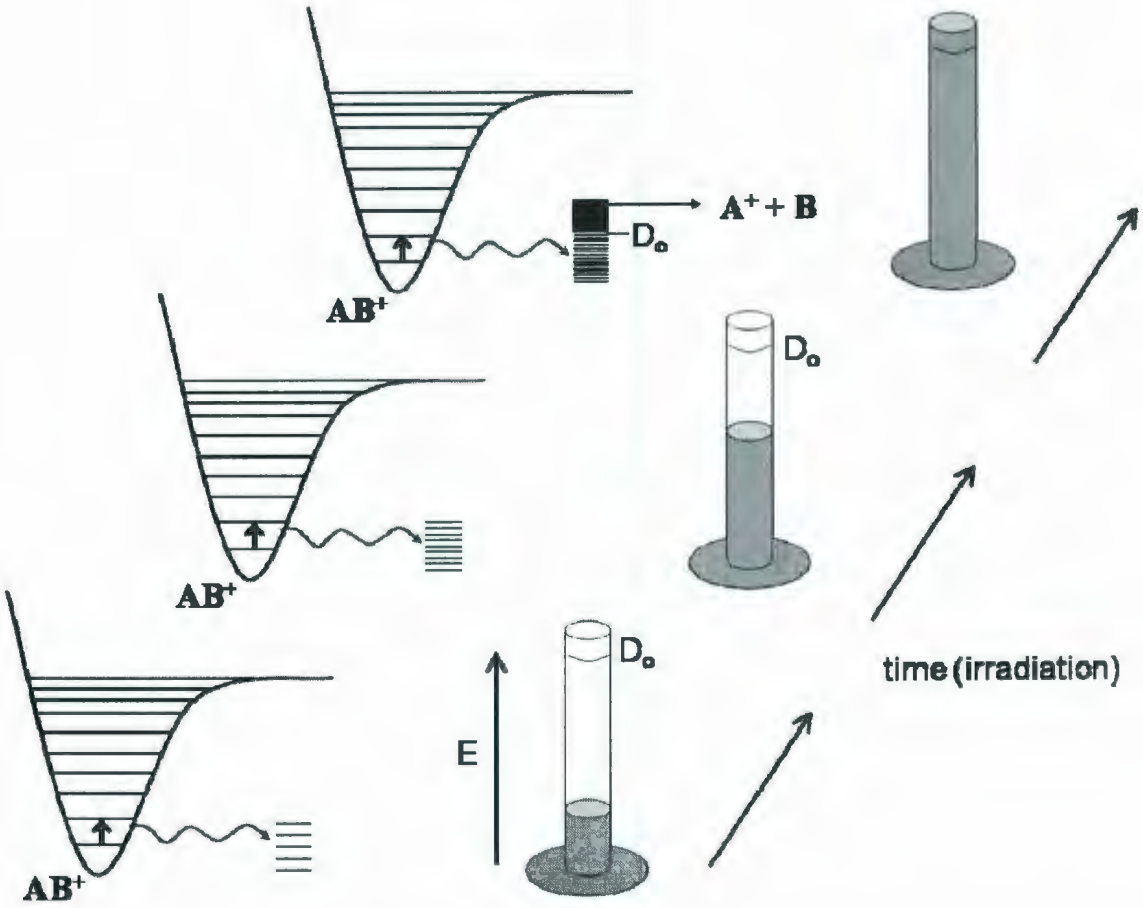

Figure 2.7 – IRMPD Mechanism. Photon absorption is followed by IVR allowing subsequent absorptions. D_o represents the ground state dissociation energy. Reproduced with permission from Dr. Travis Fridgen.

not undergo good IVR. These disadvantages are handled accordingly when they arise experimentally.

2.3 Theoretical Calculations

After receiving mention earlier in Chapter 1, the following section will introduce some background information on theoretical calculations and demonstrate how integral they are to making justifiable structural conclusions for ions in the gas phase.

To start this discussion, the reader must be made aware that software is commercially available which enables the modeling and prediction of lowest-energy structures for inputted systems. The software utilized by the Fridgen group at Memorial University is part of the Gaussian 03 suite.[35] This tool makes it possible to accurately compute electronic energies, vibrational frequencies, thermochemical quantities, and optimized equilibrium geometries for any small molecular system of interest. The theoretical methods involved in obtaining these computed values will be evaluated further. It is important to note that this theoretical approach has been previously demonstrated to be effective when studying amino acid systems.[36-39] Therefore, it has become the accepted standard for many research groups.

The initial phase in the theoretical approach, as adopted by the Fridgen group, is to analyze a vast quantity of 'initial guess' geometries using the structural optimization parameter. This operation functions to minimize a system's total energy after successive alterations to the input geometry. After analyzing an appropriate variety of initial geometries, a small library is created containing plausible arrangements for any structural features present within the system.

All structures included in the library are optimized to be real minima on the system's potential energy surface. This is verified through inspection of the calculated vibrational frequencies; the lack of an imaginary frequency indicates that the optimized structure is indeed a minimum. The structures are then ordered with respect to their energies, and therefore insight is gained into the features which inherently provide stabilization to the system. An important feature most often modeled effectively using a theoretical approach is that of hydrogen bonding. As will be shown later in Chapters 3 and 4, the stability of amino acid systems is often defined by the extent to which they undergo H-bonding.

The bulk of background theory describing the principles of theoretical calculations is beyond the scope of this thesis. However, it is important to recognize that when determining what theoretical method to use for a given system, one must compromise between computational speed and theoretical accuracy. This involves investigating the size of the system and determining the computational capacity that would be required when using a certain level of theory. As the size of the system increases, time and resources increase rapidly and become a restricting factor. Likewise, different theoretical methods vary from being largely approximate to very accurate. Common theories considered include the semi-empirical method, density functional theory (DFT), and *ab initio* methods. For modeling systems containing amino acids, it has been documented that the hybrid-functional of Becke, Lee, Yang and Parr (B3LYP)[40,41] is the best-suited compromise between speed and accuracy. In all systems studied throughout this thesis, the geometry optimization and vibrational frequency calculation were performed at the B3LYP level of theory utilizing a 6-31+G(d,p) basis set. Thermochemical data such as enthalpy and entropy were also obtained from this calculation, which will be highlighted later.

The choice of basis set can greatly affect the accuracy of a calculation. While 6-31+G(d,p) is not the most expansive basis set available, it has been consistently shown to provide reliable results in comparison to other alternatives. In particular, this basis set is designated as a split-valence double-zeta set. The numbers 6-31 are weighted to specify the quantity of primitive Gaussian functions which are used, as a linear combination, to approximate each atom's atomic orbital for its core and valence electrons. To enhance such approximations, additions to basis sets are frequently specified. The first common addition is the insertion of diffuse functions, denoted by either + or ++. These functions provide excess flexibility and allow weakly-bound electrons to localize at an appreciable distance from the bulk of the electron cloud density. For this reason, such an addition is typically desired for anionic systems. The single plus augments diffuse functions for heavy atoms, while the double plus includes diffuse functions on lighter atoms, such as hydrogen and helium. The second common addition is the insertion of polarization functions, denoted by specifying the number of added functions in brackets. Such functions account for asymmetric electron cloud distribution created with the presence of electronegative heteroatoms. For amino acid systems, using both of these additions simultaneously improves the approximation of atomic orbitals.

The second phase of the theoretical approach, as adopted by the Fridgen group, is introduced to account for a big inadequacy inherent to DFT theory: the accuracy of its electronic energy calculation. Electronic energy is the largest contributor to enthalpy as derived from thermodynamics. To determine enthalpy theoretically, a combination of the following quantities must be achieved:

$$\Delta H_{theoretical} = (Thermal\ Correction + E_{elec}) \quad (2.4)$$

where the thermal correction to enthalpy value is represented as follows:

$$Thermal\ Correction = \Delta ZPE + E_{vib} + E_{rot} + E_{trans} + RT \quad (2.5)$$

It is shown that the determination of enthalpy takes into account the zero-point energy (ZPE), as well as the energetic contributions from the other internal energy components. Since electronic energy has the largest magnitude of these terms, it would be beneficial to calculate it as accurate as possible. DFT energies for biological systems are often inaccurate due to the presence of H-bonding. Single-point energy calculations using a more intensive *ab initio* method are therefore utilized to obtain reliable electronic energies. The level of theory chosen is Møller-Plesset second order perturbation (MP2), since it has the ability to more accurately predict eletron correlation for H-bonding systems. Instead of using the same basis set as before, a more expansive triple-zeta set of 6-311++G(2d,2p) was implemented for these single-point calculations. Such a calculation approach has been successful because DFT can efficiently optimize geometries, but where it falls behind in energetic determinations, MP2 solutions reduce the undesired error inherent to the DFT method. More importantly, this combined approach reduces the computational cost (as MP2 optimizations would be very computationally demanding) and maximizes the accuracy output.

What is important to extract from this discussion on theoretical calculations, at least for highlighting their relevance towards IRMPD spectroscopy, is that lowest-energy structures can be determined and their vibrational frequencies obtained. As a result, it becomes possible to create a so-called "theoretical IR spectrum" which is compared with the experimentally-obtained gas-phase IR spectrum. Through comparison of these spectra, the presence (or absence!) of certain absorptions can clearly characterize the structure of the isolated ion. For argument's sake, opponents of this procedure may insinuate that intensities in the theoretical spectra are based on one-photon absorption while experimental spectra are produced from multiple photons. The effect this has on the success of comparison has been shown to be negligible.[42] There are also arguments that state anharmonicity intrinsic to a system should be accounted for, since calculations are done using the harmonic approximation. This issue can be addressed by applying a certain uniform scaling factor to the computed IR frequencies to account for anharmonic errors. The magnitude of the scaling factor depends on the IR range being studied, the level of theory and basis set being used, and the type of system being evaluated.[43,44]

The extraction of thermochemical data from the initial calculation is an important piece of the puzzle. The energetic information obtained acts as a forceful compliment t structural peak assignments based on spectral comparisons. Using enthalpy and entropy values to obtain calculated free energy values provides insight into the contribution made by each optimized geometry toward the overall ion population at a given temperature.

While it may not be clear how the theoretical approach functions to model atomic orbitals, the theory describing such information is not necessary. Conversely, it should be made

clear that the prescribed approach is chosen such that the computational speed and accuracy of studying amino acids is optimized. The method shows success with amino acids because they are relatively small, have low molecular weights and are organic systems comprised of merely C, H, N and possibly S. When studying amino acid systems containing large metal ions (as in Chapter 4), slight adjustments to the theoretical method must be made. Since metal ions are heavy atoms and can have many electrons, the introduction of pseudopotentials is necessary. The introduction of more electrons means there is more energy associated with electron correlation. These potentials function to represent the relativistic inner-electron core of a large metal ion and reduce the actual computational load of the process to modeling its valence electrons.

2.4 Prevalent Applications in Scientific Publications

To conclude this chapter which has discussed both the experimental and theoretical approaches for IRMPD spectroscopy, it seems pertinent to bring light to current research which has actively been using the technique in a successful manner. There has been tremendous interest for studying amino acid systems using IRMPD as such investigations provide a wealth of data for useful interpretation. Knowing that individual interactions can be isolated and then separated to determine the effect of the contribution, various groups have examined these acids interacting with protons, metal ions, and water molecules, among others. An extremely popular avenue that has been studied via all means of mass spectrometry is the determination of an amino acids gas-phase structural form and whether it is present in its canonical structure or as a zwitterion (contains a positive and a negative charge). This debate has waged onward, fueled by the fact that all natural amino acids are zwitterions when in the condensed phase but yet are

canonical when represented in the gas-phase. The implication of this result, as suggested in the introduction, is that the pathway to `bridging-the-gap` for amino acids could lie in devising an approach through which the energetic favouring of this zwitterion form would efficiently model *in vivo* systems.

Many examples could be described to highlight this idea. One of the most intriguing ones involves the study of arginine and the approaches researchers have tried to induce the formation of its zwitterion. The interaction of this amino acid with alkali metal ions was discussed earlier in section 1.2.3.2 via Cooks' kinetic method. Bush et al.[29] provided results using IRMPD spectroscopy that agreed with the conclusions presented in the kinetic study. Their work demonstrated that as the metal ion size increased, the zwitterion form became increasingly favoured until eventually the canonical-to-zwitterion transition occurred between lithium and sodium. Although both forms of arginine were observed for the sodiated species, it was observed that the zwitterion form was predominant. Approaches to obtain the same type of transition have been done by other groups, such as by Paizs and Oomens who examined clusters of tyrosine complexed with up to six water molecules.[45] They found that the neutral form of tyrosine is always lower in energy than the zwitterions, but that with each subsequent addition the energy difference between the two forms decreased. This is quite a revealing piece of information as the concept of microsolvation demonstrates that solution-phase characteristics can be mimicked in the gas-phase.

The discussion of examples similar to those mentioned above could continue endlessly. At this point, it is simply relevant for the reader to grasp a sense of the value provided by researching and characterizing amino acid systems using IRMPD. The remainder of this thesis

will present pertinent research that has been performed in the Fridgen laboratory over the course of this degree.

2.5 References

(1) Liu, J.; Huang, T.-Y.; McLuckey, S. A. *Anal. Chem.* **2009**, *81*, 1433.

(2) Benesch, J. L. P. *J. Am. Soc. Mass Spectrom.* **2009**, *20*, 341.

(3) Watson, J. D.; Crick, F. H. *Nature* **1953**, *171*, 737.

(4) Salpin, J.-Y.; Guillaumont, S.; Tortajada, J.; MacAleese, L.; Lemaire, J.; Maitre, P. *ChemPhysChem* **2007**, *8*, 2235.

(5) Topal, M. D.; Fresco, J. R. *Nature* **1976**, *263*, 285.

(6) Belcastro, M.; Marino, T.; Russo, N.; Toscano, M. *J. Mass Spectrom.* **2005**, *40*, 300.

(7) Marshall, A. G.; Hendrickson, C. L. *Mass Spectrom. Rev.* **1998**, *17*, 1.

(8) Marshall, A. G.; Hendrickson, C. L. *Int. J. Mass Spectrom.* **2002**, *215*, 59.

(9) Marshall, A. G. *Int. J. Mass Spectrom.* **2000**, *200*, 331.

(10) Fukui, K.; Takada, Y.; Sumiyoshi, T.; Imai, T.; Takahashi, K. *J. Phys. Chem. B* **2006**, *110*, 16111.

(11) Fridgen, T. D. *Mass Spectrom. Rev.* **2009**, *28*, 586.

(12) Okumura, M.; Yeh, L. I.; Lee, Y. T. *J. Chem. Phys.* **1985**, *83*, 3705.

(13) Woodin, R. L.; Bomse, D. S.; Beauchamp, J. L. *J. Am. Chem. Soc.* **1978**, *100*, 3248.

(14) Eyler, J. R. *Mass Spectrom. Rev.* **2009**, *28*, 448.

(15) Colson, W. B.; Johnson, E. D.; Kelly, M. J.; Schwettman, H. A. *Phys.Today* **2002**, *55*, 35.

(16) Fridgen, T. D.; MacAleese, L.; Maitre, P.; McMahon, T. B.; Boissel, P.; Lemaire, J. *Phys. Chem. Chem. Phys.* **2005**, *7*, 2747.

(17) Ding, Y.; Krogh-Jespersen, K. *J. Comput. Chem.* **1996**, *17*, 338.

(18) Prazeres, R.; Glotin, F.; Insa, C.; Jaroszynski, D. A.; Ortega, J. M. *Eur. Phys. J. D.* **1998**, *3*, 87.

(19) Balaj, O.-P.; Kapota, C.; Lemaire, J.; Ohanessian, G. *Int. J. Mass Spectrom.* **2008**, *269*, 196.

(20) Oomens, J.; van Roij, A. J. A.; Meijer, G.; von Helden, G. *Astrophys. J.* **2000**, *542*, 404.

(21) Maitre, P.; Le Caer, S.; Simon, A.; Jones, W.; Lemaire, J.; Mestdagh, H.; Heninger, M.; Mauclaire, G.; Boissel, P.; Prazeres, R.; Glotin, F.; Ortega, J.-M. *Nucl. Instrum. Methods Phys. Res., Section A* **2003**, *507*, 541.

(22) Polfer, N. C.; Oomens, J. *Mass Spectrom. Rev.* **2009**, *28*, 468.

(23) Armstrong, J. A.; Bloembergen, N.; Ducuing, J.; Pershan, P. S. *Phys. Rev.* **1962**, *127*, 1918.

(24) Giordmaine, J. A.; Miller, R. C. *Phys. Rev. Lett.* **1965**, *14*, 973.

(25) Zhou, J. X.; Hou, X.; Yang, K. X.; Tsai, S.-J. J.; Michel, R. G. *Appl. Spectrosc.* **1998**, *52*, 176A.

(26) Raffy, J.; Debuisschert, T.; Pocholle, J.-P.; Papuchon, M. *Appl. Opt.* **1994**, *33*, 985.

(27) Fridgen, T. D.; MacAleese, L.; McMahon, T. B.; Lemaire, J.; Maitre, P. PCCP **2006**, *8*, 955.

(28) Kamariotis, A.; Boyarkin, O. V.; Mercier, S. R.; Beck, R. D.; Bush, M. F.; Williams, E. R.; Rizzo, T. R. *J. Am. Chem. Soc.* **2006**, *128*, 905.

(29) Bush, M. F.; O'Brien, J. T.; Prell, J. S.; Saykally, R. J.; Williams, E. R. *J. Am. Chem. Soc.* **2007**, *129*, 1612.

(30) Fridgen, T. D.; McMahon, T. B. IRMPD. In *The Encylclopedia of Mass Spectrometry: Fundamentals of and Applications to Organic (and Organometallic) Compounds* Gross, M. L., Caprioli, R., Eds.; Elsevier Science, 2005; Vol. 4.

(31) Brodbelt, J. S.; Wilson, J. J. *Mass Spectrom. Rev.* **2009**, *28*, 390.

(32) Bush, M. F.; Oomens, J.; Williams, E. R. *J. Phys. Chem. A* **2009**, *113*, 431.

(33) Dunbar, R. C.; Moore, D. T.; Oomens, J. *J. Phys. Chem. A* **2006**, *110*, 8316.

(34) Dunbar, R. C. *Int. J. Mass Spectrom.* **2000**, *200*, 571.

(35) Gaussian 03, R. C., Frisch, M. J.; Trucks, G. W.; Schlegel, H. B.; Scuseria, G. E.; Robb, M. A.; Cheeseman, J. R.; Montgomery, Jr., J. A.; Vreven, T.; Kudin, K. N.; Burant, J. C.; Millam, J. M.; Iyengar, S. S.; Tomasi, J.; Barone, V.; Mennucci, B.; Cossi, M.; Scalmani, G.; Rega, N.; Petersson, G. A.; Nakatsuji, H.; Hada, M.; Ehara, M.; Toyota, K.; Fukuda, R.; Hasegawa, J.; Ishida, M.; Nakajima, T.; Honda, Y.; Kitao, O.; Nakai, H.; Klene, M.; Li, X.; Knox, J. E.; Hratchian, H. P.; Cross, J. B.; Bakken, V.; Adamo, C.; Jaramillo, J.; Gomperts, R.; Stratmann, R. E.; Yazyev, O.; Austin, A. J.; Cammi, R.; Pomelli, C.; Ochterski, J. W.; Ayala, P. Y.; Morokuma, K.; Voth, G. A.; Salvador, P.; Dannenberg, J. J.; Zakrzewski, V. G.; Dapprich, S.; Daniels, A. D.; Strain, M. C.; Farkas, O.; Malick, D. K.; Rabuck, A. D.; Raghavachari, K.; Foresman, J. B.; Ortiz, J. V.; Cui, Q.; Baboul, A. G.; Clifford, S.; Cioslowski, J.; Stefanov, B. B.; Liu, G.; Liashenko, A.; Piskorz, P.; Komaromi, I.; Martin, R. L.; Fox, D. J.; Keith, T.; Al-Laham, M. A.; Peng, C. Y.; Nanayakkara, A.; Challacombe, M.;

Gill, P. M. W.; Johnson, B.; Chen, W.; Wong, M. W.; Gonzalez, C.; and Pople, J. A.; Gaussian, Inc., Wallingford CT, 2004.

(36) Barone, V.; Adamo, C.; Lejl, F. *J. Chem. Phys.* **1995**, *102*, 364.

(37) Nguyen, D. T.; Scheiner, A. C.; Andzelm, J. W.; Sirois, S.; Salahub, D. R.; Hagler, A. T. *J. Comput. Chem.* **1997**, *18*, 1609.

(38) Stepanian, S. G.; Reva, I. D.; Radchenko, E. D.; Adamowicz, L. *J. Phys. Chem. A* **1998**, *102*, 4623.

(39) Stepanian, S. G.; Reva, I. D.; Radchenko, E. D.; Rosado, M. T. S.; Duarte, M. L. T. S.; Fausto, R.; Adamowicz, L. *J. Phys. Chem. A* **1998**, *102*, 1041.

(40) Becke, A. D. *Phys. Rev. A: At. Mol. Opt. Phys.* **1988**, *38*, 3098.

(41) Lee, C.; Yang, W.; Parr, R. G. *Phys. Rev. B: Condens. Matter* **1988**, *37*, 785.

(42) Polfer, N. C.; Oomens, J.; Moore, D. T.; Von Helden, G.; Meijer, G.; Dunbar, R. C. *J. Am. Chem. Soc.* **2006**, *128*, 517.

(43) Scott, A. P.; Radom, L. *J. Phys. Chem.* **1996**, *100*, 16502.

(44) Andersson, M. P.; Uvdal, P. *J. Phys. Chem. A* **2005**, *109*, 2937.

(45) Blom, M. N.; Compagnon, I.; Polfer, N. C.; von Helden, G.; Meijer, G.; Suhai, S.; Paizs, B.; Oomens, J. *J. Phys. Chem. A* **2007**, *111*, 7309.

Chapter 3

IRMPD spectra of proton- and sodium ion-bound glycine dimers in the N-H and O-H stretching region†

3.1 Introduction

It has been well-documented that neutral amino acids in the condensed phase are zwitterionic[1] whereas in matrix-isolation experiments[2-4] or in the gas phase,[5-9] the non-zwitterionic form is dominant. Previous work on gaseous neutral glycine, the simplest of the amino acids, has shown that its zwitterion is not even a local minimum on its potential energy surface.[10] More recent studies, however, have investigated ways to induce the isomerization of gas-phase amino acids from their neutral non-zwitterionic form to their zwitterionic state. Jensen et al.[11] introduced a novel approach whereby the addition of water molecules to such systems could aid the structural transition, and they demonstrated that a *local* minimum for the glycine zwitterion is created through its interaction with two water molecules. From this success, other attempts were made to mimic an aqueous solution with the intention of further stabilizing the zwitterionic form, perhaps even to the point where it becomes the *global* minimum. This concept of microsolvation[12-14] continues to remain a prominent interest for the hydration chemistry of various gas-phase systems.

Protonation reactions, shown to be vital for biological processes such as enzyme catalysis,[15] can occur in aqueous solutions containing amino acids and thereby alter the conformational structure of the system. Gaseous amino acids that are protonated (including protonated clusters),[16-20] those which are metal-cation associated,[20-23] or those studied as radical

† = Atkins et al., *Journal of Physical Chemistry A* **2008**, *112*, 10220.

cations[24] have received much attention from the viewpoint of structure and thermochemistry. Such information is important for a clear understanding of a variety of biological processes. As outlined in section 2.3, comparing *ab initio* and/or DFT calculations with experimental results obtained through infrared multiple photon dissociation (IRMPD) can provide information such that ionic structures can be determined and evaluated. IRMPD spectroscopy has also been used very recently to investigate the effect of alkali cation size on producing a stable salt bridge (zwitterionic) form as opposed to a charge solvated (canonical) version.[25-28] The preference for charge solvation is believed to be reduced by a strong electrostatic interaction created between the metal cation and the dipole of the zwitterion. Earlier blackbody infrared radiative dissociation (BIRD) studies, where blackbody photons emitted from the cell wall provide the radiation, have indicated that the addition of smaller cations to arginine favours charge solvated conformations whereas the addition of larger metals stabilizes the salt bridge structure.[29] BIRD studies also showed that only a few water molecules were necessary for alkali metal ion-bound valine[30,31] to adopt the zwitterionic structure. In a similar fashion, Bush et al.[32] most recently discovered that when lithiated arginine cation complexes with a single water molecule the zwitterion is the favoured structure. Recalling the kinetic method example mentioned in section 1.2.3.2, lithiated arginine was expected to be in its canonical form. The study by Bush et al.[32] demonstrates that the addition of a single water molecule to this system can stabilize the zwitterion form such that it is preferred.

While these examples have revolved around the addition of alkali cations, it has previously been demonstrated that the study of proton-bound dimers can provide interesting insight into this amino acid isomerization. Rajabi and Fridgen[33] found that the homogeneous

proton-bound dimers of glycine, alanine and valine, as well as the mixed glycine/alanine proton-bound dimer were non-zwitterionic in nature. Furthermore, they were able to demonstrate through IRMPD spectroscopy and DFT calculations that these non-zwitterionic structures most resembled an ion-dipole complex where the protonated amino acid interacts with the carbonyl end of the neutral amino acid, as was previously shown by a combination of thermochemical studies and DFT calculations.[17] Wu and McMahon[34] similarly demonstrated that the glycine molecules in the homogenous proton-bound dimer were non-zwitterionic, but their study did provide results which suggested the proline proton-bound dimer was zwitterionic in nature. The quest to characterize amino acid systems remains an important goal of many research endeavors.

The rest of this chapter involves the presentation of results for two gas-phase systems. The first portion will provide an investigation of the proton-bound glycine homodimer by IRMPD spectroscopy in the ~2400 to 3600 cm^{-1} spectral region, which is known to be inherently rich with N-H and O-H vibrational stretching modes. The second portion arises from the fact that complexes between the sodium ion and amino acids[35-40] are important in biological systems and have received an abundance of attention. For example, a recent IRMPD study of oligoglycines and oligoalanines[41] bound to a sodium ion demonstrated that the ion typically bir.ds to three basic sites and its presence greatly affects the structure of the peptides. Because of such interesting results, the second system investigated in this chapter will be the sodium ion-bound dimer of glycine. An experimental IRMPD spectrum will be provided and possible structures for this ion will be thoroughly examined with DFT calculations.

3.2 Methods

3.2.1 Experimental

The experimental information provided in section 2.2 was for the in-house FTMS at Memorial University. Experimental data in this study was obtained at the CLIO facility in Orsay, France. Details of the combination of their Bruker Apex Qe 7T FTMS with a Laser Vision IR OPO/OPA have been described previously[42] and are not repeated here. Proton-bound dimers of glycine were electrosprayed from a 0.1 mM solution of glycine in 18 Mohm (Millipore) water. The sodium ion-bound dimers were electrosprayed from the same solution to which a few drops of 1 mM NaCl were added. Following isolation in the ICR cell, ions were irradiated for 1 to 4 s with the OPO/OPA. If the wavelength of the IR laser radiation was in resonance with a vibrational mode, several photons were absorbed, leading to dissociation of the proton- or sodium ion-bound dimer. The sole dissociation pathway for both dimer systems was a loss of neutral glycine. This makes evaluation of the IRMPD efficiency easier, which was described in section 2.2.2.2. After each irradiation event, a mass spectrum was recorded. The spectral width of the laser was estimated to be < 5 cm^{-1}.

3.2.2 Computational

Absolute structural information for ionic systems can be determined an ' evaluated through comparisons of *ab initio* and/or DFT calculations with experimental IRMPD results. The process of obtaining optimized structures with corresponding electronic energies, vibrational

frequencies, and thermochemical properties were explained in section 2.3, with the Gaussian 03[43] suite of programs used for each step. Structures were geometrically optimized using B3LYP with a 6-31+G(d,p) basis set. Frequency calculations were also completed using this set of functional and basis set, which is well known for providing excellent experimentally comparable infrared spectra combined with computational speed.[44] As previously mentioned in section 2.3, the raw harmonic vibrational frequencies produced at this level of theory are on average overestimated so scaling factors are implemented.[45] The calculated frequencies used in this study were scaled by a factor of 0.955. They were furthermore convoluted with a Lorentzian profile having a 5 cm^{-1} full width at half maximum for presentation purposes. When attempting to match calculated one-photon spectra to experimental multiple photon spectra, minor deficiencies may arise which have been discussed elsewhere.[46]

Previous research has shown that for systems similar to those under study, there is a very minor effect on the relative energies when variations on the theoretical approaches are applied. In other words, relative B3LYP energies obtained from this calculation approach would be reasonably well converged with energies obtained from larger basis sets. The 298K free energy differences are reported as relative values through comparison with the reported lowest-energy structure. Single point energy calculations were performed on each structure at the MP2(full)/6-311++G(2d,2p) level of theory. The complete calculation approach as previously described was performed on all structures for both the proton- and sodium-bound glycine homodimers to determine relative enthalpies and free energies. These energies are hence denoted as MP2(full)/6-311++G(2d,2p)//B3LYP/6-31+G(d,p).

3.3. Results and Discussion

3.3.1 Glycine Proton-Bound Dimer

The IRMPD spectrum of the proton-bound glycine dimer in the ~2400 to 3650 cm^{-1} region is shown in Figure 3.1. The B3LYP/6-31+G(d,p) predicted spectra for the three lowest-energy structures are shown as well. Also in Figure 3.1 is an experimental spectrum for the proton-bound glycine dimer, as determined by Oh et al.[47] over the 3100 to 3700 cm^{-1} range. The two experimental spectra agree well, however, the free O-H stretch in our spectrum is observed at ~3555 cm^{-1}, while in the spectrum of Oh et al.[47] it is observed to be at ~3590 cm^{-1}. While there is no obvious explanation for the discrepancy, it is important to note that the free O-H stretch for neutral glycine is observed at 3564 cm^{-1} in an argon matrix.[3,4] It would be expected that via a long-range through-bond induction effect, electron density from the free O-H bond would be depleted by the positive charge, resulting in a red shift of the stretching vibration's position as compared to the neutral.

Before comparing the experimental and predicted spectra it is interesting to evaluate the three lowest energy structures to which these spectra belong. Depicted in Figure 3.2 are the corresponding three lowest energy structures. The present energetic ordering agrees with that of previous studies.[17,33] The MP2/6-311++G(2d,2p)//B3LYP/6-31+G(d,p) enthalpies and free energies provided in Figure 3.2 are at 298K and relative to structure A which is found to be the most thermodynamically stable conformer. As determined previously,[17,33] the structure of the

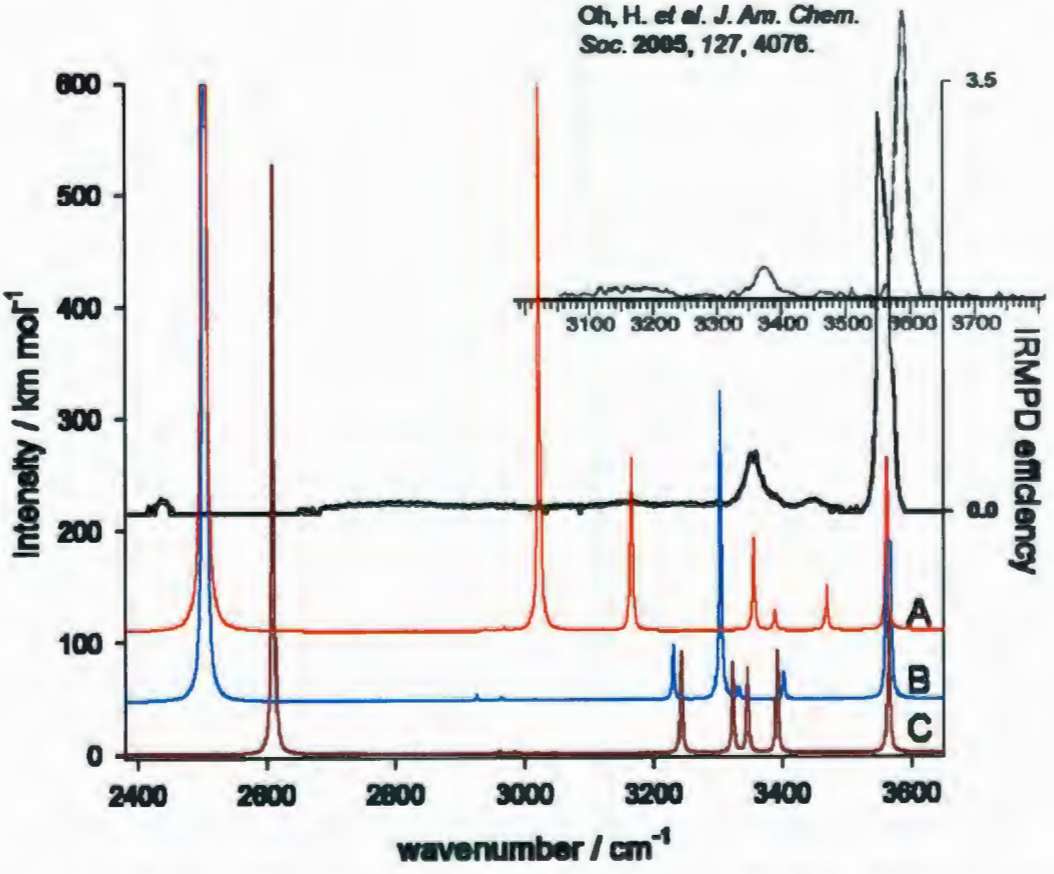

Figure 3.1 - IRMPD spectrum of proton-bound glycine dimer in the 2400 - 3600 cm^{-1} region. Also shown are B3LYP/6-31+G(d,p) theoretical infrared spectra for the three lowest energy structures. Labels (A, B and C) correspond to structures in Figure 3.2.

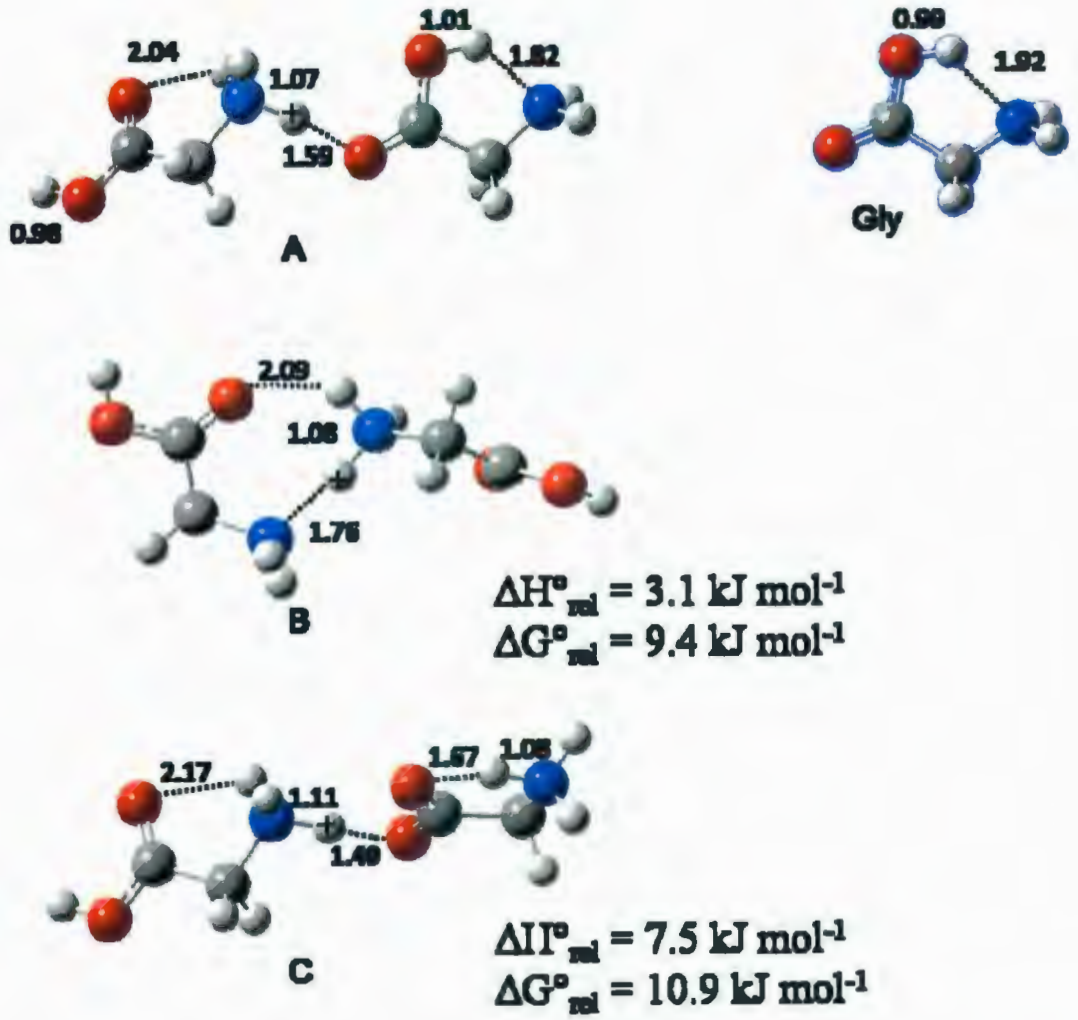

Figure 3.2 - B3LYP/6-31+G(d,p) structures for the three lowest energy isomers of the glycine proton-bound dimer. Structure labels (A, B, C) correspond to the predicted spectra in Figure 3.1. Bond lengths are in angstroms and the relative thermochemistries were calculated using MP2(full)/6-311++G(2d,2p)//B3LYP/6-31+G(d,p).

lowest energy conformer resembles an ion-dipole complex[33] involving N-protonated glycine bound to the carbonyl oxygen of the neutral amino acid. The binding proton resides closer to the amine nitrogen atom, a feature consistent with the most probable structure for protonated glycine.[48] There are also stabilizing intramolecular N-H···O and O-H···N hydrogen bonds within each amino acid moiety which are important aspects of the structure and show up in the infrared spectrum discussed below. Structure B, where the proton binds the amino acids via the amino groups, was previously determined by some to be the lowest energy conformer.[47,49] This binding proton is found significantly closer to one of the amino groups. There is also a N-H···O hydrogen bond between a carbonyl oxygen of one amino acid and the amino group of the other. This structure is higher in free energy by 9.4 kJ mol^{-1}. Structure C, which is also higher in free energy by 10.9 kJ mol^{-1}, is similar to the structure A; however, the hydroxyl hydrogen has been transferred to the amino group resulting in a zwitterionic structure. In this case the binding proton shifts closer to the carboxyl oxygen than what is seen for structure A.

The experimental spectra are compared to the predicted spectra for structures A, B and C in Figure 3.1 and Table 3.1. Within the 3300 to 3650 cm^{-1} region, the predicted spectrum for structure A clearly agrees best with the experimental spectrum. The free O-H stretch observed at 3555 cm^{-1} is fairly sharp and intense. The NH_2 asymmetric stretch for the free NH_2 group is observed at 3450 cm^{-1}. The other fully resolved feature in this region is the non-hydrogen bonded N-H stretch (the left glycine) at 3360 cm^{-1}. The shoulder on the high frequency side of this feature, at 3390 cm^{-1}, constitutes the free NH_2 symmetric stretch.

Table 3.1 - Table of observed and predicted wavenumber positions (structure A) for the glycine proton-bound dimer.

Observed position / cm^{-1}	Assignment	Predicted[a] position (A) / cm^{1}
3555	free OH str	3562
3450	free NH_2 asym str	3438
3390 shoulder	free NH_2 sym str	3387
3360	non H-bonded N-H str	3355
2650 - 3300 very broad	H-bonded NH str/	3165/
	H-bonded OH str	3022
2440	shared proton str	2503

a: B3LYP/6-31+G(d,p) scaled by 0.955.

The band at 2440 cm^{-1} is assigned to the shared proton asymmetric stretch. The predicted absorption for this stretch is significantly blue shifted from the experimentally observed feature. Harmonic calculations are not expected to adequately predict strongly anharmonic vibrations, such as the shared proton asymmetric stretch. It has been seen in the past that shared proton stretches for heterogeneous proton bound dimers are observed at significantly lower frequency than the predicted spectra.[50-52] The glycine proton-bound dimer is expected to be transparent in this region of the infrared, except for its shared-proton stretch, so this assignment at 2440 cm^{-1} is made with confidence. It would still be beneficial to observe the spectrum of the deuterium-labeled ion for confirmation of this assignment.

There are two bands predicted to occur at 3165 and 3022 cm^{-1} corresponding to the hydrogen bonded N-H and O-H stretches, respectively. While the experimental spectrum in this region may resemble noise, there is in fact an authentic broad absorption observed between ~2650 and 3300 cm^{-1}. This is confirmed by simply blocking the laser radiation before it enters the ICR cell. By doing so, it is observed that the dissociation ceases to occur thereby assuring that the feature is due to actual modes. Evidence supporting the existence of this broad spectral absorption has been provided in various scientific publications. For neutral species which have strong intramolecular hydrogen bonds such as acetylacetone and malonaldehyde, for which the enol isomer is dominant, the strongly hydrogen bonded O-H stretch is also observed to be very broad, occurring between 1800 and 3400 cm^{-1} and lacking the intensity that harmonic calculations predict.[53-55] The broadness of this feature has been associated with a double-minimum type of potential energy surface along the O-H-O stretching coordinate, strong

anharmonicity, and strong coupling to low-frequency modes.[55,56] Progress has been made in attempts to model this anharmonic vibration by means of molecular dynamics calculations.[57] The broad bands in the present experimental spectrum between 2650 and 3300 cm^{-1} are assigned to the hydrogen bonded N-H and O-H stretching modes.

It is worthwhile to compare the hydrogen bonded O-H stretch to that observed for the neutral with a similar conformation (Figure 3.2). This O-H stretch for the neutral has been demonstrated to occur at 3200 cm^{-1} in an argon matrix.[4] Unscaled harmonic calculations place this vibration at 3462 cm^{-1} using MP2/aug-cc-pVDZ,[58] 3451 cm^{-1} using B3LYP/aug-cc-pVDZ,[4] and 3466 cm^{-1} using B3LYP/6-31+G(d,p) for neutral glycine as depicted in Figure 3.2. Therefore, these calculations are all in agreement and would require a more extreme scaling factor (about 0.92) compared to the typical 0.96 for the "less anharmonic" vibrations. The B3LYP/6-31+G(d,p) structures of the proton-bound dimer and for neutral glycine, in Figure 3.2, reveal that the O-H--N hydrogen bond in the proton-bound dimer is significantly stronger resulting in a longer O-H bond and would be expected to have an absorption which is red-shifted with respect to the neutral. In fact, the anharmonic vibration (as determined by B3LYP/6-31+G(d,p)) is predicted to occur at 3164 cm^{-1} and when scaled by an appropriate 'extreme' scaling factor would be 2910 cm^{-1} in reasonable agreement with the broad band observed in Figure 3.1.

The spectrum in Figure 3.1, along with the spectra in the 700 to 2000 cm^{-1} region[33,34] represent a complete and assigned IR spectrum for the glycine proton-bound homodimer. These experiments, along with the thermochemical experiments[17] and the calculated thermochemistries, support the exclusive existence of structure A in the gas-phase at 298 K. As

mentioned previously, deuterium substitution experiments would be beneficial for this system.

3.3.2 Sodium Ion-Bound Glycine Dimer

The experimental IRMPD spectrum for the sodium ion-bound dimer of glycine from 3000 to 3700 cm^{-1} is shown in Figure 3.3 along with the B3LYP/6-31+G(d,p) predicted spectra for the five lowest-energy structures as determined by the MP2/6-311++G(2d,2p)//B3LYP/6-31+G(d,p) energy calculations. The inset in Figure 3.3 is simply a repeat of the experiment in the NH_2 region with a slower scanning rate of the infrared laser. The corresponding structures for the theoretical spectra are depicted in Figure 3.4A with the rest of the structures which have been determined in Figure 3.4B. The predicted thermodynamic properties associated with these structures are provided in Table 3.2.

Structure I is predicted to be lowest in both enthalpy and free energy by 20.8 and 20.0 kJ mol^{-1}, respectively, over structure II. Structure I is symmetric and composed of two bidentate glycine ligands. This is consistent with the lowest energy glycine-Na^+ monomeric complex determined in previous studies.[20,36,48,59] Structure II is similar to structure I in that each amino acid is bidentate, bound to Na^+ through the amine and carbonyl group. However, one of the OCOH dihedrals is rotated from 0° to about 180° such that the hydroxy hydrogen is sterically congesting a hydrogen on the CH_2 group, probably accounting for most of the 20 kJ mol^{-1} thermodynamic instability compared with structure I. Structure III differs from structure I in that there is a 180° rotation about the C-C bond so that the hydroxy oxygen on one amino acid is interacting with Na^+ rather than the carbonyl oxygen. There also exists two structures related to II and III (IIa and IIIa, also shown in Figure 3.4A) which are the symmetric versions and are significantly higher in energy than II and III. Structure IV is similar to the lowest energy glycine

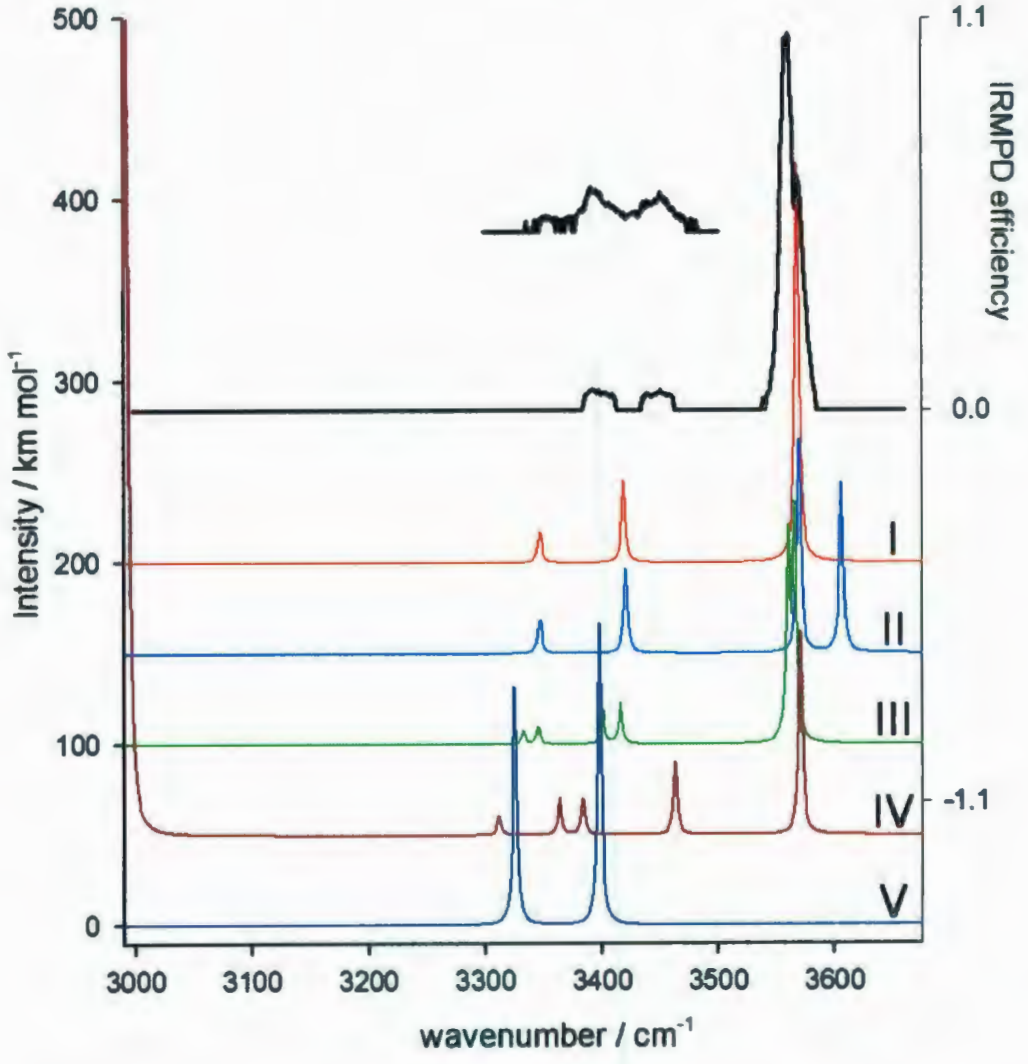

Figure 3.3 - IRMPD spectrum of sodium ion-bound glycine dimer in the 3000 - 3700 cm^{-1} region. Also shown are the B3LYP/6-31+G(d,p) theoretical infrared spectra for the five lowest energy structures. Labels (I-V) correspond to those in Figure 3.4 and Table 3.2.

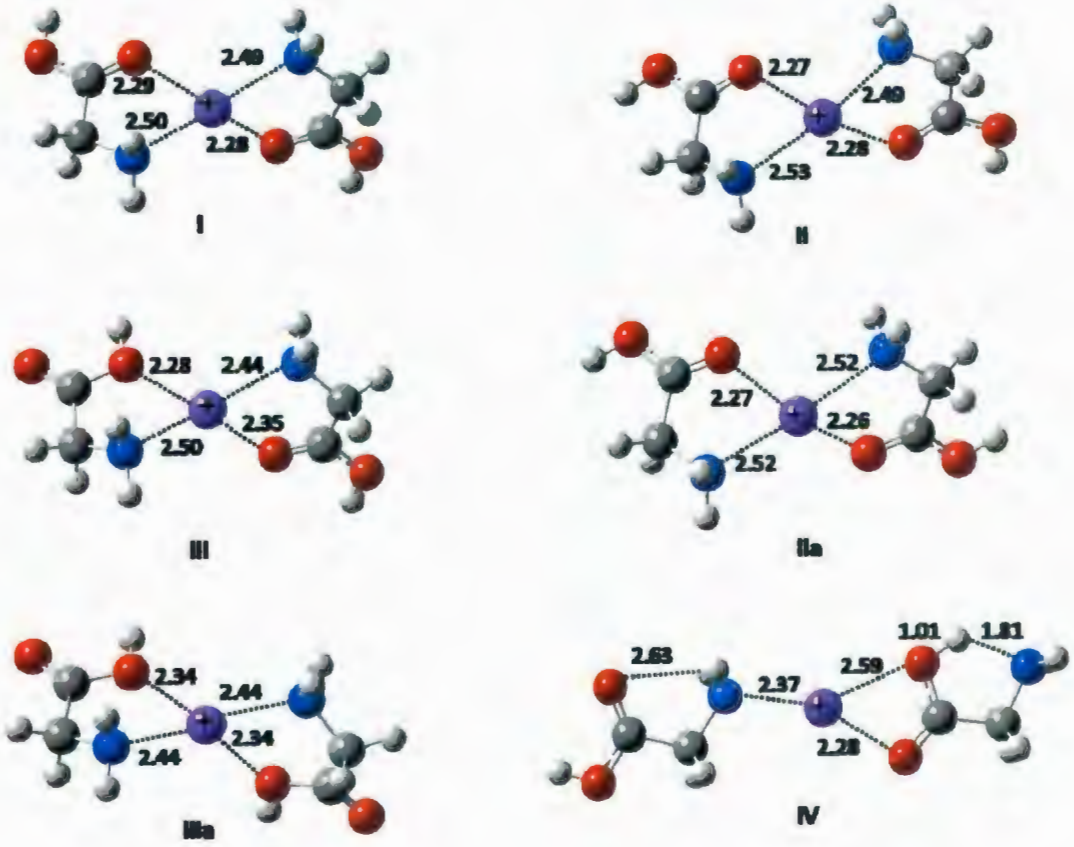

Figure 3.4A - B3LYP/6-31+G(d,p) structures for isomers of the glycine sodium ion-bound dimer. Structure labels (I-V) correspond to the predicted spectra in Figure 3.3. The relative thermochemistries of all structures, calculated using MP2(full)/6-311++G(2d,2p)//B3LYP/6-31+G(d,p), are provided in Table 3.2.

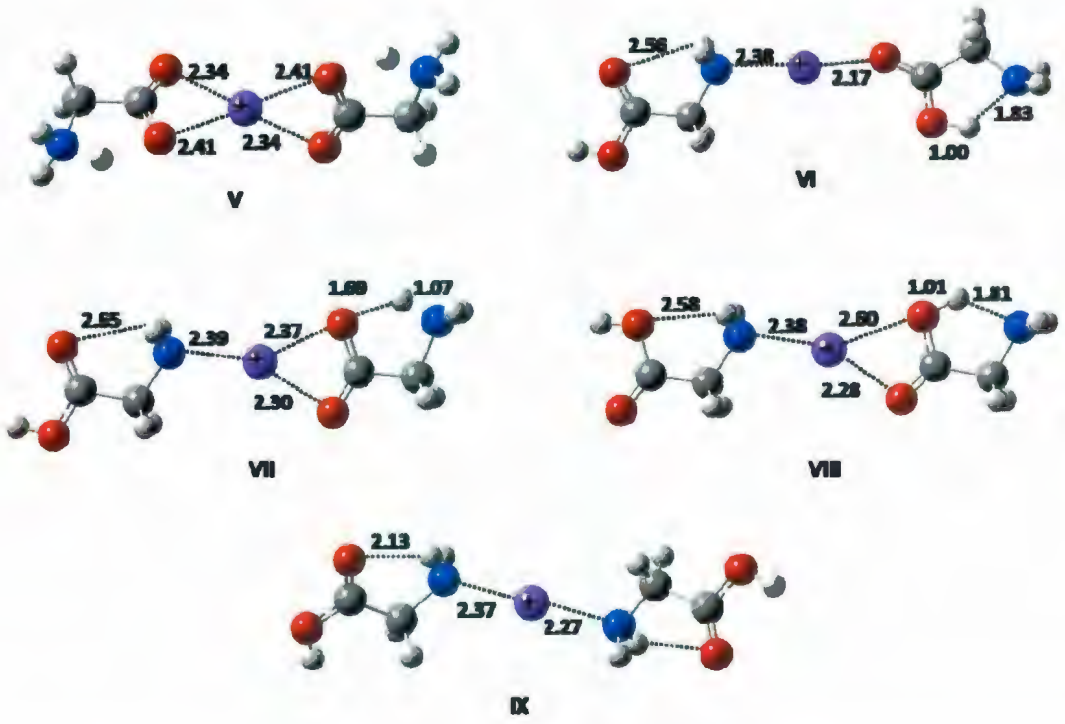

Figure 3.4B - B3LYP/6-31+G(d,p) structures for isomers of the glycine sodium ion-bound dimer. V-IX are higher-energy isomers. The relative thermochemistries of all structures, calculated using MP2(full)/6-311++G(2d,2p)//B3LYP/6-31+G(d,p), are provided in Table 3.2.

Table 3.2 - Thermochemistries[a] of sodium ion-bound dimers of glycine. Labels (I - IX) correspond to those in Figures 3.3 and 3.4.

Structure	Relative Enthalpy[a] / kJ mol^{-1}	Relative Free Energy[a] / kJ mol^{-1}
I	0	0
II	20.8	20.0
IIa	41.4	39.8
III	30.0	30.1
IIIa	60.6	60.6
IV	49.5	38.1
V	37.0	38.4
VI	51.5	38.6
VII	55.1	47.3
VIII	61.6	51.1
IX	122.8	104.7

a: MP2(full)/6-311++G(2d,2p)//B3LYP/6-31+G(d,p)

proton-bound dimer that was discussed above. The zwitterionic structure, V, is the next highest in energy, nearly 40 kJ mol^{-1} higher than I. The remaining structures are presented (as well as I-V) in Figure 3.4B and their relative enthalpies and free energies in Table 3.2

The IRMPD spectrum for the sodium ion-bound dimer of glycine (Figure 3.3) is not as rich as that for the proton-bound dimer, consisting of three main features. The O-H stretch is observed at 3560 cm^{-1} and the asymmetric and symmetric NH_2 stretching absorptions are observed at 3450 and 3390 cm^{-1}, respectively (see also Table 3.3). These bands are of course, doubly degenerate. These band positions are virtually identical to those observed for the proton-bound glycine dimer.

The predicted spectrum for structure I compares more favourably with the experimental IRMPD spectrum than any of the higher energy isomers. It should be noted, however, that we cannot rule out the other structures solely on the basis of the IRMPD spectrum. For example, structure III (or even IIIa) cannot be completely ruled out by comparison of its predicted infrared spectrum with the experimental work, however, it is predicted to be higher in energy by 30.1 kJ mol^{-1} which would mean that its contribution to a mixture would be minimal. Structures II and IIa can be ruled out based on the predicted position of the free O-H stretching vibration(s) which would occur at significantly higher energy than that observed. Structure IV can probably be ruled out based on the number of bands observed since the predicted spectrum is significantly more complicated in this region. While the predicted spectrum for the zwitterionic structure V does not agree with the experimental spectrum since an O-H stretch is observed. However, the observation of the O-H stretch in the experimental spectrum does not preclude V from existing

Table 3.3 - Table of observed and predicted wavenumber positions (structure I) for the glycine sodium ion-bound dimer.

Observed position / cm^{-1}	Assignment	Predicted[a] position (I)[b] / cm^{-1}
3560	OH str	3569
3450	NH_2 asym str	3419
3390	NH_2 sym str	3347

a: B3LYP/6-31+G(d,p) scaled by 0.955.

b: note that these predicted bands are doubly degenerate due to the symmetry of the sodium ion-bound dimer.

in the mixture since the NH_2 stretching vibrations still occur at roughly the same position as in the lowest energy isomer. However, all the higher energy structures which we have reported are significantly higher in enthalpy and free energy, by between 20 and 105 kJ mol^{-1} than the lowest energy structure and are not likely important. Thermochemical studies would be beneficial and might provide further evidence for one or a mixture of structures. The IRMPD spectrum presented agrees with that predicted for the lowest energy structure which is consistent with and confirms the results of the thermochemical calculations.

3.4 Conclusions

The IRMPD spectrum of the proton-bound dimer of glycine was extended to 2400 cm^{-1} from a previously published spectrum[47] whose low energy limit was ~3100 cm^{-1}. This extension allowed for the observation and assignment of the shared proton stretch at 2440 cm^{-1} and the hydrogen-bonded O-H and N-H stretching vibrations which is a weak and very broad feature spanning ~2650-3300 cm^{-1}. The fragmentation was confirmed to be dissociation-induced by the OPO laser since it ceased to occur when the laser radiation was blocked. The present spectrum also allowed the assignment of the free O-H stretch, the NH_2 symmetric and asymmetric stretching vibrations, as well as the N-H stretch corresponding to non-hydrogen bonded NH. The experimental IRMPD spectrum clearly allows the assignment of the structure of the glycine proton-bound dimer to the ion-dipole complex and rules out any of the higher energy structures. The calculated region below 3300 cm^{-1} cannot easily be accurately modeled due to the anharmonic nature of these hydrogen-bonded modes.

The IRMPD spectrum for the sodium ion-bound dimer of glycine is a much simpler spectrum, consisting of three bands which coincide very well with the positions of the same modes for the proton-bound dimer. Unlike they glycine proton-bound dimer, where agreement between the experimental and theoretical spectra provided a more definite assignment of structure, the IRMPD spectrum alone cannot be used to rule out all possible structures. However, the electronic structure calculations show that the lowest energy structure is such by some 20 kJ mol^{-1}. The experimental spectrum is consistent with the predicted spectrum for the lowest energy structure. This leads to the conclusion that the sodium ion-bound dimer is composed of two glycine molecules bound in a bidentate fashion through the carbonyl oxygen and the amino nitrogen and that glycine monomers are not zwitterionic.

3.5 References

(1) Levy, H. A.; Corey, R. B. *J. Am. Chem. Soc.* **1941**, *63*, 2095.

(2) Stepanian, S. G.; Reva, I. D.; Radchenko, E. D.; Adamowicz, L. *J. Phys. Chem. A* **1998**, *102*, 4623.

(3) Stepanian, S. G.; Reva, I. D.; Radchenko, E. D.; Rosado, M. T. S.; Duarte, M. L. T. S.; Fausto, R.; Adamowicz, L. *J. Phys. Chem. A* **1998**, *102*, 1041.

(4) Stepanian, S. G.; Reva, I. D.; Radchenko, E. D.; Adamowicz, L. *J. Phys. Chem. A* **1999**, *103*, 4404.

(5) Blanco, S.; Lesarri, A.; Lopez, J. C.; Alonso, J. L. *J. Am. Chem. Soc.* **2004**, *126*, 11675.

(6) Lesarri, A.; Cocinero, E. J.; Lopez, J. C.; Alonso, J. L. *Angew. Chem. Int. Ed.* **2004**, *120*, 6191.

(7) Godfrey, P. D.; Firth, S.; Hatherley, L. D.; Brown, R. D.; Pierlot, A. P. *J. Am. Chem. Soc.* **1993**, *115*, 9687.

(8) Godfrey, P. D.; Brown, R. D. *J. Am. Chem. Soc.* **1995**, *117*, 2019.

(9) Csaszar, A. G.; Perczel, A. *Prog. Biophys. Mol. Biol.* **1999**, *71*, 243.

(10) Ding, Y.; Krogh-Jespersen, K. *Chem. Phys. Lett.* **1992**, *199*, 261.

(11) Jensen, J. H.; Gordon, M. S. *J. Am. Chem. Soc* .**1995**, *117*, 8159.

(12) Ahn, D.; Park, S.; Jeon, I.; Lee, M.; Kim, N.; Han, Y.; Lee, S. *J. Phys. Chem. B* **2003**, *107*, 14109.

(13) Bachrach, S. M. *J. Phys. Chem. A* **2008**, *112*, 3722.

(14) Xu, S.; Nilles, J. M.; Bowen, K. H., Jr. *J. Chem. Phys.* **2003**, *119*, 10696.

(15) Alberty, R. A. *Biophys. Chem.* **2007**, *125*, 328.

(16) Wu, R.; McMahon, T. B. *J. Am. Chem. Soc.* **2008**, *130*, 3065.

(17) Raspopov, S. A.; McMahon, T. B. *J. Mass Spectrom.* **2005**, *40*, 1536.

(18) Lioe, H.; O'Hair, R. A. J.; Gronert, S.; Austin, A.; Reid, G. E. *Int. J. Mass Spectrom.* **2007**, *267*, 220.

(19) Jones, C. M.; Bernier, M.; Carson, E.; Colyer, K. E.; Metz, R.; Pawlow, A.; Wischow, E. D.; Webb, I.; Andriole, E. J.; Poutsma, J. C. *Int. J. Mass Spectrom.* **2007**, *267*, 54.

(20) Wyttenbach, T.; Witt, M.; Bowers, M. T. *J. Am. Chem. Soc.* **2000**, *122*, 3458.

(21) Shoeib, T.; Siu, K. W. M.; Hopkinson, A. C. *J. Phys. Chem. A* **2002**, *106*, 6121.

(22) Wang, P.; Ohanessian, G.; Wesdemiotis, C. *Int. J. Mass Spectrom.* **2008**, *269*, 34.

(23) Marino, T.; Russo, N.; Toscano, M. *J. Phys. Chem. B* **2003**, *107*, 2588.

(24) Zhao, J.; Siu, K. W. M.; Hopkinson, A. C. *PCCP* **2008**, *10*, 281.

(25) Armentrout, P. B.; Rodgers, M. T.; Oomens, J.; Steill, J. D. *J. Phys. Chem. A* **2008**, *112*, 2248.

(26) Bush, M. F.; O'Brien, J. T.; Prell, J. S.; Saykally, R. J.; Williams, E. R. *J. Am. Chem. Soc.* **2007**, *129*, 1612.

(27) Dunbar, R. C.; Polfer, N. C.; Oomens, J. *J. Am. Chem. Soc.* **2007**, *129*, 14562.

(28) Forbes, M. W.; Bush, M. F.; Polfer, N. C.; Oomens, J.; Dunbar, R. C.; Williams, E. R.; Jockusch, R. A. *J. Phys. Chem. A* **2007**, *111*, 11759.

(29) Jockusch, R. A.; Price, W. D.; Williams, E. R. *J. Phys. Chem. A* **1999**, *103*, 9266.

(30) Jockusch, R. A.; Lemoff, A. S.; Williams, E. R. *J. Phys. Chem. A* **2001**, *105*, 10929.

(31) Lemoff, A. S.; Williams, E. R. *J. Am. Soc. Mass Spectrom.* **2004**, *15*, 1014.

(32) Bush, M. F.; Prell, J. S.; Saykally, R. J.; Williams, E. R. *J. Am. Chem. Soc.* **2007**, *129*, 13544.

(33) Rajabi, K.; Fridgen, T. D. *J. Phys. Chem. A* **2008**, *112*, 23.

(34) Wu, R.; McMahon, T. B. *J. Am. Chem. Soc.* **2007**, *129*, 4864.

(35) Wang, P.; Wesdemiotis, C.; Kapota, C.; Ohanessian, G. *J. Am. Soc. Mass Spectrom.* **2007**, *18*, 541.

(36) Moision, R. M.; Armentrout, P. B. *J. Phys. Chem. A* **2002**, *106*, 10350.

(37) Kish, M. M.; Wesdemiotis, C.; Ohanessian, G. *J. Phys. Chem. B* **2004**, *108*, 3086.

(38) Cerda, B. A.; Hoyau, S.; Ohanessian, G.; Wesdemiotis, C. *J. Am. Chem. Soc.* **1998**, *120*, 2437.

(39) Dunbar, R. C. *J. Phys. Chem. A* **2000**, *104*, 8067.

(40) Kapota, C.; Lemaire, J.; Maitre, P.; Ohanessian, G. *J. Am. Chem. Soc.* **2004**, *126*, 1836.

(41) Balaj, O.-P.; Kapota, C.; Lemaire, J.; Ohanessian, G. *Int. J. Mass Spectrom.* **2008**, *269*, 196.

(42) Bakker, J. M.; Besson, T.; Lemaire, J.; Scuderi, D.; Maitre, P. *J. Phys. Chem. A* **2007**, *111*, 13415.

(43) Gaussian 03, R. C., Frisch, M. J.; Trucks, G. W.; Schlegel, H. B.; Scuseria, G. E.; Robb, M. A.; Cheeseman, J. R.; Montgomery, Jr., J. A.; Vreven, T.; Kudin, K. N.; Burant, J. C.; Millam, J. M.; Iyengar, S. S.; Tomasi, J.; Barone, V.; Mennucci, B.; Cossi, M.; Scalmani, G.; Rega, N.; Petersson, G. A.; Nakatsuji, H.; Hada, M.; Ehara, M.; Toyota, K.; Fukuda, R.; Hasegawa, J.; Ishida, M.; Nakajima, T.; Honda, Y.; Kitao, O.; Nakai, H.; Klene, M.; Li, X.; Knox, J. E.; Hratchian, H. P.; Cross, J. B.; Bakken, V.; Adamo, C.; Jaramillo, J.; Gomperts, R.; Stratmann, R. E.; Yazyev, O.; Austin, A. J.; Cammi, R.; Pomelli, C.; Ochterski, J. W.; Ayala, P. Y.; Morokuma, K.; Voth, G. A.; Salvador, P.; Dannenberg, J. J.; Zakrzewski, V. G.; Dapprich, S.; Daniels, A. D.; Strain, M. C.; Farkas, O.; Malick, D. K.; Rabuck, A. D.; Raghavachari, K.; Foresman, J. B.; Ortiz, J. V.; Cui, Q.; Baboul, A. G.; Clifford, S.; Cioslowski, J.; Stefanov, B. B.; Liu, G.; Liashenko, A.; Piskorz, P.; Komaromi, I.; Martin, R. L.; Fox, D. J.; Keith, T.; Al-Laham, M. A.; Peng, C. Y.; Nanayakkara, A.; Challacombe, M.; Gill, P. M. W.; Johnson, B.; Chen, W.; Wong, M. W.; Gonzalez, C.; and Pople, J. A.; Gaussian, Inc., Wallingford CT, 2004.

(44) Andersson, M. P.; Uvdal, P. *J. Phys. Chem. A* **2005**, *109*, 2937.

(45) Scott, A. P.; Radom, L. *J. Phys. Chem.* **1996**, *100*, 16502.

(46) Oomens, J.; Sartakov, B. G.; Meijer, G.; von Helden, G. *Int. J. Mass Spectrom.* **2006**, *254*, 1.

(47) Oh, H.-B.; Lin, C.; Hwang, H. Y.; Zhai, H.; Breuker, K.; Zabrouskov, V.; Carpenter, B. K.; McLafferty, F. W. *J. Am. Chem. Soc.* **2005**, *127*, 4076.

(48) Jensen, F. *J. Am. Chem. Soc.* **1992**, *114*, 9533.

(49) Price, W. D.; Schnier, P. D.; Williams, E. R. *J. Phys. Chem. B* **1997**, *101*, 664.

(50) Burt, M. B.; Fridgen, T. D. *J. Phys. Chem. A* **2007**, *111*, 10738.

(51) Fridgen, T. D.; MacAleese, L.; Maitre, P.; McMahon, T. B.; Boissel, P.; Lemaire, J. *PCCP* **2005**, *7*, 2747.

(52) Fridgen, T. D.; MacAleese, L.; McMahon, T. B.; Lemaire, J.; Maitre, P. *PCCP* **2006**, *8*, 955.

(53) Chiavassa, T.; Roubin, P.; Pizzala, L.; Verlaque, P.; Allouche, A.; Marinelli, F. *J. Phys. Chem.* **1992**, *96*, 10659.

(54) Chiavassa, T.; Verlaque, P.; Pizzala, L.; Roubin, P. *Spectrochim. Acta* **1994**, *50A*.

(55) Matanovic, I.; Doslic, N. *J. Phys. Chem. A* **2005**, *109*, 4185.

(56) Tayyari, S. F.; Zeegers, -. H., Th.; Wood, J. L. *Spectrochim. Acta* **1979**, *35A*, 1289.

(57) Jezierska, A.; Panek, J. J. *Journal of Chem. Theory Comput.* **2008**, *4*, 375.

(58) Bludsky, O.; Chocholousova, J.; Vacek, J.; Huisken, F.; Hobza, P. *J. Chem. Phys.* **2000**, *113*, 4629.

(59) Hoyau, S.; Ohanessian, G. *Chem. Eur. J.* **1998**, *4*, 1561.

Chapter 4

The structure of $Pb(Gly-H)^+$ and the monosolvated water and methanol solvated species by infrared multiple photon dissociation spectroscopy, energy-resolved collision-induced dissociation, and electronic structure calculations†

4.1 Introduction

Recently, metal ions have captured the interest of researchers for a broad range of applications in gas-phase chemistry. For example, complexation with aromatic groups has provided a more complete picture of cation-π interactions.[1-3] In metal ion complexes of amino acids, the size of the metal cation has been found to influence the propensity for amino acids to adopt zwitterionic structures.[4-15] For example glycine complexed with Li^+, Na^+ or Be^{2+} adopts a charge solvated structure, whereas K^+, Cu^{2+}, Mg^{2+}, Ca^{2+}, Sr^{2+} and Ba^{2+} promote a zwiterionic structure.[5, 16-19]

One of the more intriguing avenues of gas-phase research involves the development of a detailed picture of how biological systems fundamentally interact. Metal ions are known to play a role in the formation of certain peptides[20] and obtaining a quantitative scale for their binding energies to small biological molecules is desirable.[21] However, unlike the alkali and alkaline earth metals which have been the focus in the majority of studies referenced above, human exposure to certain heavy metals (Pb, Cd, Tl, Hg, etc.) and their respective ionic forms have been known to lead to adverse chemical responses within cells. The degree of toxicity typically depends on how efficiently the heavy metal ion competes for binding sites on proteins and peptides.[22] Acquiring structural information about fundamental interactions between toxic ions

and simple biological building blocks can pave the way for modeling the actual physiological response by the larger systems which would be responsible for detoxification.

The tripeptide glutathione (γ-Glu-Cys-Gly, GSH) is well known to be responsible for detoxification, due to its large concentration within the cell and its ability to chelate metals.[23] Attempts to understand such a process have been undertaken in the past through various means such as NMR[24] and pulse polarography.[25] Burford, Eelman and LeBlanc[26] used electrospray mass spectrometry to examine the complexes of various heavy metal cations (Pb^{2+}, Cd^{2+}, Hg^{2+}, Tl^{+}, Bi^{3+}) with all 20 standard amino acids as well as homocysteine. The mass spectra revealed that in most cases the most abundant complexes for the dication systems involved the heavy metal ions bound to the conjugate base of the amino acid, $(MAa-H)^{+}$ (M = metal, Aa = amino acid, H = hydrogen). Higher order complexes involving multiple amino acids and metal ions were also identified. Later they expanded upon this work to examine complexes of the same metal ions with gluthathione.[27] CID experiments on the complexes showed no neutral fragments containing sulfur, suggesting the importance of cysteine's sulfur atom in chelating the metal species. With these types of experiments, though, it is not possible to provide a more definitive structural characterization.

Many experimental and theoretical approaches have been utilized to study the structures of amino acids when complexed with a metal ion. One of the most recent approaches involves the coupling of a mass spectrometer to a broadly tunable infrared (IR) source for the observation of IR-induced dissociation. As the absorption of multiple photons is necessary for the dissociation to occur, a so-called IRMPD "consequence" spectrum is produced, which has been shown in most cases to correlate well with absorption spectra obtained from theoretical calculations.[28] The radiation sources utilized for this experimental approach include the free

electron lasers (FEL) of FELIX[29] and CLIO[30], and groups have also started taking advantage of a table-top OPO/OPA laser set-up.[9, 19, 31-34]

CID, another technique used largely for structural investigations, employs two stages of mass analysis combined in one experiment. In this method a selected precursor ion, upon dissociation by collisions with an inert gas, produces a product ion spectrum in which all fragment ions are derived from the selected precursor ion. Applying this technique, Ohanessian and coworkers, for example, have been able to elucidate structures of solvated zinc(II) complexes with carboxylic acids[35] and glycine.[36]

The history of lead derivatives as anti-knocking agents in gasoline makes the lead dication an interesting prospect for study; understanding the Pb^{2+} ion interacting with amino acids may lead to rationalizing the effect of its contamination and exposure. Analytical chemists have investigated the ion through various means.[37, 38] Here we will provide ou gas-phase energy-resolved CID and IRMPD spectroscopy studies on $[Pb(Gly-H)]^+$. Comparisons will be drawn to theoretical spectra with the intention of elucidating intrinsic structural features of these ions. Also included is a study of the structure of the water and methanol solvated $[Pb(Gly-H)]^+$ complexes, $[Pb(Gly-H)H_2O]^+$ and $[Pb(Gly-H)CH_3OH]^+$.

4.2 Methods

4.2.1 Experimental

4.2.1.1 IRMPD Spectroscopy.

Ions were electrosprayed from solutions containing approximately 1 mM glycine (Sigma Aldrich) and 1 mM lead nitrate in a 50/50 mixture of 18 MΩ water (Millipore) and methanol

using the Apollo II ion source on a Bruker Apex Qe70 Fourier transform ion cyclotron resonance (FTICR) mass spectrometer. Flow rates were typically 100 μL h^{-1}. Ions were initially mass selected in the quadrupole mass filter prior to accumulation in a hexapole trap for 1-2 s and then transferred to the ICR cell where they were irradiated with tunable infrared radiation from an optical parametric oscillator (OPO) for 2 - 7 s at each wavelength in 1 cm^{-1} intervals.

The OPO laser system/FTICR spectrometer set up will be discussed thoroughly in a forthcoming paper. A brief description will be provided here. The potassium titanyl phosphate (KTP) crystal of the OPO laser (Euroscan, Belgium) was pumped with the fundamental line (1064 nm) from a Brilliant B Nd: YAG laser (Big Sky Laser) with 6 ns pulses at 10 Hz and an output of 850 mJ. The output of the OPO has a 2 cm^{-1} bandwidth. The OPO laser radiation entered the vacuum chamber through a BaF_2 window, and the entire laser path from the laser to the ICR cell, including the bore of the magnet, was purged with dry CO_2-free air and dry N_2. The wavelength of the laser was scanned in 1 cm^{-1} steps and 2 mass spectra were averaged per wavelength.

For the IRMPD experiments, ions were solvated according to the method developed previously.[39] Briefly, a second transfer line was directed into the hexapole accumulation cell. The first one is for argon collision gas, and the second is a vapor inlet line. The argon flow was typically minimized while vapor from the liquid was flowing. Either water, methanol, or ^{18}O-labeled water was degassed by three freeze-pump-thaw cycles. The pressure in the hexapole accumulation cell is estimated to be about 10^{-2} mbar, but the micro-valve between the liquid and the accumulation cell was opened slowly to effect almost complete single solvation of the selected ion.

4.2.1.2 Energy-Resolved MS/MS

Experiments were performed using a MDS SCIEX API 2000 triple quadrupole mass spectrometer with a TurboIonSpray ion source. Equimolar solutions of lead derived from lead nitrate (BDH) and glycine (Aldrich) were prepared in methanol or in water (100 μM each). Solutions were introduced into the electrospray source at a typical flow rate of 3 μL min^{-1} and electrospray voltage of 5500 V. H/D exchange was investigated with a mixture of D_2O-CH_3OD (70:30) as a solvent for glycine and lead nitrate solutions.

The relative stabilities of different parent and product ions were evaluated by recording breakdown dissociation profiles under multiple collision conditions (nitrogen collision gas, pressure approx 2 mTorr) using the multiple reaction monitoring (MRM) scan mode with laboratory collision voltages between 0 to 100 V. Relative ion intensities were plotted as a function of collision voltage, and the steepest part of the intensity curve was extrapolated to zero by linear regression, onset voltage represented by the intercept. The final values reported here are averages of at least three individual measurements, represented in the center of mass reference frame (E_{CM}). The uncertainty of the measured onset energy was estimated to be up to ±10%.

4.2.2 Computational

All calculations were done using the Gaussian 03 software package.[40] Geometry optimizations and harmonic vibrational frequency calculations were performed using the B3LYP density functional theory. For Pb, the LANL2DZ basis set and relativistic core potential were used[41] while the 6-31+G(d,p) basis set was used for all other atoms. Geometries, thermal

corrections to the thermochemical data as well as entropies were extracted from this DFT calculation. Single point energy calculations were then performed on all optimized structures using the MP2 level of theory, with the same basis set and core potential for Pb and the larger 6-311++G(2d,2p) basis set for all other atoms. The energies derived by this method are abbreviated as MP2/6-311++G(2d,2p)//B3LYP/6-31+G(d,p) but one should keep in mind that the LANL2DZ basis set and core potential was used for Pb in all calculations. Computed harmonic frequencies were scaled by a factor of 0.955[42] and convoluted with a Lorentzian profile having 10 cm^{-1} full width at half maximum. The reported enthalpies and 298K free energy differences are reported relative to the lowest-energy structures.

Transition state structures were verified by the presence of one imaginary frequency which corresponded to the reaction coordinate. Intrinsic reaction coordinate calculations were also performed to verify the reactant and product from the transition state.

4.3 Results and Discussion

4.3.1 IRMPD Spectroscopy

The combination of IR radiation sources with mass spectrometry has provided researchers with a significant tool capable of elucidating intrinsic structural information regarding gas-phase ions. In IRMPD, once the impinging IR radiation is in resonance with a vibrational mode of the isolated ion, it becomes energized through absorption of a photon. Rapid IVR to other vibrational modes occurs, allowing the absorption of another photon exciting the same mode. As this process continues, the internal energy of the ion surpasses the threshold dissociation and dissociation is observed.

4.3.1.1 $[Pb(Gly\text{-}H)H_2O]^+$

Initially, our attempts at obtaining the IRMPD spectrum of bare $[Pb(Gly\text{-}H)]^+$ were unsuccessful, presumably because the lowest-energy dissociation threshold was too high (see below) so that the IRMPD process was not efficient enough to be observed. Therefore, we added water to $[Pb(Gly\text{-}H)]^+$ producing $[Pb(Gly\text{-}H)H_2O]^+$ which was found to undergo IRMPD when the laser was tuned to be resonant with a vibrational mode. The only dissociation product of this IRMPD process was a loss of neutral water. The experimental IRMPD spectrum for the $[Pb(Gly\text{-}H)H_2O]^+$ in the 3200 – 3800 cm^{-1} region is shown at the top of Figure 4.1 and will be compared to theoretical IR spectra after discussing plausible structures.

The spectrum of $[Pb(Gly\text{-}H)H_2O]^+$ in Figure 4.1 has three prominent features, two strong absorptions at 3661 cm^{-1} and 3550 cm^{-1}, and a weaker absorption in the NH stretching region at 3365 cm^{-1}. Initially it was predicted that the structure of $[Pb(Gly\text{-}H)H_2O]^+$ resembles 1 in Scheme 4.1, where Pb^{2+} has been ligated by zwitterionic glycine which has also lost a proton from the NH_3^+ group. Water would conceivably be bound to Pb^{2+} as well. The positions of the two strong bands are quite interesting and provide telltale signs of the structure which is inconsistent with 1 in Scheme 4.1. Previous spectroscopic work on the sodium ion- and proton-bound dimers of glycine[19] determined that the O-H stretching vibrations of the carboxylic acid groups are at 3555 cm^{-1} and 3569 cm^{-1}, respectively. Similarly, the O-H stretch of canonical matrix isolated glycine is at 3577 cm^{-1}.[43] Furthermore, a matrix-isolation study of $Pb(OH)_2$ in solid Ar[44] found the PbO-H stretch to be located at 3640 cm^{-1}. Finally, if water were intact on the ion, two bands associated with the symmetric and asymmetric stretch would be expected, probably slightly red shifted from ~3660 cm^{-1} and 3760 cm^{-1}, respectively. For example, the asymmetric and symmetric

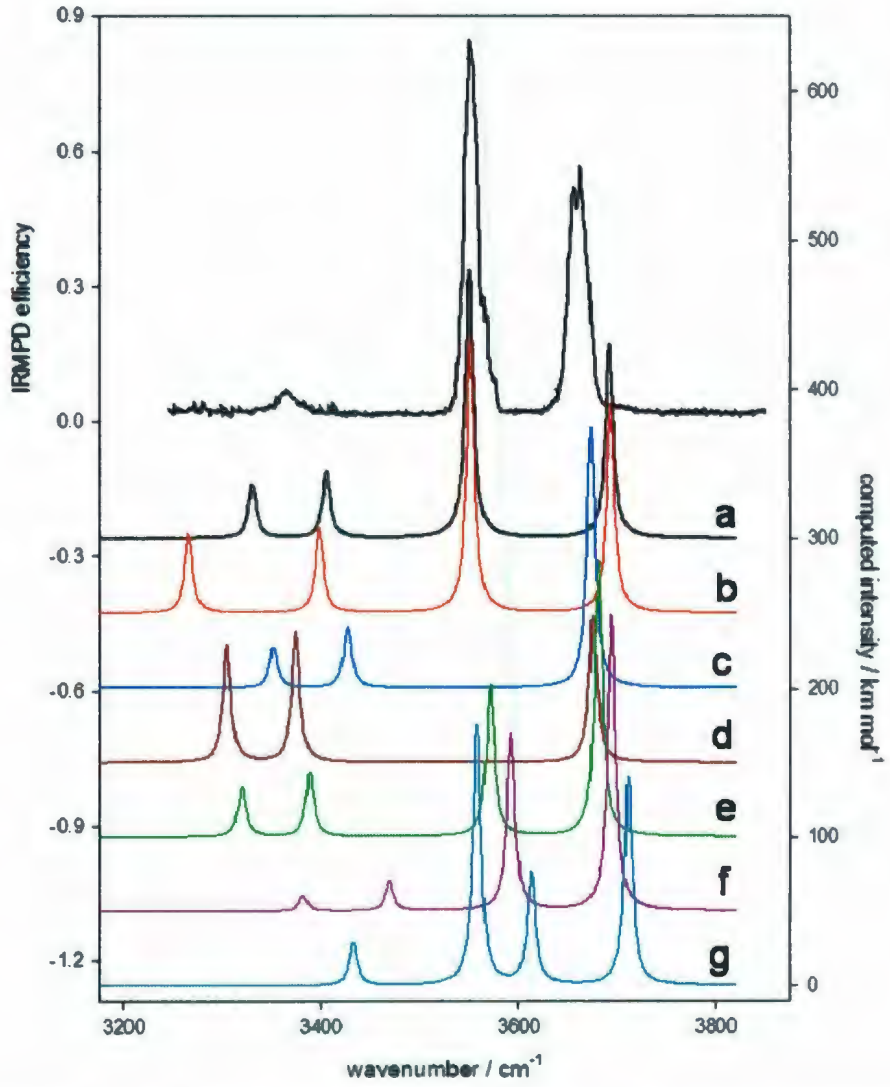

Figure 4.1 - IRMPD spectrum of $[Pb(Gly\text{-}H)H_2O]^+$ (top trace) and the B3LYP/6-31+G(d,p) computed spectra for 7 isomers. See Figure 4.3 for corresponding structures.

Scheme 4.1 - $[Pb(Gly\text{-}H)H_2O]^+$ structures

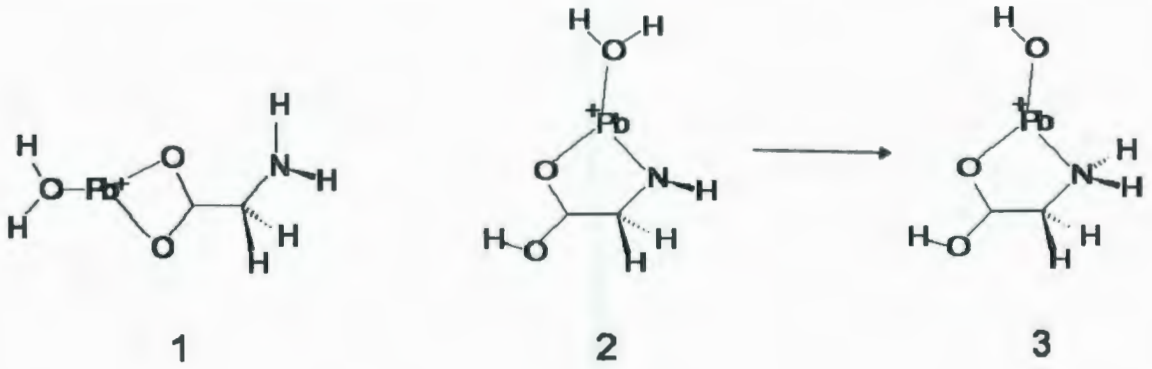

1 2 3

stretching vibrations of water complexed to Li^+ in Li^+-bound dimers of thymine and uracil occur at ~3730 cm^{-1} and 3650 cm^{-1}.[45] The similarities of these previous assignments with the band positions observed in the spectrum of $[Pb(Gly\text{-}H)H_2O]^+$ (Figure 4.1) indicated a structure similar to 3 in Scheme 4.1. An initial entrance channel complex in the reaction of H_2O with $[Pb(Gly\text{-}H)]^+$ (2 in Scheme 4.1) transfers a proton from water to the amino acid nitrogen.

One implication of this hypothesis on the structure of $[Pb(Gly\text{-}H)H_2O]^+$ is that bare $[Pb(Gly\text{-}H)]^+$ is non-zwitterionic and the net proton loss from the amino acid is from the N-group rather than from the carboxylic acid group. In other words, the carboxylic acid group is not deprotonated. Calculations were therefore done on various structures of $[Pb(Gly\text{-}H)]^+$, and are four lowest-energy structures are displayed in Figure 4.2. The lowest-energy structure based on these MP2/6-311++G(2d,2p)//B3LYP/6-31+G(d,p) calculations is i) in which the proton has been lost from N and still remains on the carboxylic acid group. Interestingly, the structure that was initially hypothesized to be the most favorable, iii), is the third lowest in energy. The highest energy isomer is iv) where the proton has been lost from the methylene group. Note that without the spectroscopic data, calculations of structure i) would likely not have been attempted due to its unexpected likelihood of having a substantial contribution.

From this new theoretical data, calculations were performed on a number of these structures where water was attached as well. The results of these calculations are presented in Figure 4.3. Although a, b, c, and d are all very similar in energy, only the conformers a and b are structures which could stem from i) in Figure 4.2 without extensive hydrogen atom shift isomerization. Structure g is also possible, stemming from i) and is the entrance channel

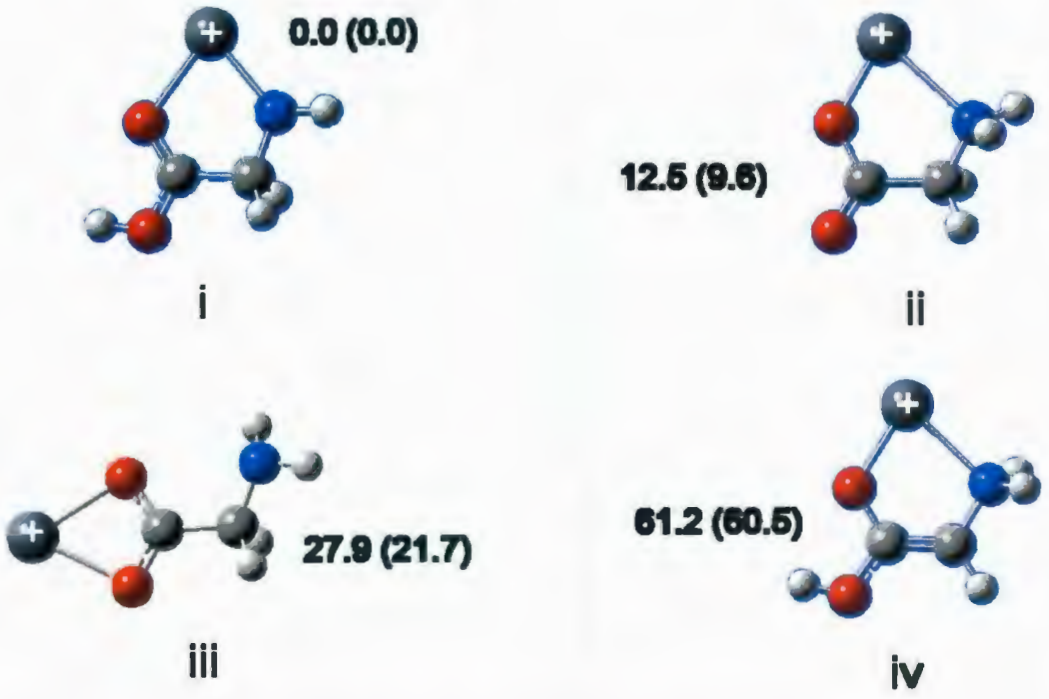

Figure 4.2 - Computed structures for the four lowest-energy isomers of $[Pb(Gly\text{-}H)]^+$ along with the relative enthalpies and 298 K entropies in parentheses.

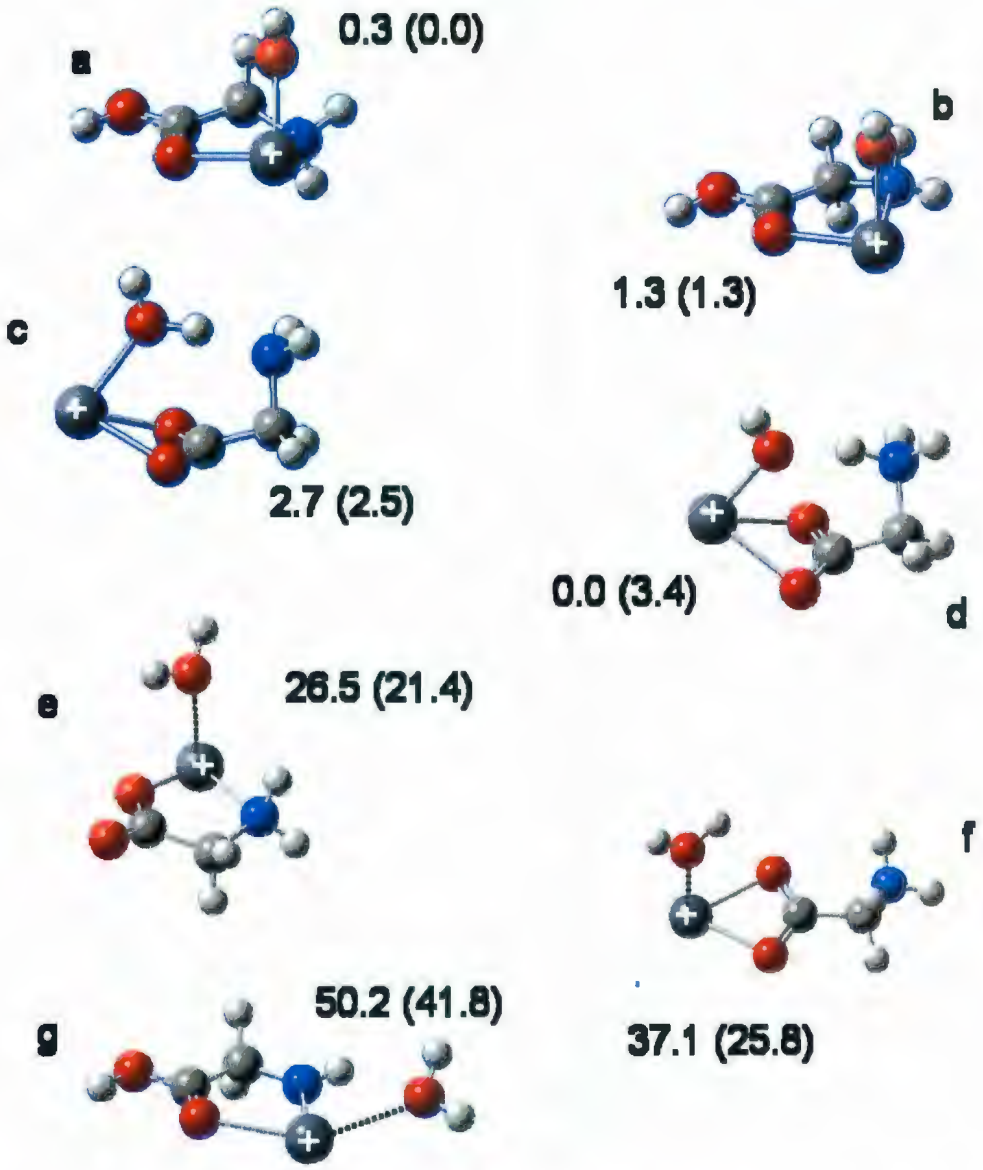

Figure 4.3 - Computed structures for the seven isomers of $[Pb(Gly\text{-}H)H_2O]^+$ along with the relative enthalpies and 298 K entropies in parentheses.

complex formed upon reaction of neutral water with $[Pb(Gly-H)]^+$. It is significantly higher in energy, and the energy barrier for isomerization to structure b is only about 10 kJ mol^{-1} (Figure 4.4). Structures c, d and f stem from iii) in Figure 4.2, the first two of which are strongly stabilized by intramolecular hydrogen bonding interactions.

In Figure 4.1 the computed IR spectra for a through g are compared to the experimental IRMPD spectrum of $[Pb(Gly-H)H_2O]^+$. The predicted spectra for structures a and b match well with the IRMPD spectrum, but spectroscopically structures c and d cannot be ruled out as being present simply based on the absence of a band predicted to be at 3550 cm^{-1} where a band is observed in the experimental spectrum. The remaining experimental features compare favorably with the other predicted bands for c and d. All that can be concluded spectroscopically is that structures c and d are, at most, minor contributors. However, one can surmise that since i) is the lowest energy $[Pb(Gly-H)]^+$ isomer, then the addition of a water molecule in the gas phase should initially give g and then a mixture of a and b. To obtain structures such as c and d, many rearrangements, including a proton shift and a Pb^{2+} ion shift, with significant energy barriers would not likely occur rapidly. Structures e and f cannot be ruled out by comparing the experimental and computed spectra. An IRMPD spectrum of $[Pb(Gly-H)H_2O]^+$ where the water was labeled with ^{18}O is shown in Figure 4.5. If the two intense bands in the IRMPD spectrum of $[Pb-(Gly-H)H_2O]^+$ were due to the symmetric and asymmetric O-H stretching absorptions of the water, as in structures e and f, then both bands would be expected to shift to lower wavenumber position, by approximately 10 cm^{-1}. However, the only one that shows a red shift is the 3661 cm^{-1}, as expected if the structure of the observed ion were as represented by structures a and b.

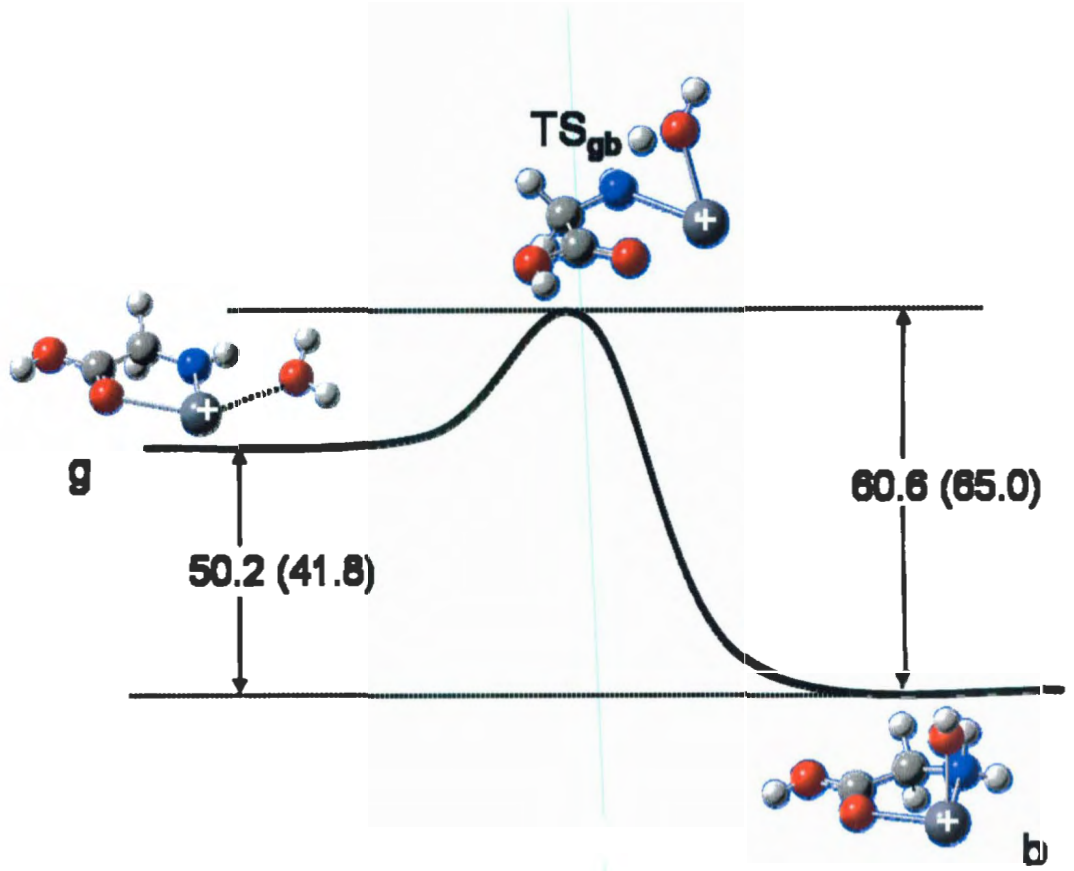

Figure 4.4 - Proton-transfer isomerization profile between structure g and b of $[Pb(Gly\text{-}H)H_2O]^+$.

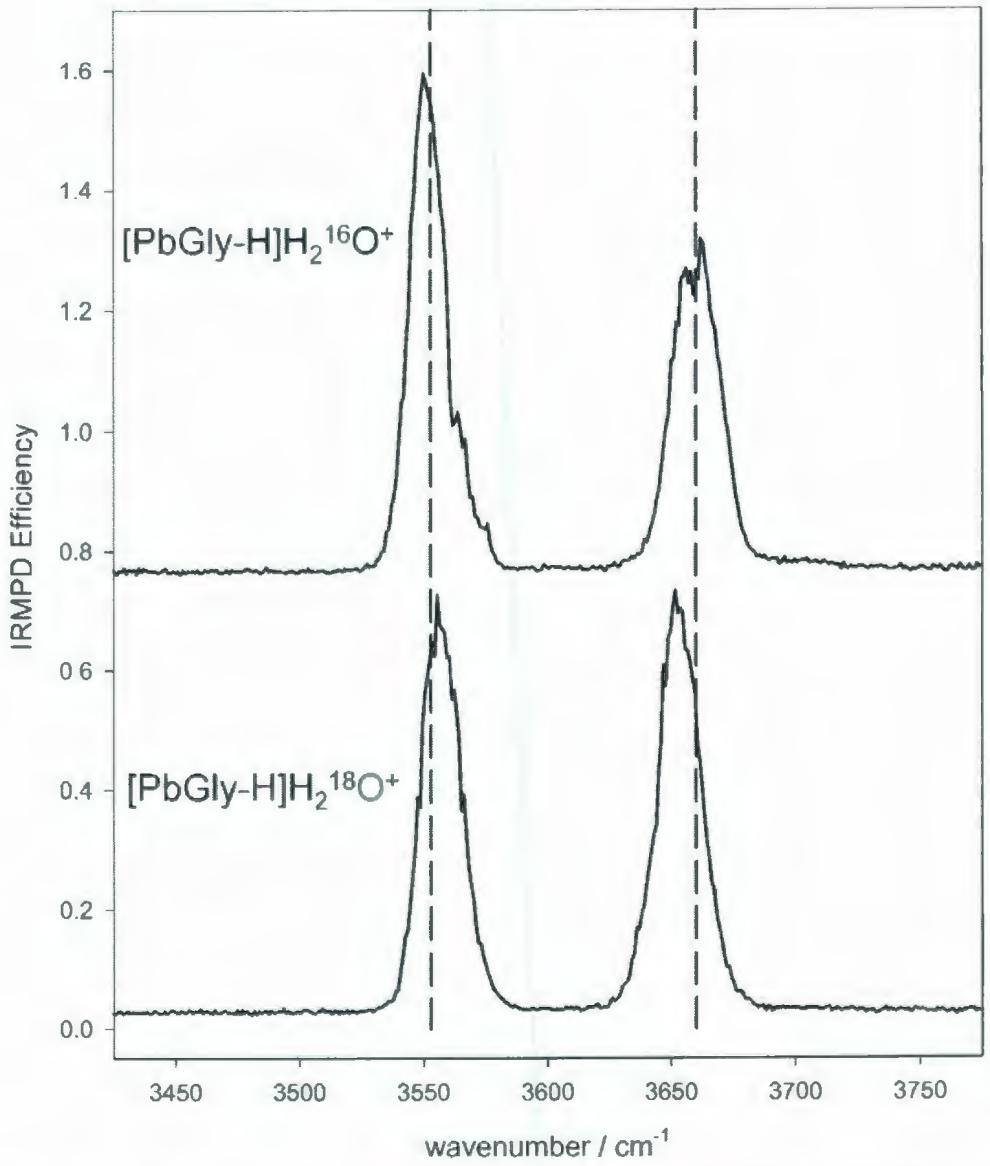

Figure 4.5 - IRMPD spectrum of $H_2{}^{16}O$ (top trace) and $H_2{}^{18}O$ (bottom trace) labeled $[Pb(Gly\text{-}H)H_2O]^+$. Dashed lines are present to emphasize the location of the red shift.

4.3.1.2 [Pb(Gly-H)]$^+$

By heating the vacuum chamber housing the ICR cell with a heating jacket (which is cooled on the outside to protect the magnet), the internal ICR cell temperature was increased to 73 °C. At this temperature the internal energy of $[Pb(Gly\text{-}H)]^+$ was high enough to observe IRMPD and the predominant fragmentation pathway observed upon absorption of the OPO laser was CO loss, with a very small amount of H_2O loss (9 % of CO loss). The IRMPD spectrum is shown in Figure 4.6 along with the IR absorption spectra predicted for the four structures in Figure 4.2. The band observed at 3552 cm^{-1}, in virtually the same position as that assigned to the carboxylic acid O-H stretch for $[Pb(Gly\text{-}H)H_2O]^+$, is still present in the absence of water, consistent with there being a –COOH group in the complex and the proton being lost from N in $[Pb(Gly\text{-}H)]^+$ as in structure i). The computed spectrum for this lowest energy structure, i), is also the best match to the experimental infrared spectrum confirming this structure. This is also consistent with the conclusion that $[Pb(Gly\text{-}H)H_2O]^+$ is most likely structures a and b and not c through f. Experiments of Rogalewicz, Hoppilliard and Ohanessian[36] on $[Zn(Gly\text{-}H)]^+$ also predict that glycine is preferentially deprotontated at N in this complex even though deprotonation at N is some 200 kJ mol^{-1} higher in energy.[46] The present work is the first experimental evidence for deprotonation at N of these complexes of metal cations and deprotonated amino acids.

4.3.1.3 [Pb(Gly-H)CH_3OH]$^+$

Methanol was complexed to $[Pb(Gly\text{-}H)]^+$ in the accumulation cell producing $[Pb(Gly\text{-}H)CH_3OH]^+$. Upon absorption of the infrared laser, the only fragmentation pathway observed was loss of methanol. The IRMPD spectrum is shown in Figure 4.7. The band at 3552 cm^{-1} is

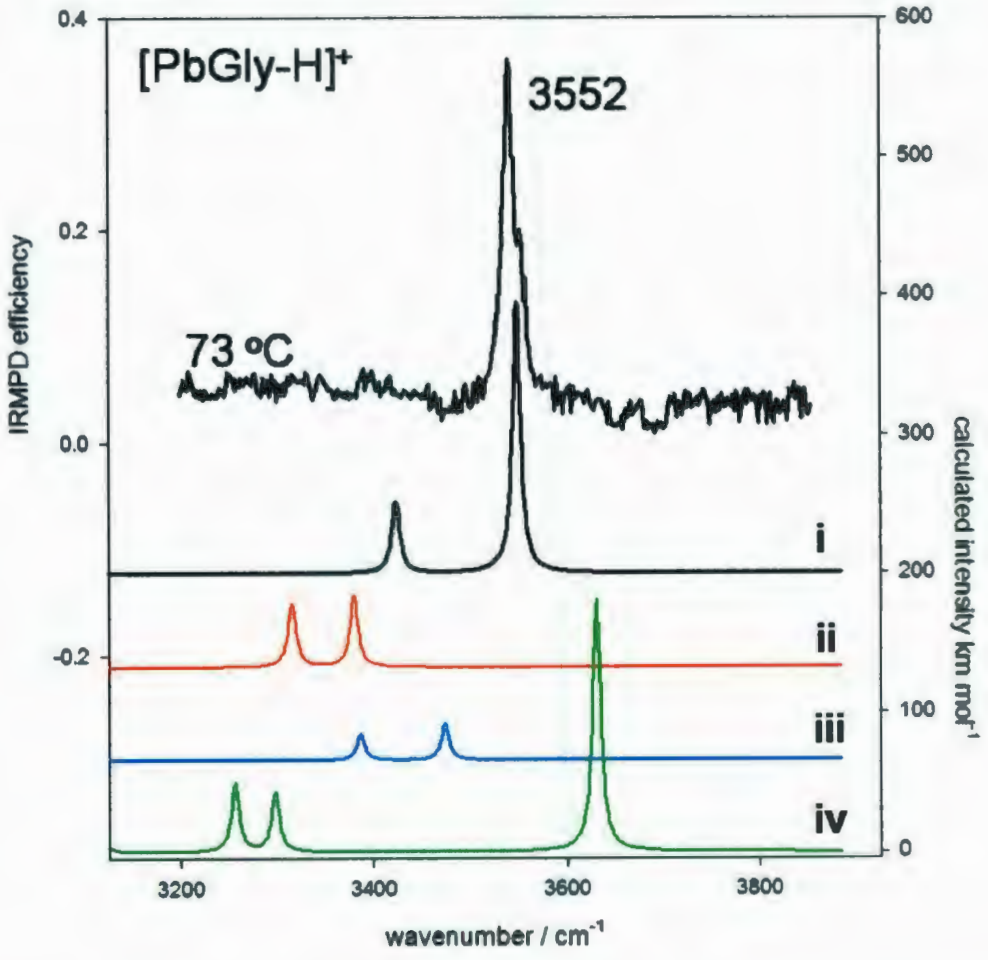

Figure 4.6 - IRMPD spectrum of $[Pb(Gly-H)]^+$ at 73 °C compared with the computed spectra for the four lowest energy isomers (see Figure 4.2 for structures).

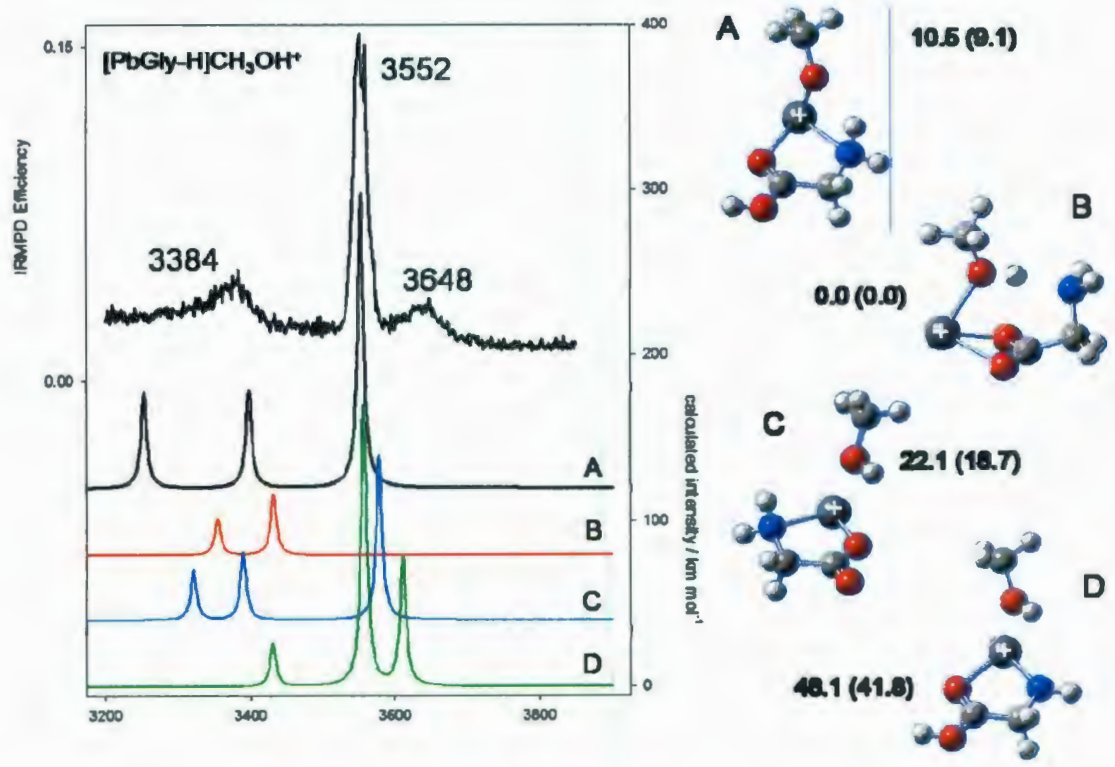

Figure 4.7 - IRMPD spectrum of $[Pb(Gly\text{-}H)CH_3OH]^+$ compared with the computed spectra for four isomeric structures.

present, indicative of a carboxylic acid O-H stretch. Since it is anticipated that there would be a transfer of a proton from the hydroxyl group of methanol to N in the complex, there would be a $PbOCH_3$ group rather than a PbOH group. The absence of a strong band ~3660 cm^{-1} as there was in $[Pb(Gly\text{-}H)H_2O]^+$ is expected. Comparing the experimental spectrum with the computed spectra, it is evident that structures B and C could not be the only species present. Even though structure B is the lowest energy structure, it would only be formed via extensive rearrangement from structure i) involving a proton transfer from the carboxylic acid end to the NH group. Solvation of $[Pb(Gly\text{-}H)]^+$, structure i), would initially produce D and would be expected to rearrange to structure A through a transition state which is similar to that shown in Figure 4.4 for the H_2O solvated species. The energy barrier for this proton shift isomerization is also calculated to be similar, ~10 kJ mol^{-1}.

There is a diffuse band centred at 3648 cm^{-1} which may suggest that methanol is not dissociated or not completely dissociated and that there is at least a mixture of structures A and D. The diffuseness of the 3648 cm^{-1} band is explained by some hydrogen bonding interaction between the absorbing O-H group on methanol with the nitrogen atom of glycine as seen in Figure 4.7. This 3648 cm^{-1} band is most likely explained by the presence of structure D.

4.3.1.4 Ethyl ester, $[Pb(GlyOOEt\text{-}H)H_2O]+$

The complex between Pb^{2+} and the conjugate base of glycine ethyl ester, $[Pb(GlyOOEt\text{-}H)]^+$ was electrosprayed and singly hydrated in the accumulation cell. Upon absorption of the infrared laser, $[Pb(GlyOOEt\text{-}H)H_2O]^+$ was observed to lose water as the sole dissociation process. The spectrum of $[Pb(GlyOOEt\text{-}H)H_2O]^+$ is shown in Figure 4.8 and compared with the spectra of the other species previously presented in this chapter. There are two important observations

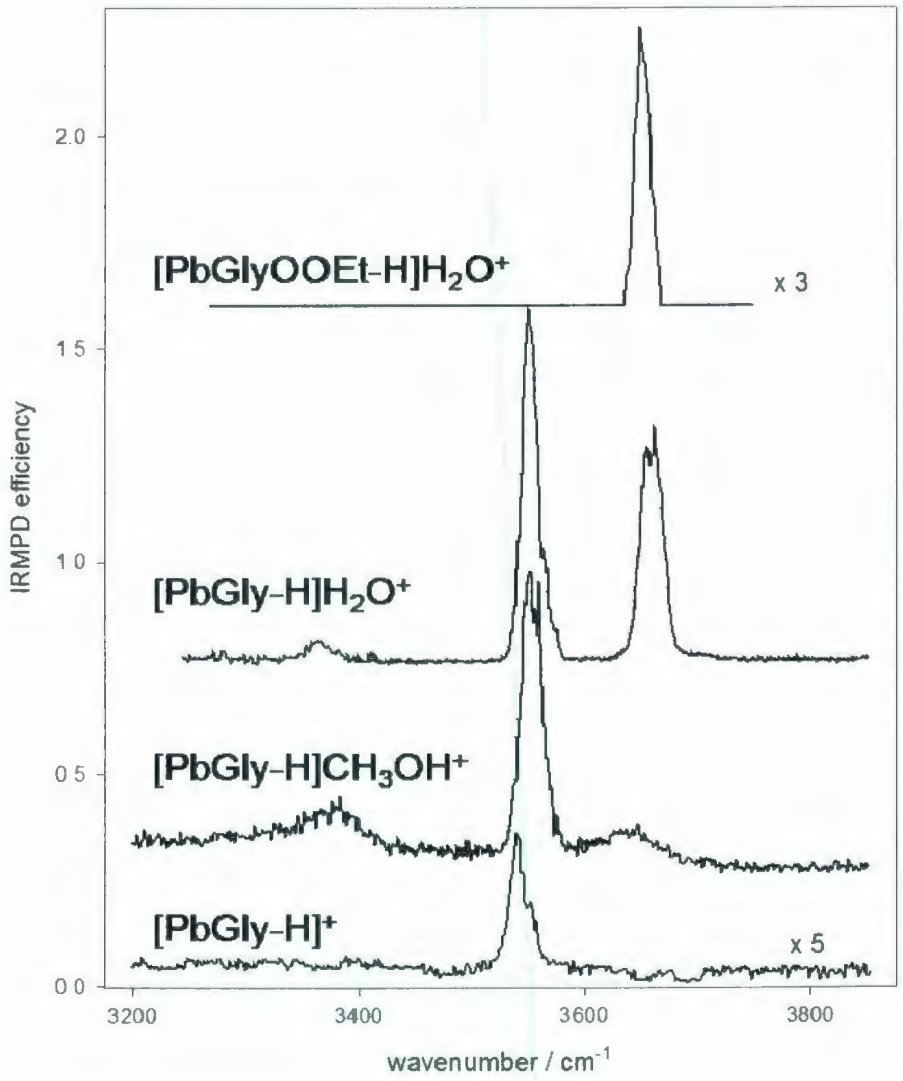

Figure 4.8 - Comparison of the experimental IRMPD spectra of $[Pb(GlyOOEt-H)H_2O]^+$, $[Pb(Gly-H)H_2O]^+$, $[Pb(Gly-H)CH_3OH]^+$, and $[Pb(Gly-H)]^+$.

made by comparing this spectrum to the others. First, the band observed in the spectra of the other species around 3550 cm^{-1} and assigned to the –COO-H stretch is not present in the $[Pb(GlyOOEt\text{-}H)H_2O]^+$ as expected since the -H has been replaced by $-CH_2CH_3$ (or probably more precisely the –OH has been replaced by $-OCH_2CH_3$). This is consistent with our assignment of the 3550 cm^{-1} band to the –COO-H stretch. Second, the band at about 3660 cm^{-1}, also present in the spectrum of $[Pb(Gly\text{-}H)H_2O]^+$, confirms the assignment of this band to the PbO-H stretching absorption.

4.3.2 CID Results

In Figure 4.9 are the MRM profiles recorded for the dissociation of the $[Pb(Gly\text{-}H)S]^+$ complex ions (S=solvent) generated in pure water and in pure methanol solutions. Both primary and higher order collision-induced dissociations were observed. The onset voltages for the dissociation of product ions are listed in Table 4.1 and these provide insight into the sequence of dissociation. The higher onset energies from the solvated ions are expected because of the extra energy required for desolvation. The increasing differences in the onsets with increasing onset energies that are evident in Table 4.1 can be attributed to increasing excess energy of the collisions being stored in the solvent molecules. In effect the solvent molecule acts to dampen the collisions, and the extent of dampening will increase with the collision energy. There are some slight differences in onset energies between ions created in water and methanol that may reflect a larger dampening by methanol, but these are within the error margins of the experiment.

Figure 4.9 shows that the solvated ions first lose the solvent molecule upon collision according to reaction 4.1.

Table 4.1. Onset energies (CM)[a] for product ion formation initiated by the dissociation of $[Pb(Gly-H)]^+$ or $[Pb(Gly-H)S]^+$.

Dissociation channel of $[Pb(Gly-H)]^+$	Onset energy (CM), eV			
	Solvent: H_2O		Solvent: MeOH	
	$[Pb(Gly-H)H_2O]^+$	$[Pb(Gly-H)]^+$	$[Pb(Gly-H)MeOH]^+$	$[Pb(Gly-H)]^+$
1) CO loss	0.7 ± 0.1	0.5± 0.1	0.6 ± 0.1	0.5 ± 0.1
2) H_2O loss	0.7 ± 0.1	0.5 ± 0.1	0.7 ± 0.1	0.3 ± 0.1
3) $PbNHCH^+$ formation	1.1 ± 0.1	0.8 ± 0.1	1.1 ± 0.1	0.9 ± 0.1
4) $PbOH^+$ formation	1.5 ± 0.1	1.0 ± 0.1	1.5 ± 0.1	1.1 ± 0.1
5) PbH^+ formation	1.7 ± 0.1	1.4 ± 0.1	1.7 ± 0.1	1.3 ± 0.1
6) Pb^+ formation	2.1 ± 0.1	1.7 ± 0.1	2.3 ± 0.1	1.6 ± 0.1

[a] Onset energy (CM) = $E_{lab}m_{N2}/(m_{N2} + m_c)$, where E_{lab} is the laboratory collision voltage, m_{N2} is the mass of the collision gas molecules, and m_c is the mass of the complex ion.

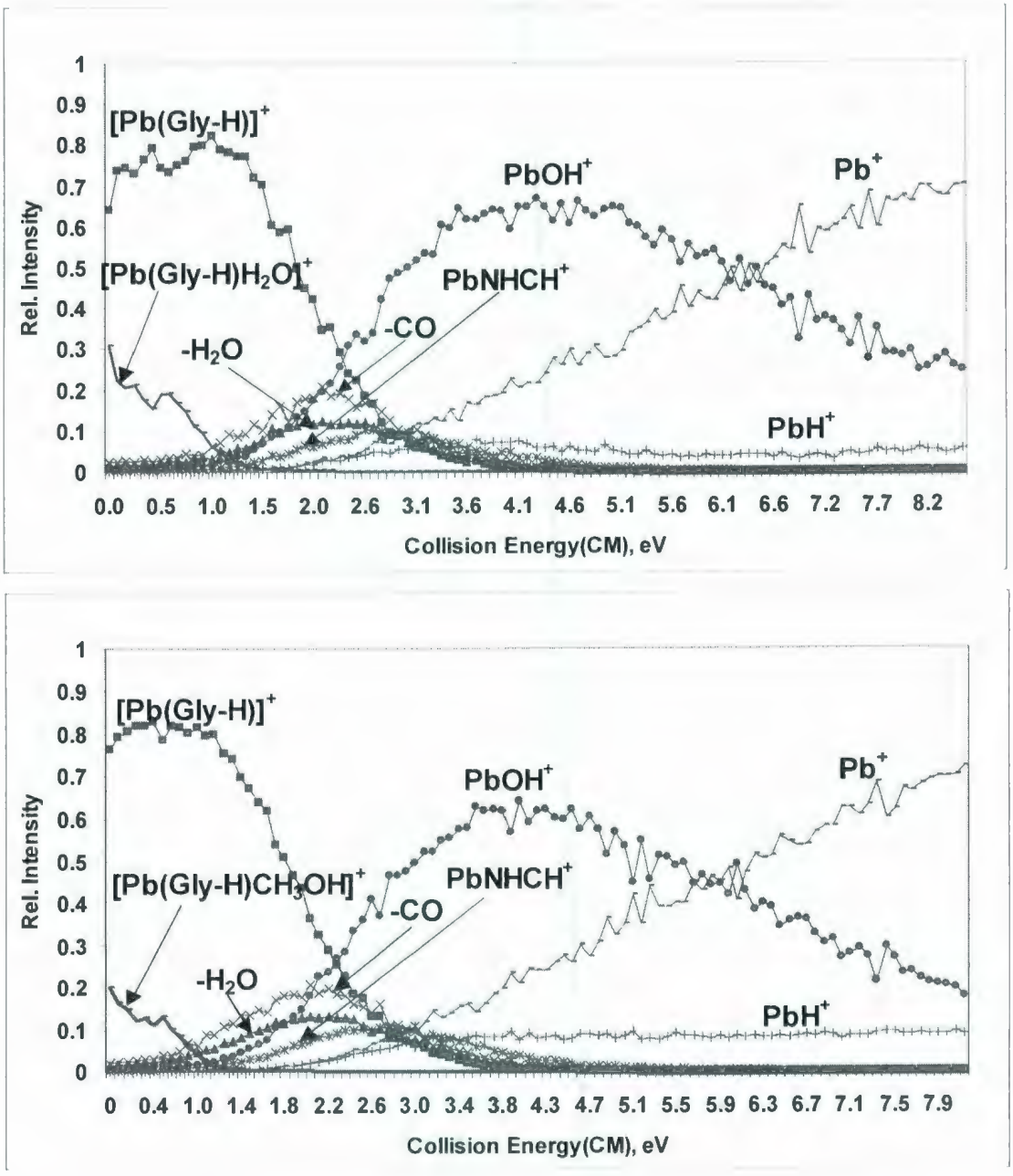

Figure 4.9 - Dissociation profiles obtained for $[Pb(Gly-H)S]^+$ ions, where S is a solvent molecule of water (top) or methanol (bottom).

$$[Pb(Gly\text{-}H)S]^+ \xrightarrow{CID} [Pb(Gly\text{-}H)]^+ + S \quad (4.1)$$

Two primary covalent bond dissociations are observed following desolvation: the elimination of carbon monoxide, reaction 4.2, and the elimination of water, reaction 4.3.

$$[Pb(Gly\text{-}H)]^+ \xrightarrow{CID} [Pb(Gly\text{-}H\text{-}CO)]^+ + CO \quad (4.2)$$

$$[Pb(Gly\text{-}H)]^+ \xrightarrow{CID} [Pb(Gly\text{-}H\text{-}H_2O)]^+ + H_2O \quad (4.3)$$

Further dissociation of the resulting ion $[Pb(Gly\text{-}H\text{-}CO)]^+$ leads to $PbOH^+$ and then Pb^+ according to reaction 4.4:

$$[Pb(Gly\text{-}H\text{-}CO)]^+ \xrightarrow{CID} PbOH^+ + NHCH_2 \xrightarrow{CID} Pb^+ + OH \quad (4.4)$$

$[Pb(Gly\text{-}H\text{-}H_2O)]^+$ undergoes successive loses of CO and HCN to form PbH^+ according to reaction 4.5:

$$[Pb(Gly\text{-}H\text{-}H_2O)]^+ \xrightarrow{CID} [PbNHCH]^+ + CO \xrightarrow{CID} PbH^+ + HCN \quad (4.5)$$

Scheme 4.2. Proposed mechanism for the dissociation of the (1:1) lead-glycine complex, $[Pb(Gly\text{-}H)]^+$.

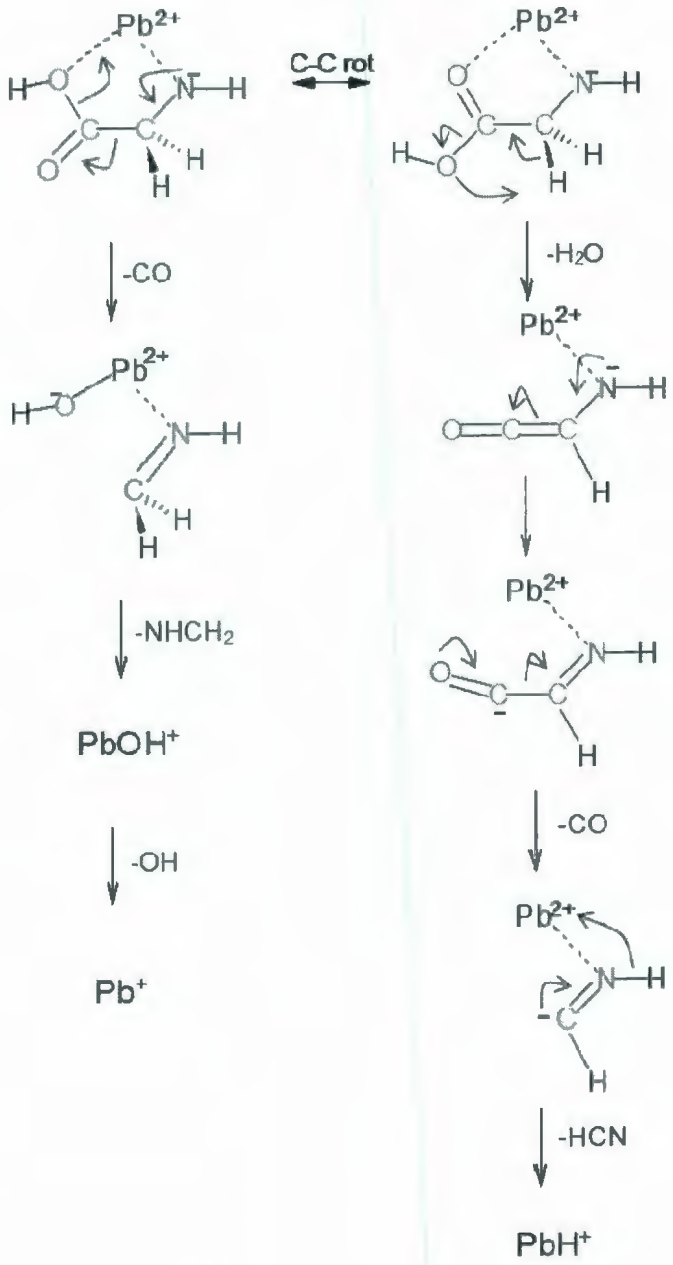

The observed dissociation of the desolvated complex $[Pb(Gly-H)]^+$ can be understood with the mechanism proposed in Scheme 4.2. The structure of the $[Pb(Gly-H)]^+$ formed initially in the electrospray process is not necessarily reflected in the product ions resulting from the CID experiments since the multi-collisional nature of the CID process may lead to isomerization of the $[Pb(Gly-H)]^+$ complex prior to dissociation (Scheme 4.2). The CID studies suggest that losses of CO and H_2O from $[Pb(Gly-H)]^+$ are relatively isoenergetic processes, while the much softer process of IRMPD on $[Pb(Gly-H)]^+$ shows that CO loss is preferred. The mechanism proposed in Scheme 4.2 shows both pathways. The initial loss of CO requires an isomerization of i) to a higher energy structure. While both losses of CO and H_2O have similar onset energies, loss of H_2O requires the transfer of a hydrogen atom, shown to originate from the methylene group. Although the presence of lead makes the amino hydrogens quite mobile, as shown by the formation of $[PbOH(Gly)]^+$ when $[Pb(Gly-H)]^+$ is hydrated, the transfer of the last hydrogen from N is not likely. Furthermore, hydrogen transfer from the methylene group necessitates a tight transition state such that at higher collision energies CO loss is kinetically more favorable as seen experimentally.

4.4. Conclusions

Prior gas-phase work had identified the ion produced when Pb^{2+} is complexed with glycine as being of the form $[Pb(Gly-H)]^+$.[26] Taking such experimentation one step further, energy-resolved CID and IRMPD spectroscopy in the 3200 – 3700 cm^{-1} range can be combined to elucidate the actual structures of these species. Using IRMPD spectroscopy the ability to deduce the structure *a posteriori* was clearly shown for these systems. The structure of $[Pb(Gly-H)H_2O]^+$

from the IRMPD experiments has an intact –COOH group meaning that glycine is deprotonated on N. The results of these experiments guided the theoretical calculations which confirmed that the lowest energy structure was indeed that deduced from experiment. Energy-resolved collision-induced dissociation experiments are analyzed in terms of the structure determined from the IRMPD spectroscopy experiments. Plausible mechanisms of final CID products, PbH^+ and Pb^+, from $[Pb(Gly-H)]^+$, and in fact from the solvated structures as well, are proposed. Detailed calculations of the potential energy surface for $[Pb(Gly-H)]^+$ dissociation could help in the mechanistic proposal but are beyond the scope of this work.

Further experimentation is needed on cysteine and glutamic acid with the Pb^{2+} ion in order to proceed onward with attempts to understand the binding of such heavy metal ions with glutathione.

4.5 References

(1) Dunbar, R. C. *J. Phys. Chem. A* **2000**, *104*, 8067.

(2) Gapeev, A.; Yang, C.-N.; Klippenstein, S. J.; Dunbar, R. C. *J. Phys. Chem. A* **2000**, *104*, 3246.

(3) Grimm, R. L.; Mangrum, J. B.; Dunbar, R. C. *J. Phys. Chem. A* **2004**, *108*, 10897.

(4) Dunbar, R. C.; Polfer, N. C.; Oomens, J. *J. Am. Chem. Soc.* **2007**, *129*, 14562.

(5) Strittmatter, E. F.; Lemoff, A. S.; Williams, E. R. *J. Phys. Chem. A* **2000**, *104*, 9793.

(6) Bush, M. F.; Oomens, J.; Saykally, R. J.; Williams, E. R. *J. Am. Chem. Soc.* **2008**, *130*, 6463.

(7) Drayss, M. K.; Blunk, D.; Oomens, J.; Schaefer, M. *J. Phys. Chem. A* **2008**, *112*, 11972.

(8) Kapota, C.; Lemaire, J.; Maitre, P.; Ohanessian, G. *J. Am. Chem. Soc.* **2004**, *126*, 1836.

(9) Bush, M. F.; O'Brien, J. T.; Prell, J. S.; Saykally, R. J.; Williams, E. R. *J. Am. Chem. Soc.* **2007**, *129*, 1612.

(10) Bush, M. F.; Oomens, J.; Williams, E. R. *J. Phys. Chem. A* **2009**, *113*, 431.

(11) Forbes, M. W.; Bush, M. F.; Polfer, N. C.; Oomens, J.; Dunbar, R. C.; Williams, E. R.; Jockusch, R. A. *J. Phys. Chem. A* **2007**, *111*, 11759.

(12) O'Brien, J. T.; Prell, J. S.; Steill, J. D.; Oomens, J.; Williams, E. R. *J. Phys. Chem. A* **2008**, *112*, 10823.

(13) Hoyau, S.; Ohanessian, G. *Chem. Eur. J.* **1998**, *4*, 1561.

(14) Remko, M.; Rode, B. M. *J. Phys. Chem. A* **2006**, *110*, 1960.

(15) Wyttenbach, T.; Witt, M.; Bowers, M. T. *J. Am. Chem. Soc.* **2000**, *122*, 3458.

(16) Bertran, J.; Rodriguez-Santiago, L.; Sodupe, M. *J. Phys. Chem. B* **1999**, *103*, 2010.

(17) Hoyau, S.; Pelicier, J.-P.; Rogalewicz, F.; Hoppilliard, Y.; Ohanessian, G. *Eur. J. Mass Spectrom.* **2001**, *7*, 303.

(18) Wyttenbach, T.; Witt, M.; Bowers, M. T. *Int. J. Mass Spectrom.* **1999**, *182/183*, 243.

(19) Atkins, C. G.; Rajabi, K.; Gillis, E. A. L.; Fridgen, T. D. *J. Phys. Chem. A* **2008**, *112*, 10220.

(20) Rode, B. M. *Peptides* **1999**, *20*, 773.

(21) Hoyau, S.; Norrman, K.; McMahon, T. B.; Ohanessian, G. *J. Am. Chem. Soc.* **1999**, *121*, 8864.

(22) Belcastro, M.; Marino, T.; Russo, N.; Toscano, M. *J. Mass Spectrom.* **2005**, *40*, 300.

(23) Meister, A. *J. Biol. Chem.* **1988**, *263*, 17205.

(24) Fuhr, B. J.; Rabenstein, D. L. *J. Am. Chem. Soc.* **1973**, *95*, 6944.

(25) Cruz, B. H.; Diaz-Cruz, J. M.; Diaz-Cruz, M. S.; Arino, C.; Esteban, M.; Tauler, R. *J. Electroanal. Chem.* **2001**, *516*, 110.

(26) Burford, N.; Eelman, M. D.; LeBlanc, W. G. *Can. J. Chem.* **2004**, *82*, 1254.

(27) Burford, N.; Eelman, M. D.; Groom, K. *J. Inorg. Biochem.* **2005**, *99*, 1992.

(28) Oomens, J.; Tielens, A. G. G. M.; Sartakov, B. G.; von Helden, G. *Astrophys. J.* **2003**, *591*, 968.

(29) Oepts, D.; van der Meer, A. F. G.; van Amersfoort, P. W. *Infrared Phys.Technol.* **1995**, *36*, 297.

(30) Ortega, J. M.; Berset, J. M.; Chaput, R.; Glotin, F.; Humbert, G.; Jaroszynski, D.; Joly, P.; Kergosien, B.; Lesrel, J. *Nucl. Instrum. Methods Phys. Res., Sect. A* **1996**, *375*, 618.

(31) Oh, H.; Breuker, K.; Sze, S. K.; Ge, Y.; Carpenter, B. K.; McLafferty, F. W. *PNAS* **2002**, *99*, 15863.

(32) Eyler, J. R. *Mass Spectrom. Rev.* **2009**, *28*, 448.

(33) Fridgen, T. D. *Mass Spectrom. Rev.* **2009**, *28*, 586.

(34) Polfer, N. C.; Oomens, J. *Mass Spectrom. Rev.* **2009**, *28*, 468.

(35) Rogalewicz, F.; Louazel, G.; Hoppilliard, Y.; Ohanessian, G. *Int. J. Mass Spectrom.* **2003**, *228*, 779.

(36) Rogalewicz, F.; Hoppilliard, Y.; Ohanessian, G. *Int. J. Mass Spectrom.* **2001**, *206*, 45.

(37) Lobinski, R.; Adams, F. C. *Anal. Chim. Acta* **1992**, *262*, 285.

(38) Gorecki, T.; Pawliszyn, J. *Anal.Chem.* **1996**, *68*, 3008.

(39) Rajabi, K.; Easterling, M. L.; Fridgen, T. D. *J. Am. Soc. Mass Spectrom.* **2009**, *20*, 411.

(40) Gaussian 03, R. C., Frisch, M. J.; Trucks, G. W.; Schlegel, H. B.; Scuseria, G. E.; Robb, M. A.; Cheeseman, J. R.; Montgomery, Jr., J. A.; Vreven, T.; Kudin, K. N.; Burant, J. C.; Millam, J. M.; Iyengar, S. S.; Tomasi, J.; Barone, V.; Mennucci, B.; Cossi, M.; Scalmani, G.; Rega, N.; Petersson, G. A.; Nakatsuji, H.; Hada, M.; Ehara, M.; Toyota, K.; Fukuda, R.; Hasegawa, J.; Ishida, M.; Nakajima, T.; Honda, Y.; Kitao, O.; Nakai, H.; Klene, M.; Li, X.; Knox, J. E.; Hratchian, H. P.; Cross, J. B.; Bakken, V.; Adamo, C.; Jaramillo, J.; Gomperts, R.; Stratmann, R. E.; Yazyev, O.; Austin, A. J.; Cammi, R.; Pomelli, C.; Ochterski, J. W.; Ayala, P. Y.; Morokuma, K.; Voth, G. A.; Salvador, P.; Dannenberg, J. J.; Zakrzewski, V. G.; Dapprich, S.; Daniels, A. D.; Strain, M. C.; Farkas, O.; Malick, D. K.; Rabuck, A. D.; Raghavachari, K.; Foresman, J. B.; Ortiz, J. V.; Cui, Q.; Baboul, A. G.; Clifford, S.; Cioslowski, J.; Stefanov, B. B.; Liu, G.; Liashenko, A.; Piskorz, P.; Komaromi, I.; Martin, R. L.; Fox, D. J.; Keith, T.; Al-Laham, M. A.; Peng, C. Y.; Nanayakkara, A.; Challacombe, M.; Gill, P. M. W.; Johnson, B.; Chen, W.; Wong, M. W.; Gonzalez, C.; and Pople, J. A.; Gaussian, Inc., Wallingford CT, 2004.

(41) Cornard, J. P.; Dangleterre, L.; Lapouge, C. *Chem. Phys. Lett.* **2006**, *419*, 304.

(42) Kamariotis, A.; Boyarkin, O. V.; Mercier, S. R.; Beck, R. D.; Bush, M. F.; Williams, E. R.; Rizzo, T. R. *J. Am. Chem. Soc.* **2006**, *128*, 905.

(43) Linder, R.; Seefeld, K.; Vavra, A.; Kleinermanns, K. *Chem. Phys. Lett.* **2008**, *453*, 1.

(44) Wang, X.; Andrews, L. *J. Phys. Chem. A* **2005**, *109*, 10689.

(45) Gillis, E. A. L.; Rajabi, K.; Fridgen, T. D. *J. Phys. Chem. A* **2009**, *113*, 824.

(46) O'Hair, R. A. J.; Blanksby, S.; Styles, M.; Bowie, J. H. *Int. J. Mass Spectrom.* **1999**, *182/183*, 203.

Chapter 5

Summary

Through IRMPD spectroscopy of protonated and metalated complexes of glycine, structural characterization of such ions has been obtained in the gas phase. Experiments of this nature are able to specify whether an amino acid is present as its zwitterion or non-zwitterion form when complexed with cations in the gas phase. A vast amount of research interest has been directed towards this structural quandary with certain results suggesting that the zwitterion form can be preferentially stabilized depending on the influence of noncovalent interactions. The implications of such studies are quite revealing as it becomes possible to demonstrate, for example, that an aqueous solution can be mimicked in the gas-phase through the stepwise addition of water molecules. This gas-phase "aqueous solution" is obtained when the zwitterion form of the amino acid becomes favoured as opposed to the non-zwitterion. Other published results have demonstrated similar structural transitions through the complexation of amino acids with metal cations of an appreciable size. By studying similar types of noncovalent interactions with glycine, the simplest of the twenty standard amino acids, it was anticipated that elucidating any presence of zwitterionic forms would be possible. On the whole, the goal was merely to evaluate with certainty the most-abundant ion structure of complexes involving glycine.

The two studies discussed in Chapters 3 and 4 demonstrate that IRMPD spectroscopy can be utilized for determining the gas-phase structure of a proton-/sodium ion-bound dimer of glycine and of a lead-glycine complex. The connecting feature between these systems was the

enhanced stability observed when strong noncovalent interactions were present. In structure A of the proton-bound glycine dimer, an *N*-protonated glycine was shown to bind to a neutral glycine. This structure, known as an ion-dipole complex, was stabilized by *two* intramolecular hydrogen bonds. Similarly in the sodium ion-bound glycine dimer, structure I demonstrated beautiful symmetry bound in a bidentate fashion to each of the glycine molecules, creating *four* important interaction sites. In determining the structure of the lead-glycine complex ion, our chemical intuition was challenged as the structure of [Pb(Gly-H)]+ was shown to involve a deprotonation on the amine nitrogen of glycine and *not* on its carboxylic acid. This fact implies that the complex is more stable with the Pb^{2+} cation interacting with oxygen and a deprotonated nitrogen than with the delocalized electron density of a carboxylate functionality. After consulting theoretical calculations to allow for valid confirmations, it was demonstrated that for all of complexes discussed in this thesis, the most abundant gas-phase ion did not have any contributions from the zwitterionic form of glycine.

A major portion of this thesis corroborates that IRMPD spectroscopy is an applicable and direct means to study ions in the gas-phase. Other approaches that are more common in practice can provide insight into ion structure, but their indirect nature is a considerable drawback, since they must often rely heavily on theoretical calculations to validate what was observed experimentally. As shown in Chapter 4, the IRMPD approach is advantageous for its ability to reveal structural information solely from the experimental information. It is important that analyzing experimental data first, before leaning on theoretical explanations, remains to be the primary approach of IRMPD spectroscopists. The future of IRMPD spectroscopy is a bright one, as gas-phase studies of this nature allow for the investigation of fundamental interactions that have significant application to our collective understanding of condensed phase systems.

At the conclusion of this summary, the opportunity for future work is undeniable. Investigating proton- and sodium ion-bound dimers of other amino acids would be beneficial to provide comparison. Similarly, changing the binding ion of the dimer from sodium to other alkali metals would perhaps illicit an energetic switch whereby the zwitterion form of the amino acid could be favoured. With respect to investigating complexes of gaseous Pb^{2+}, expanding the results obtained for glycine to other amino acids will provide a more in-depth understanding of its exposure effects from a fundamental perspective. The information provided for glycine will also serve as a stepping stone to characterizing the detoxification of Pb^{2+} through its interactions with the tripeptide glutathione.

VITA

Name: Chad Garry Atkins

Birth Date: June 28th, 1984

Education: Memorial Graduate Program, Department of Chemistry, Memorial University of Newfoundland, St. John's, Newfoundland (2007-2009)

B.Sc. (Co-Operative Honours Chemistry) 2007, University of Waterloo, Waterloo, Ontario (2002-2007)

Publications: Chad G. Atkins, Laura Banu, Mark Rowsell, Voislav Blagojevic, Diethard K. Bohme, and Travis D. Fridgen, **2009**, "The structure of $Pb(Gly\text{-}H)^+$ and the monosolvated water and methanol solvated species by infrared multiple photon dissociation spectroscopy, energy-resolved collision-induced dissociation, and electronic structure calculations," *Journal of Physical Chemistry B*, submitted for publication June 18th, 2009.

Robert J. Nieckarz, Chad G. Atkins, and Terry B. McMahon, **2008**, "Effects of isomerization on the measured thermochemical properties of deprotonated glycine/protic-solvent clusters," *ChemPhysChem*, Volume 9, pages 2816-2825.

Chad G. Atkins, Khadijeh Rajabi, Elizabeth A.L. Gillis, and Travis D. Fridgen, **2008**, "Infrared Multiple Photon Dissociation Spectra of Proton- and Sodium Ion-Bound Glycine Dimers in the N-H and O-H Stretching Region," *Journal of Physical Chemistry A*, Volume 112, pages 10220-10225.

Conferences: **26th Annual Trent Conference on Mass Spectrometry,** Orillia, Ontario, July 27th - July 31st, 2008. **Poster Presentation:** "*The structure of $Pb(Gly\text{-}H)^+$ and the water and methanol solvated species by IRMPD spectroscopy, energy-resolved CID, and electronic structure calculations.*" Chad G. Atkins, Laura Banu, Mark Rowsell, Voislav Blagojevic, Diethard K. Bohme, Travis D. Fridgen.

Gordon Conference – *Gaseous Ions: Structures, Energetics, & Reactions*, Galveston, Texas, U.S.A., March 1st - March 6th, 2009. **Poster Presentation:** *"Structural Investigation of Pb^{2+}-amino acid complexes using IRMPD spectroscopy."* Chad G. Atkins, Mark Rowsell, Travis D. Fridgen.

57th ASMS Conference on Mass Spectrometry, 2009. **Poster Presentation:** *"Conformational and Thermochemical Properties of Deprotonated Amino Acid Clusters from High Pressure Mass Spectrometry."* Robert J. Nieckarz, Chad G. Atkins, Opal Courtney, Terry B. McMahon.

25th Annual Trent Conference on Mass Spectrometry, Orillia, Ontario, July 27th-July 31st, 2008. **Oral Presentation:** *"Characterizing Intermolecular Interactions and Structures of Glycine Homodimers using IRMPD Spectroscopy in the N-H/O-H Stretching Region."* Chad G. Atkins, Khadijeh Rajabi, Elizabeth A.L. Gillis, Travis D. Fridgen.

25th Annual Trent Conference on Mass Spectrometry, Orillia, Ontario, July 27th - July 31st, 2008. **Poster Presentation:** *"Effects of Isomers on the Thermochemical Properties of Deprotonated Glycine···ROH (R = H, CH_3, C_2H_5) Clusters obtained via PHPMS."* Robert J. Nieckarz, Chad G. Atkins, Terry B. McMahon.

24th Annual Trent Conference on Mass Spectrometry, Orillia, Ontario, July 27th – July 31st, 2007. **Oral Presentation:** *"Implementing High Pressure Mass Spectrometry as a Tool for Investigating Structural and Energetic Properties of Deprotonated Glycine with Alcohols."* Chad G. Atkins, Robert J. Nieckarz, Terry B. McMahon.

35th Southern Ontario Undergraduate Student Chemistry Conference (SOUSCC), Oshawa, Ontario, March 17th, 2007. **Oral Presentation:** *"Investigating Glycine···ROH (R = H, CH_3, C_2H_5) with High Pressure Mass Spectrometry to Determine Structural and Energetic Properties."* Chad G. Atkins, Robert J. Nieckarz, Terry B. McMahon.